NUCLEATION IN BULK SOLUTIONS AND CRYSTAL GROWTH ON HEAT-TRANSFER SURFACES DURING EVAPORATIVE CRYSTALLIZATION OF SALTS COMPOSED OF Na_2CO_3 AND Na_2SO_4

A Dissertation
Presented to
The Academic Faculty

By

Daniel D. Euhus

In Partial Fulfillment
Of the Requirements for the Degree
Doctor of Philosophy in Chemical Engineering

Georgia Institute of Technology

September, 2003

Copyright © Daniel D. Euhus 2003

NUCLEATION IN BULK SOLUTIONS AND CRYSTAL GROWTH ON HEAT-TRANSFER SURFACES DURING EVAPORATIVE CRYSTALLIZATION OF SALTS COMPOSED OF Na_2CO_3 AND Na_2SO_4

Dr. W. James Frederick Jr.
Chemical and Biomolecular Engineering
Georgia Institute of Technology

Dr. Charles A. Eckert
Chemical and Biomolecular Engineering
Georgia Institute of Technology

Dr. David I. Orloff
Mechanical Engineering
Georgia Institute of Technology

Dr. David T. Clay
International Paper

Committee Chair
Dr. Ronald W. Rousseau
Chemical and Biomolecular Engineering
Georgia Institute of Technology

9-25-03

Date Approved

To my loving wife, Kimberly:
Without her patience and encouragement and her willingness to delay her own life goals,
this thesis would not have been possible.

ACKNOWLEDGEMENTS

I would like to express my appreciation to my advisors, Dr. Ronald W. Rousseau and Dr. W. James Frederick Jr. Their combined expertise was invaluable to me. I would also like to thank the remaining members of my thesis committee, Dr. Charles Eckert, Dr. David Orloff, and Dr. David Clay for their interest and input into my research.

I appreciate the help and guidance from a number of current and previous crystallization group members including, Thomas Paxton, Bing Shi, Izumi Kurosawa, Karsten Bartling, Jennifer Sherard, Jose Mendez-del Rio, Young-soo Kim, and Jennifer Luk. Special thanks to the suggestions provided by former graduate student Jason Smith who acted as a great sounding board for many of my ideas. Special thanks are due to Wolfgang Schmidl, Steve Lien, and Chris Verrill at the Institute of Paper Science and Technology for their collaboration on this research.

I wound like to acknowledge and thank the various sources of funding for the Evaporator Research Consortium, the US Department of Energy, the Georgia Research Alliance, Andritz Company, International Paper Company, Lasentec Corporation, Mead-Westvaco Company, Potlatch Corporation, and Weyerhaeuser Company. Special thanks to International Paper Company and Weyerhaeuser Company for their continued support of my research after the Evaporator Research Consortium issued its report. Special thanks to the National Science Foundation for their support of my Graduate Research Fellowship. Any opinions, findings, conclusions or recommendations expressed in this thesis are those of the author and do not necessarily reflect the views of the National Science Foundation.

TABLE OF CONTENTS

LIST OF TABLES

LIST OF FIGURES

LIST OF SYMBOLS

A Heat-transfer surface area, m^2

A' Adherence parameter, Equation 2.7

a Fouling rate fitting parameter, $m^4K^2W^{-2}s^{-1}$, Equation 2.8

a' Fouling rate fitting parameter, $m^2K{\cdot}W^{-1}s^{-1}$, Equation 2.9

a Chemical activity

b Fouling rate fitting parameter, $m^4K^2W^{-2}$, Equation 2.8

b' Fouling rate fitting parameter, $m^2K{\cdot}W^{-1}$, Equation 2.9

b FBRM laser width, m

C Concentration, $mol{\cdot}m^{-3}$

C_O Clean plate viscosity constant

$c(l)$ Chord-count density, m^{-3}

$C(l)$ Chord count, s^{-1}

ΔC_i Number of chords measured in the i^{th} channel, s^{-1}

C_1 Fitting parameter, Equation 5.5

C_2 Fitting parameter, Equation 5.6

d_i Diameter of i^{th} particle, m

d_P Particle diameter, m

ΔG_v Free energy change for the transformation from dissolved solute to crystal per unit volume, $J{\cdot}m^{-3}$

G Growth rate, $m{\cdot}s^{-1}$

G_S Growth rate of scale on the heat-transfer surface, $m{\cdot}s^{-1}$

h Heat transfer coefficient, $W{\cdot}m^{-2}K^{-1}$

ΔH_V Heat of vaporization, $J \cdot kg^{-1}$

J_O Nucleation rate, $m^{-3}s^{-1}$ (Volume) or $m^{-2}s^{-1}$ (Surface)

k Boltzmann constant, 1.380658E-23 $J \cdot molecule^{-1}K^{-1}$

k_F Effective thermal conductivity of the fouling deposit, $W \cdot m^{-1}K^{-1}$

k_i Shape factor, $_V$ indicates volume, $_A$ indicates surface area

k_G Growth rate parameter, $m \cdot s^{-1}$

k_N Nucleation rate parameter, $m^{-3}s^{-1}$

k_S Surface growth rate parameter, $m \cdot s^{-1}$

l_i Chord length at the start of the i^{th} channel

$\bar{l}$ Square-weighted mean chord length, m

L Characteristic particle length, m

m_j j^{th} moment of the particle population, m^{j-3}

$\dot{m}$ Mass flow rate, $kg \cdot s^{-1}$

m Inverse solubility profile slope, K^{-1}

$\dot{m}_T$ Mass transfer rate, $kg \cdot s^{-1}$

n^O Surface nucleation site count, m^{-2}

$n(L)$ Particle population density, m^{-3}

$N(L)$ Particle population, s^{-1}

P_S Steam pressure, bara

Q Heat, J

q Heat transfer rate, W

r_c Critical radius, m

R Thermal Resistance – subscript indicates what the resistance is measured through, $m^2K \cdot W^{-1}$

R Gas Constant, 8.31451 $J \cdot mol^{-1}K^{-1}$ (Equation 2.10 only)

R_E Electrical Resistance, Ω

Re Reynolds number

S Supersaturation

SFR Surface fouling rate, $m^2K \cdot W^{-1}s^{-1}$

T Temperature, K

t Time, s

U Overall heat transfer coefficient, $W \cdot m^{-2}K^{-1}$

v Crystal molar volume, m^3mol^{-1}

V Voltage, V

V_S Sample volume, m^3

$\dot{v}_S$ FBRM laser rotation speed

$\bar{V}_S$ Volume scan rate of the solution by the FBRM, m^3s^{-1}

WP Wetted perimeter, m

x Thickness, m

z Measured effect

α Fitting parameter

α Fitting parameter, Equation 5.6

ε_{Surf} Interfacial surface energy, $J \cdot m^{-2}$

γ Activity coefficient

μ Chemical potential, $J \cdot mol^{-1}$

μ Viscosity, $kg \cdot m^{-1}s^{-1}$

σ Relative Supersaturation

θ_D Induction time, s

λ Effective laser penetration depth, m

Φ_D Fouling deposition rate, $m \cdot s^{-1}$

Φ_R Fouling removal rate, $m \cdot s^{-1}$

ρ Density, $kg \cdot m^{-2}$

ρ_C Crystal density, $kg \cdot m^{-3}$

τ Scale initiation time, s

τ Shear rate, s^{-1}

Superscripts and Subscripts

$_1$ First event

$_2$ Second event

$_0$ Clean plate conditions

$_B$ Bulk Condition

$_C$ Clean plate condition

$_F$ Fouling

$_g$ Growth rate order, typically equals 1

$_i$ Chemical species

$_I$ Inlet Condition

^{i} Nucleation order

$_L$ Liquor

M	Metastable condition
O	Outlet Condition
S	Surface Condition
S	Steam or steam side condensate
Sat	Saturated condition
W	Wall, stainless steel heat transfer surface
*	Chemical equilibrium
*	Solubility limit
Γ	Plate (Reynolds number)

SUMMARY

Introduction

The capacity of many black liquor evaporators and high-solids concentrators suffers from fouling of their heat transfer surfaces. The fouling problem in about 30% of these evaporators and concentrators results from deposition of double salts composed of Na_2CO_3 and Na_2SO_4. Reduction or elimination of fouling by these double salts through improved design of black liquor evaporators and improved operating practices requires an understanding of the crystallization processes that produce the deposits. The overall objective of the research conducted in this study was to provide at least part of that knowledge.

The outcome of the research conducted was new, fundamental results in four areas of crystallization of Na_2CO_3 and Na_2SO_4 and its relationship to fouling in black liquor evaporators. First, the initiation mechanisms for heat-transfer fouling by Na_2CO_3-Na_2SO_4 based salts were determined, and an important relationship between nucleation of crystals and fouling was discovered. Second, a methodology for the estimation and application of rate parameters for primary nucleation and growth in bulk solutions and growth of crystals on a heat-transfer surface was developed. This methodology created an analytical tool for modeling and for comparative analysis of experimental results. The influence of several variables on the rate parameters was determined for both aqueous solutions of Na_2CO_3 and Na_2SO_4 and black liquor. Third, calcium was shown to inhibit the crystallization behavior of double salts of Na_2CO_3 and Na_2SO_4. Finally, fouling was dependant on liquor composition (because of a transition in crystallizing species from

burkeite to dicarbonate) and on nucleation phenomena, which can be more important in fouling than crystal growth.

Initiation Mechanisms for Heat-Transfer Fouling by Na_2CO_3-Na_2SO_4 Based Salts.

- Rapid fouling events during evaporation of black liquor were found to correspond with the primary bulk nucleation of dicarbonate[1].
- Direct nucleation of crystals on the heat-transfer surface was determined to be the mechanism by which burkeite[2] deposition was initiated.
- Adhesion of crystals from the bulk solution to the heat-transfer surface was determined to be the mechanism by which dicarbonate deposition was initiated.

Estimation and Application of Rate Parameters for Primary Nucleation and Growth in Bulk Solutions and Growth of Crystals on a Heat-Transfer Surface

- Nucleation rates for crystals suspended in a bulk solution were estimated from chord length distributions of the crystal population obtained by FBRM. This research marked the first time that FBRM had been utilized for this purpose.
- Rate parameters for primary nucleation and growth in a bulk solution and crystal growth on the heat transfer surface were estimated from FBRM measurements of the crystal population with time, measurements of the change in the heat-transfer resistance with time, and values of relative supersaturation derived from solubility predictions and experimental observations.

[1] Double salt with a nominal composition of $2Na_2CO_3$:Na_2SO_4
[2] Double salt with a nominal composition of $2Na_2SO_4$:Na_2CO_3

- A correlative model estimating the dependence of the rate parameter for primary bulk nucleation on the thermal driving force, the rate of circulation of the suspension, and the solution composition was developed for aqueous solutions of Na_2CO_3 and Na_2SO_4.
- A correlative model estimating the dependence of the rate parameter for crystal growth on heat-transfer surfaces on the rate of circulation of the suspension, and the solution composition was developed for aqueous solutions of Na_2CO_3 and Na_2SO_4.
- Estimated rate parameters were used to show that increasing the ratio of Na_2CO_3:Na_2SO_4 in black liquor increased the rate of fouling of heat-transfer surfaces during evaporation.
- The sizes of crystals on the heat-transfer surface were measured with time using analysis of digital imagery. The rate of growth of these crystals was determined from the images obtained.
- The growth rate of a layer of crystals on a heat-transfer surface was estimated from the heat-transfer resistance and thermal conductivity of the fouling deposit. This estimated growth rate was found to be very nearly the same as the observed growth rate of crystals on the heat-transfer surface.

Influences of Calcium on the Crystallization of Na_2CO_3-Na_2SO_4 Based Salts.

- Calcium inhibited bulk nucleation and crystal growth on the heat-transfer surface for both burkeite and dicarbonate.

Implications of Crystallization Behavior on Control of Fouling

- Nucleation and subsequent adherence of dicarbonate crystals on heat transfer surfaces causes rapid fouling in black liquor evaporators. Supersaturation at the heat-transfer surface due only to the temperature difference (and the inverse solubility with temperature of Na_2CO_3 and Na_2SO_4) does not.
- A number of alternatives to reduce fouling in black-liquor evaporators were evaluated in pilot evaporation experiments. The estimated rate parameters for crystal growth on the heat-transfer surface were used to compare the different alternatives. The most promising alternative was addition of anhydrous sodium carbonate to black liquor whose total solids concentration was above the solubility limit for Na_2CO_3 and Na_2SO_4. One plausible explanation for this result is that the anhydrous sodium carbonate provides a surface for growth that reduces the dissolved Na_2CO_3 and avoids nucleation of dicarbonate.

Chapter I: Research Scope and Objectives

1.1. Introduction

The capacity of many black liquor evaporators and high-solids concentrators suffers from fouling of their heat transfer surfaces. The fouling problem in about 30% of these evaporators and concentrators results from deposition of double salts composed of Na_2CO_3 and Na_2SO_4. The scale formed is often referred to as soluble scale because these sodium salts are moderately soluble in water and are readily removed by washing with hot water. [1]

In 1997 Schmidl and Frederick [2] conducted a survey of pulp mills to document problems with fouling in black liquor evaporators. This study found that no generally applicable method to reduce soluble scale fouling in black liquor evaporation had been found. Schmidl and Frederick compare their results to a similar study conducted by Grace in the early 1970s [3]. Their analysis indicates that the number of mills experiencing no fouling problems had dropped to nearly zero in the 25 years since Grace's study. Furthermore, the percentage of mills with soluble scale problems increased. During this same time, the total solids content[1] of the liquor being produced also increased at nearly all mills.

The pulp and paper industry continues to use kraft (alkaline) pulping for a number of reasons. Kraft pulping produces strong fibers. Chemical and energy recovery in kraft pulp mills involves well-established and mature operations. The current industrial infrastructure is designed around kraft pulping. This last issue creates perhaps the

[1] Total solids content is the primary industrial measurement for the concentration of black liquor. It is the solvent-free (water-free) mass divided by the total mass of black liquor.

greatest resistance to industrial change. At the present time, capital available to the industry is limited, and industrial production facilities are being expected to produce more with their existing equipment. Due to its high capital costs, the recovery boiler and associated operations eventually become the bottleneck in most mills. Thus, any incremental increase in recovery capacity translates into an incremental increase in production. While many mills are recovery boiler limited, a number do experience significant evaporator problems as well.

1.2. Research Objectives

This research obtained new, fundamental results in four areas of crystallization of Na_2CO_3 and Na_2SO_4 and determined how these results related to fouling in black liquor evaporators. The first objective was to determine the initiation mechanisms for heat-transfer fouling by Na_2CO_3-Na_2SO_4 based salts. The second objective was to develop a methodology for the estimation and application of rate parameters for primary nucleation and growth in bulk solutions and growth of crystals on a heat-transfer surface. This methodology could then be applied as an analytical tool for modeling heat-transfer fouling as a crystallization process and for comparative analysis of experimental crystallization and fouling results. The third objective was to determine the effect of calcium on the crystallization behavior of double salts of Na_2CO_3 and Na_2SO_4, particularly as it relates to fouling on a heat-transfer surface. The final objective was to determine the dependence of fouling on liquor composition, particularly the influence of the transition in crystallizing species from burkeite to dicarbonate identified by Shi [4], and on nucleation phenomena.

1.2.1. Initiation Mechanisms for Heat-Transfer Fouling by Na_2CO_3-Na_2SO_4 Based Salts

In order to identify the nucleation mechanism(s) for fouling of heat-transfer surfaces, a bench-scale apparatus to observe crystal nucleation and growth on a heat-transfer surface was constructed. It was used to determine the mechanism(s) for the initiation of fouling by burkeite and dicarbonate. Identifying and observing the mechanism by which fouling of heat-transfer surfaces are initiated provided two benefits. First, it determined whether addressing fouling as a crystallization problem is appropriate. It is possible that the fouling in black liquor evaporators occurs due to non-crystallization processes such as adhesion of crystals produced in the bulk solution, and that supersaturation driven crystal nucleation or growth do not occur directly on the surface. Second, identifying the initiation mechanism may lead to a method to control fouling on heat-transfer surfaces in black liquor evaporators.

1.2.2. Estimation and Application of Rate Parameters for Primary Nucleation and Growth in Bulk Solutions and Growth of Crystals on a Heat-Transfer Surface

Methodologies to analyze pilot-scale bulk crystallization and heat-transfer coefficient data were developed in order to obtain rate parameters for the crystallization phenomena. Nucleation rates were estimated for the first time from Focused-Beam Reflectance Measurement (FBRM) techniques. Rate parameters for primary bulk nucleation and for crystal growth on the heat-transfer surface were estimated using conventional crystallization models. The rate parameters estimated were used to

determine the influence of the Reynolds number, the thermal driving force, and the composition of the dissolved salts on the fouling process and to evaluate potential strategies to reduce fouling on heat-transfer surfaces.

This research developed correlative models for the dependence of the rate parameters for primary bulk nucleation and for crystal growth on the heat-transfer surface from aqueous solutions of sodium carbonate and sodium sulfate. These models correlated the influence of the previously mentioned experimental variables on the rate parameters.

This research also determined the dependence of the rate parameters for primary bulk nucleation and for crystal growth on the heat-transfer surface on the composition of black liquor solutions. In addition, the viability of a number of potential strategies that could be employed to reduce fouling at an industrial facility was determined by comparison of their estimated rate parameters.

The sizes of crystals on the heat-transfer surface were measured as a function of time from digital imagery. The rate of growth of these crystals was determined using the measurements obtained. The growth rate of a layer of crystals on a heat-transfer surface was estimated from the heat-transfer resistance and thermal conductivity of the fouling deposit. This estimated growth rate was compared to the observed growth rate of crystals on the heat-transfer surface.

1.2.3. Influence of Calcium on the Crystallization of Na_2CO_3-Na_2SO_4 Based Salts

The influence of calcium on primary bulk nucleation and crystal growth on the heat-transfer surface was determined. Of particular interest was the influence of calcium on the mechanism by which initiation of scale occurs on heat-transfer surfaces.

1.2.4. Implications of Crystallization Behavior on Control of Fouling.

Shi identified a new double salt of sodium carbonate and sodium sulfate [4]. Termed "dicarbonate," this double salt has a nominal composition of $2Na_2CO_3$:Na_2SO_4. Dicarbonate crystallization occurs in the range of dissolved liquor compositions where rapid fouling has been observed in industrial evaporators. This research determined the influence of the composition of solutions containing sodium carbonate and sodium sulfate on fouling and particularly the role played by the new dicarbonate salt in fouling of black liquor evaporators at high total solids content.

1.3. Bibliography

1. Shi, B., Euhus, D.D., Rousseau, R.W., Frederick, Jr., W.J., "Crystallization and Control of Sodium Salt Scales in Black Liquor Concentrators," Submitted to *TAPPI Journal*
2. Schmidl, W. and Frederick, Jr., W.J., "Current Trends in Evaporator Fouling," *1998 International Chemical Recovery Conference*, TAPPI Press, Atlanta, pp. 367-377
3. Grace, T.M. and B.D. Andrews, *Study of Evaporator Scaling: Soluble Carbonate-Sulfate Scales Project 3234 Report 2*, January 25, 1977

4. Shi, B., "Crystallization of Solutes that Lead to Scale Formation in Black Liquor Evaporation," *Ph.D. Thesis*, Georgia Institute of Technology, 2002

Chapter II: Background and Review of Work Related to Fouling in Black Liquor Evaporation

2.1. Introduction

Research focused on reducing fouling of black-liquor evaporators has been conducted for the past 40 years. The level of research has advanced from reporting observations of fouling in industrial evaporators to phenomenological investigation of the underlying microscopic crystallization processes responsible for fouling. This chapter presents a review of research in black liquor evaporation. In addition, it presents reviews of heat transfer and fouling of heat-transfer surfaces, the solubility of Na_2CO_3 and Na_2SO_4, and crystallization phenomena as related to fouling in black liquor evaporators.

2.2 Overview of Black Liquor Evaporation

The chemical recovery area of a kraft pulp mill is an economically critical component of modern pulp and paper mills because without the recovery and regeneration of the inorganic chemicals used in the pulping process and energy recovery as electricity and steam, the cost of producing kraft pulp would be prohibitive. However, because the chemical recovery area does not make a product for external sale as a paper machine does for example, it often does not receive as much attention. Evaporation of black liquor is a critical part of the chemical recovery process.

Black liquor is a mixture of dissolved inorganic sodium salts consumed in pulping and their residues (primarily hydroxide, carbonate, sulfate, sulfide and thiosulfate), sodium salts of anionic, dissolved organic material (mostly lignin, hemicellulose and cellulose degradation products), suspended organic material, and water. It is the feed

material to the recovery process shown in Figure 2.1. Weak black liquor, at 15-20% total solids content[1], is fed to steam-heated, multiple-effect evaporators. The evaporator product is strong black liquor with total solids content between 65-85%. Strong liquor is fired in a recovery boiler at this total solids content.

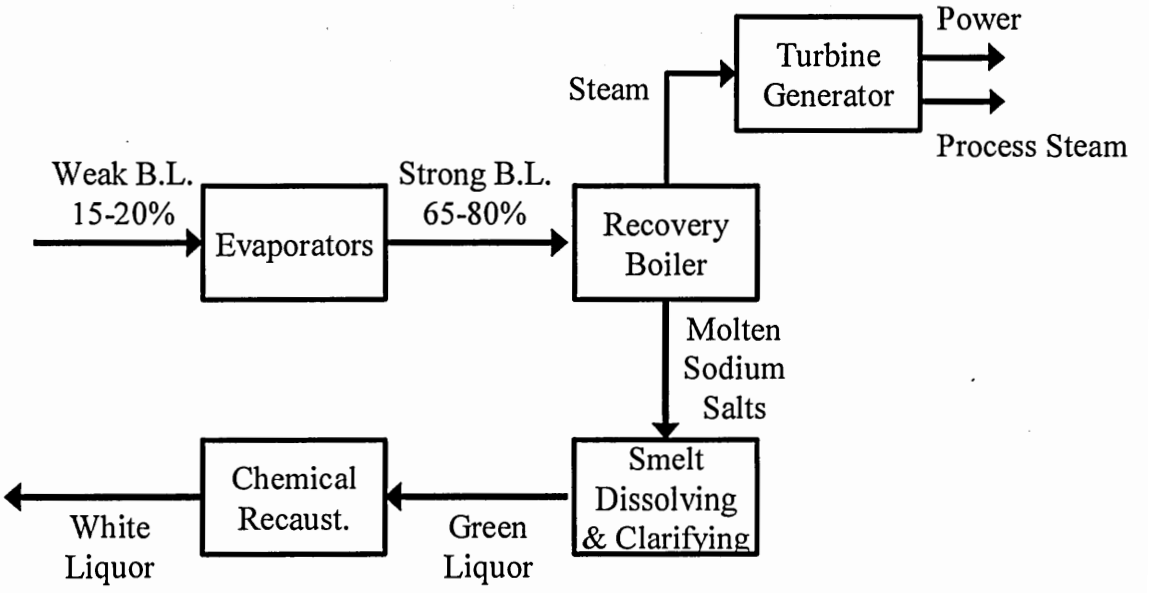

Figure 2.1: Basic kraft chemical recovery cycle.

The evaporation of black liquor is typically accomplished using one of four different types of process equipment. Prior to the 1970s, direct contact heat exchangers were often used to concentrate black liquor in North America. Direct-contact evaporation utilized flue gas from the recovery boiler as the heat source for evaporation. However, direct-contact evaporation allowed for the transfer of reduced sulfur compounds from the black liquor to the flue gas, causing significant release of these odorous compounds. Also, direct-contact evaporation is less energy efficient than indirect-contact evaporation. For these reasons, in the late 1960's and early 1970's the

[1] Total solids content is the primary industrial measurement for liquor concentration. It is the solvent-free (water-free) mass divided by the total mass of black liquor.

North American pulp and paper industry shifted away from direct-contact evaporation technology. One type of indirect-contact evaporator installed at many pulp mills is the so-called Long Tube Vertical (LTV) rising-film evaporators. While these pieces of equipment provide excellent heat-transfer coefficients, they are unfit for operating above the solubility limit[2] of the dissolved salts in black liquor where they invariably foul quickly. Many pulp mills now use one or two different technologies to concentrate black liquor above the solubility limit. The first is the falling-film evaporator and its close relative the falling-film crystallizing evaporator. In this type of evaporator a film of black liquor flows down the heated surface with evaporation occurring at the film-vapor interface. Falling-film evaporators provide good heat-transfer coefficients and reduced potential for plugging, particularly when heated plates are used as the heat-transfer surface. Plugging can be a serious problem with LTV evaporators. The crystallizing variant of falling-film evaporators employs an enlarged sump to increase retention time so that crystal growth in the sump is able to reduce supersaturation more completely. The final type of indirect-contact evaporators are forced-circulation evaporators. This type of evaporator uses flooded tubes for the heat transfer, creating a superheated liquid. Evaporation occurs in a subsequent flash tank, where crystallization also occurs.

Crystallization of various sodium salts is likely to occur during evaporation of black liquor. This crystallization often occurs on the heat-transfer surfaces of evaporators, and it requires cleaning. One result is higher equipment costs as black liquor evaporators are designed with excess capacity so as to reduce the cleaning frequency. A

[2] The solubility limit is essentially the first point at which crystal may exist in the system. It is the thermodynamic equilibrium point.

second result is the possibility of lost pulp production capacity if limitations in capacity of the black liquor evaporators act as a bottleneck for the pulp mill.

More detailed discussions of the chemical recovery process in general and black liquor evaporation specifically are available from a number of sources. [1-4]

2.3. Background and Review of Heat Transfer Fouling

The fouling of heat-transfer surfaces is a well-developed field of study. The traditional methodology for studying fouling is well outlined in the papers compiled by Somerscales and Knudsen [5]. Heat transfer is the process of moving heat through the various materials that exist between the heat sink and the heat source. The overall heat transfer coefficient, U, is defined as the ratio of the heat flux to the product of the temperature difference between the heat source to the heat sink and the area of the heat transfer surface:

$$U = \frac{q}{A\Delta T}. \tag{2.1}$$

Using the electrical circuit analogy [6], the total resistance to heat transfer ($1/U$) can be shown to be,

$$\frac{1}{UA} = R_L + R_F + R_W + R_S. \tag{2.2}$$

where $1/UA$ is the sum of all the resistances, R_i where i represents each individual resistance.

Fouling is defined to be any deposit on a heat transfer surface that is resistive to the flow of heat through it. In industrial processes, fouling can occur for a number of reasons. In this work, only precipitation fouling will be considered. Hasson defined

precipitation fouling as "the phenomena of a solid layer deposition on a heat transfer surface, arising primarily from the presence of dissolved inorganic salts in the flowing solution which exhibit supersaturation under the process conditions [7]." This type of fouling is referred to as crystallization fouling when the inorganic salts crystallize from solution.

The resistance due to fouling, R_F, is the difference between the reciprocal of the heat-transfer coefficient under fouling conditions ($1/UA$) and that of the heat-transfer coefficient for the clean surface ($1/U_0A$).

$$R_F = \frac{1}{UA} - \frac{1}{U_0 A} \tag{2.3}$$

The rate at which fouling occurs is the derivative of R_F with respect to time:

$$\frac{dR_F}{dt} = \frac{\frac{1}{A} d\left(\frac{1}{U} - \frac{1}{U_i}\right)}{dt}. \tag{2.4}$$

In many cases, the rate of fouling can be expressed in terms of the difference between the rates of deposition and removal of the fouling species using the so-called Kerns model [7, 8, 9],

$$k_F \frac{dR_F}{dt} = \frac{dx_F}{dt} = \Phi_D - \Phi_R. \tag{2.5}$$

In his review of fouling models, Hasson [7] noted that, when the rate of deposition is controlled by mass transfer, the deposition and removal terms are frequently expressed as

$$\Phi_D = \frac{\dot{m}_T}{A\rho_F}, \tag{2.6}$$

$$\Phi_R = \frac{x_F \tau}{A'}, \tag{2.7}$$

The combination of these equations allows fouling rates to be predicted if the value of A', the sticking coefficient, the rate of mass transfer (m_T) and the shear stress (τ) are known. Values for A' are usually obtained by fitting the Kern equation to experimental data. While the Seaton equation is useful as a correlating equation, it contains no information about the underlying phenomena responsible for fouling.

When the rate of fouling depends upon the temperature at the interface between the solution and the scale deposited, the decrease in the heat transfer coefficient with time is often described in terms of one of two limiting cases. In the first of these, the overall thermal driving force remains constant, and deposition of scale causes the temperature at the scale-liquid interface and the heat flux to decrease with time. In this case, the relationship between the fouling resistance ($1/U$) and time is

$$\frac{1}{U^2} = at + b. \tag{2.8}$$

In the other case, the thermal driving force is increased with time as fouling proceeds, to maintain a constant heat flux. In this case, the temperature at the scale-liquid interface remains constant with time, and the relationship between the fouling resistance ($1/U$) and time is

$$\frac{1}{U} = a't + b', \tag{2.9}$$

Berry tried to use Equation 2.8 to fit operating data obtained from an industrial black liquor evaporator [10]. He recognized the futility of this approach because most black liquor evaporators were operated at essentially constant heat flux. As fouling

occurred, the steam pressure was increased to maintain a constant evaporation rate, effectively maintaining a constant heat flux. Equation 2.9 would have been a more appropriate model.

One important problem with previous work in crystallization fouling of heat-transfer surfaces is that the fouling phenomena are never described in terms of the underlying crystallization phenomena.

2.4. Solubility of Inorganic Salts in Aqueous and Black Liquor Solutions

Grace was the first to recognize that the solubility behavior of Na_2CO_3 and Na_2SO_4 in black liquor was a critical part of why fouling occurred in black liquor evaporators. His starting point was the solubility data for Na_2CO_3 and Na_2SO_4 in aqueous solutions reported by Green and Frattali [11]. Figure 2.2 shows their three-component diagram for Na_2CO_3-Na_2SO_4-H_2O in equilibrium at 100°C. They reported the crystal and solution compositions in seven distinct regions of the diagram at 100°C. The different crystals that appear in one or more of these regions are anhydrous sodium carbonate, sodium carbonate monohydrate, burkeite, and anhydrous sodium sulfate. In Figure 2.2, the solid solution refers burkeite.

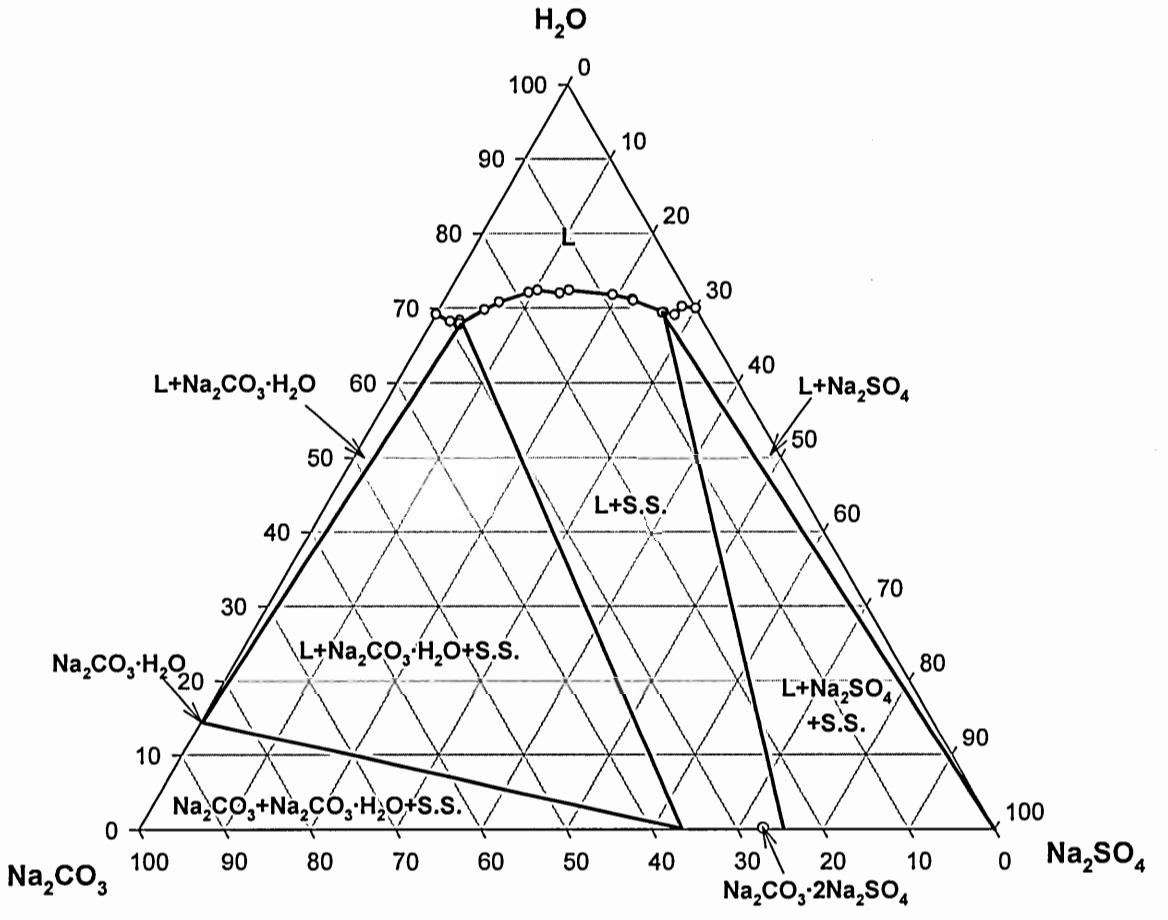

Figure 2.2: Solubility data for the Na_2CO_3-Na_2SO_4-H_2O system from Green & Fratteli [11]. (Figure from Shi [12], L - liquid; S.S. - solid solution)

Grace recognized that Green and Frattali's data, along with similar data compiled by Seidell and Linke [13], might describe the solubility of Na_2CO_3 and Na_2SO_4 in black liquor. However, the impact of other inorganic sodium salts (Na_2S, Na_2SO_3) and the sodium salts of organic compounds were not known. Grace conducted a number of equilibrium experiments with a variety of black liquors over a range of compositions [14, 15]. From the work of Green and Frattali and his collected data, Grace developed the first correlation for predicting the total solids content of black liquor at which the solubility limit for Na_2CO_3 and Na_2SO_4 mixtures was reached. The correlation was based on the assumption that all of the sodium compounds in black liquor other than Na_2SO_4

and Na_2CO_3 had an impact equivalent to that of NaOH on the solubility of Na_2SO_4 and Na_2CO_3. Grace reported his correlation to be accurate to within 5-10%. His graphical correlation made possible, for the first time, prediction of where crystallization of sodium carbonate and sodium sulfate salts would occur. Besides providing a useful predictive tool for mills struggling to understand their fouling problems, Grace's solubility work also provided the first, and only, extensive data source for the solubility of Na_2SO_4 and Na_2CO_3 in black liquor. Because of this, subsequent models have been both developed from and compared to the Grace data. To this day it stands as a landmark in research on fouling of black liquor evaporators, and continues to be used and reanalyzed extensively.

Sinquefield [16] developed a chemical equilibrium simulator for calculating the composition of aqueous solutions of inorganic chemicals at specified total composition and temperature. The advanced chemical equilibrium predictor created, NAELS (Non-Ideal Aqueous Electrolyte Systems), includes a subroutine for estimating the activity coefficients of ions that is based on the Pitzer formalism [17] and a robust equation solver.

The free energy data and ion interaction parameters in the databases of software such as NAELS are values that have been obtained from experimental measurements with solutions of single salts and of binary salt mixtures. In principle, the software can predict the solubility of individual salts in solutions that contain many compounds. In practice, the predictions are sometimes quite good (e.g. [18]) and sometimes not. Harvie and co-workers [19, 20] found that the agreement between the predicted and measured solubility of inorganic salts in the system sodium-potassium-magnesium-calcium-chlorine-sulfate-water could be improved greatly by adjusting very slightly one of the

free energy values. It has become normal practice to improve the agreement between predicted and measured solubility in multicomponents by adjusting one or more of the free energy and activity coefficient parameters.

Recognizing the utility of Sinquefield's NAELS model, Weyerhaeuser Company developed the NAELS software further. Golike et al. [21] fit Grace's black liquor solubility data to estimate the Pitzer ion interaction parameters of the sodium salt of an organic anion that would represent all of the sodium phenolates and carboxylates among the dissolved organic matter in black liquor. In effect, the properties of this species accounted for all of the influences not explained by the inorganic anions already modeled (CO_3^{-2}, SO_4^{-2}, OH^-, $SH^-$and Cl^-). After this new species was included in the NAELS database, the NAELS software predicted the combined solubility of Na_2SO_4 and Na_2CO_3 in black liquor in Grace's experiments within ±10% of the measured values.

Golike et al. also identified a transition in the sodium salt species crystallized that they termed the "second critical solids point." This transition was a shift from burkeite to sodium carbonate as the solid species that was crystallizing. The ratio of Na_2CO_3:Na_2SO_4 in solution increases as burkeite crystallizes from black liquor. This occurs because the sulfate is depleted from solution more rapidly than the carbonate.

Recently, Verrill et al. [22] measured the solubility of Na_2CO_3 and Na_2SO_4 in black liquor at total solids content as high as 70%. Theirs was the first to be reported at total solids content substantially higher than Grace's. They compared their solubility data with predictions from the NAELS software, and showed that even though the NAELS software does not necessarily predict the correct solid species after the transition from burkeite, the concentrations of the dissolved sodium salts predicted were within the

range of their experimental accuracy. Their experimental work was conducted with two black liquors. To either validate the NAELS software or to re-evaluate some of the thermodynamic parameters in its database would require many more experiments with a larger number of liquors.

Permission was obtained from Weyerhaeuser Company, one of the industrial supporters of this thesis research, to use their proprietary version of the NAELS software. All solubility data in this thesis have been estimated using the NAELS software. However, due to limitations imposed by the confidentiality agreement, only the results of the calculations are presented.

2.5. Fouling of Black Liquor Evaporators

Observations prior to the solubility work conducted by Grace into the fouling of black liquor evaporators were limited to mills experiencing problems with fouling. For example, Berry identified fouling as a crystallization problem [10]. He identified seven different forms of scale, but not burkeite[3], one of the sodium salt species most likely to crystallize initially from many black liquors. The omission of burkeite is most likely due to his confusing sodium sulfate scaling with burkeite scaling. This may have been due to a lack of familiarity with the solubility behavior and solubility limit of sodium carbonate and sodium sulfate.

Arhippainen and Jungerstam [23] presented a discussion of operating experiences, including scaling concerns, for black liquor at total solids contents from 60-65%. Their paper focused on the opportunities to reduce evaporator fouling by employing forced-circulation heat exchangers. The authors recognized the importance of burkeite, and also

[3] Burkeite is a naturally occurring double salt with a nominal molar ratio of $2Na_2SO_4 \cdot Na_2CO_3$.

commented that "the scaling properties of the liquor should be closely related to the stability of the colloidal particles in the liquor." [23, p. 1097] It is not clear if they were referring to nucleating crystals that may agglomerate and adhere to the heat transfer surface or to something else.

After Grace conducted his solubility research, his next step was to study the actual fouling phenomena. He first conducted an extensive survey of evaporator fouling in the pulp and paper industry to define the problem more completely and also to determine the operating variables that might be significant with regard to fouling [24]. He concluded that calcium carbonate scales[4] and soluble scales[5] were the most common in the mills investigated. At the time of Grace's report, calcium scales caused more severe problems than did soluble scales. Grace was surprised that no correlation existed between the severity of scaling and the solubility limit of the sodium salts in black liquor. In crystallization terms it is not the solubility limit, but the supersaturation that determines whether scaling will be severe or not. Thus, this observation should not be surprising.

Despite an obvious interest in calcium carbonate scales, Grace and Andrews conducted research into soluble-scale fouling [25, 26]. They note that soluble-scale fouling was dependant on the supersaturation and metastable limit, and it occurred when black liquor was concentrated above a limit that he termed the "critical solids content." Today, the use of this term creates some confusion. The critical solids content, as defined by Grace, represents the total solids content of black liquor at the solubility limit of Na_2CO_3 and Na_2SO_4, the concentration where crystals might first nucleate. However, in

[4] Calcium carbonate scales are nominally defined as those scales that contain calcium as the primary cation and are not easily dissolved by hot water.

[5] Soluble scales are nominally defined as scales composed of sodium carbonate and sodium sulfate and are easily dissolved by hot water.

the industry, the term "critical solids content" is often used when describing the point at which crystallization of Na_2CO_3 and Na_2SO_4 began as black liquor was concentrated. Grace and Andrews concluded that local conditions at the hot surface were not a significant factor leading to scaling. From a crystallization perspective this is difficult to believe given that the salts crystallizing exhibit inverse solubility[6] and thus the supersaturation would be greater at the heated surface. They also noted that the amount of scale could increase very rapidly once fouling began. Taken together, these two observations might indicate that high supersaturation, beyond that generated by the wall temperature alone for an inverse solubility solution, existed at the time of scale initiation.

Although the formation of calcium scale is outside the scope of this research, one observation by Westervelt et al. [27, 28] should be mentioned. They concluded that it was the presence of Ca-organic complexes in black liquor and the influence of increased liquor temperature on their stability that caused calcium carbonate scaling. Nearly all of the dissolved calcium in black liquor is coordinated, or bound, by organic ions in solution. As the liquor temperature is increased, the hydrogen ion concentration decreases. This shifts the distribution of phenolate groups in the ligands that bind calcium ions from O^--R-O^- toward O^--R-OH. This causes some of the calcium-organic complexes to dissociate, releasing calcium ions that crystallize with the abundant carbonate ions in solution. Since higher temperature favors dissociation of these complexes and release of calcium ion, this process occurs most rapidly at the heat transfer surface, and the $CaCO_3$ crystallizes on that surface. The findings of Westervelt et al. are important to the issue of the impact of free calcium ions on crystallization of burkeite and dicarbonate. This is discussed further in portions of Chapters 5, 6 and 7.

[6] The solubility limit for a salt displaying inverse solubility will increase as the temperature decreases.

Many scaling problems in kraft pulp mills were addressed by some portion of Grace's work. Publications after his work have focused on two application areas: (a) improving operability of existing equipment, and (b) design of new equipment. Some of the articles on improving evaporator operation simply reformulated Grace's data into a form that was more accessible to mill personnel [29, 30]. The problem with this is that much of Grace's work was conducted near the solubility limit. As total solids content for liquor being fired in recovery boilers continued to rise, the total solids content in product black liquors in many mills reached and then exceeded the transition region identified by Golike et al. [21], and applying the same methods as at lower total solids contents to solutions didn't necessarily work. This was also true for others looking to apply the lessons learned from Grace's work to solve fouling problems in newer evaporators that concentrated black liquor to higher total solids content [31, 32, 33, 34].

Branch [35, 36] and Novak [9, 37] measured fouling rates using the methodology outlined in section 2.3 to develop deposition and removal rate models dependent upon Reynolds numbers, heat fluxes and temperature differences. Novak even used a pseudo-supersaturation term dependant on bulk and surface temperatures. However, both neglected to see that the changing x_F they were estimating was really the growth rate of crystals on the heat-transfer surface. Their works were among the most significant fundamental studies into the fouling of heat-transfer surfaces while evaporating black liquor since Grace's. Unfortunately, not addressing their observations on the most fundamental level (crystallization) was a missed opportunity.

Even after all of the previous work reviewed here, fouling continues to be a major problem in many pulp mills. As the total solids content of black liquors being fired in

recovery boilers increased, so did operational difficulties in evaporation. Schmidl and Frederick [38] found that evaporator fouling had gotten worse, not better, in the 25 years since Grace's initial survey [24]. Insoluble scale fouling problems had been reduced, presumably due to lessons learned from Grace's work on calcium carbonate fouling. However, a greater number of pulp mills now had problems with soluble-scale fouling.

2.6. Crystallization Background

Before delving into the most recent work that has provided a starting point for this thesis, the fundamentals of crystallization are reviewed and their relationship to fouling of heat transfer surfaces are considered. A more detailed review of this topic is available from Rousseau [39].

Supersaturation is one of the most important variables in determining crystallization kinetics. Relative supersaturation, σ, (often referred to simply as supersaturation) is derived from the chemical potential for a single species,

$$\Delta\mu_i = \mu_i - \mu_i^* = RT \ln \frac{a_i}{a_i^*}, \tag{2.10}$$

where R is the gas constant. Equation 2.10 can be restricted to ideal solutions (activity coefficients ≈ 1) or to those in which ($\gamma_i \approx \gamma_i^*$). Recalling that $\gamma_i C_i = a_i$, and defining $S_i \equiv C_i/C_i^*$,

$$\frac{\Delta\mu_i}{RT} \approx \ln S_i . \tag{2.11}$$

If the supersaturation is further restricted to a range $S_i < 1.1$ [39], then $\ln S_i \approx S_i - 1 = \sigma_i$; that is,

$$\frac{\Delta\mu_i}{RT} \approx S_i - 1 = \sigma_i . \tag{2.12}$$

Nucleation mechanisms can be divided into primary (homogeneous and heterogeneous) and secondary categories. An expression for primary nucleation kinetics can be developed from classical nucleation theory:

$$J_0 = A\exp\left(-\frac{16\pi\varepsilon_{Surf}{}^3\upsilon^2}{3k^3T^3[\ln(\sigma+1)]^2}\right), \tag{2.13}$$

Equation 2.13 can be modified empirically for use with chemically complex solutions such as black liquor, such that,

$$J_0 = k_N\sigma_{max}{}^i . \tag{2.14}$$

Mullin [40], another excellent source for in-depth background in crystallization, notes that i in Equation 2.14, referred to as the nucleation order, is a fitted parameter and has no physical significance.

Mullin [40] also provides the theoretical derivation for the size of a critical nucleus, which is the smallest crystal that is stable in the prevailing solution:

$$r_c = \frac{-2\varepsilon_{Surf}}{\Delta G_v}, \tag{2.15}$$

where γ is the interfacial surface tension and ΔG_v is the free energy change of the transformation from dissolved solute to crystal per unit volume. Essentially, this value indicates when a group of ions or molecules has reached a size that will continue to grow rather than redissolve. Trace impurities can have a significant influence on the interfacial surface tension, making the size of a critical nucleus difficult to compute for a solution of aqueous sodium carbonate and sodium sulfate. It would be extremely difficult to determine for a complex solution with numerous impurities such as black liquor.

Estimates by Shi [12] indicate that the critical nucleus size is smaller than can be measured *in situ* by the experimental techniques available.

The growth kinetics for a crystal can be related to supersaturation using an empirical power-law function:

$$G = k_G \sigma^g . \tag{2.16}$$

Mullin notes that for many systems, $g = 1$ [40].

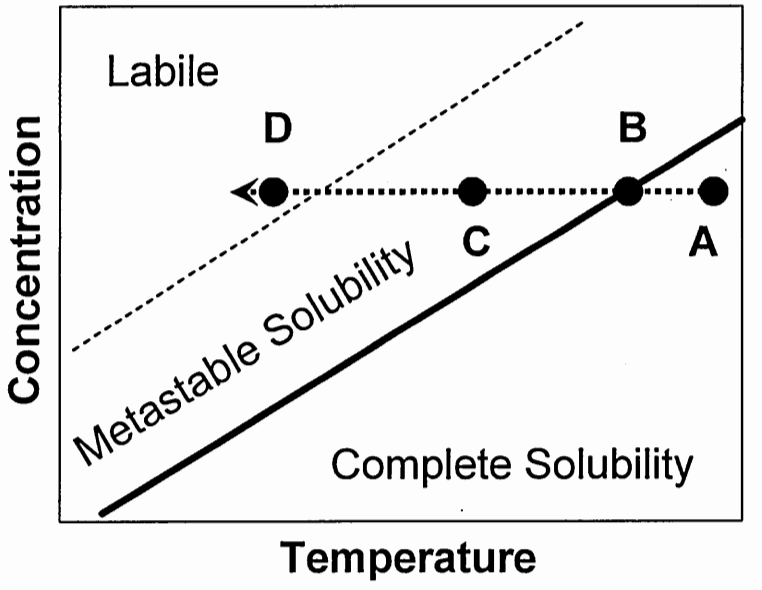

Figure 2.3: Solubility diagram illustrating the soluble region, the metastable region and the labile region (adapted from Mullin [40])

Solubility diagrams can be divided into three regions as illustrated in Figure 2.3: the soluble region, the metastable region and the labile region. Mullin provides a useful discussion of the metastable region [40], which is an ill-defined region of solution compositions where nucleation occurs only through secondary mechanisms. In the labile region, nucleation occurs by primary mechanisms, and no crystallization occurs in the soluble region.

The horizontal dashed line in Figure 2.3 indicates graphically what will occur during a cooling process, assuming that solubility increases with temperature. At the highest temperature, point A, the solute is completely soluble. No amount of time or agitation will induce crystal nucleation or growth. Cooling moves the operating point to B, the solubility limit (shown as a solid curve) where thermodynamic equilibrium exists for the given temperature and concentration. Cooling beyond point B moves the solution into the metastable region where crystal growth can occur on existing crystals, and primary nucleation is possible but might not occur in a finite time period. Continued cooling will move the operating point past the metastable limit into the labile region where primary nucleation occurs. The metastable limit is process- and solution-dependant.

Both Rousseau [39] and Mullin [40] provide additional information on the general crystallization phenomena that are critical to understanding and approaching fouling of heat-transfer surfaces as a crystal nucleation and growth problem.

2.7. Crystallization and Fouling of a Heat-Transfer Surface

The concept of fouling of heat-transfer surfaces by Na_2CO_3 and Na_2SO_4 being a crystallization process has not been missed completely in previous work. Reducing fouling of heat-transfer surfaces through manipulation of crystallization behavior can be accomplished by reducing the supersaturation in black liquor during evaporation. The only way to reduce supersaturation while concentrating the solution by evaporation is through nucleation and growth of crystals. Both of these phenomena can occur either in

the bulk solution or on the heat-transfer surface as postulated in Figure 2.4. This figure is developed from a similar diagram for crystallization in bulk solutions [40].

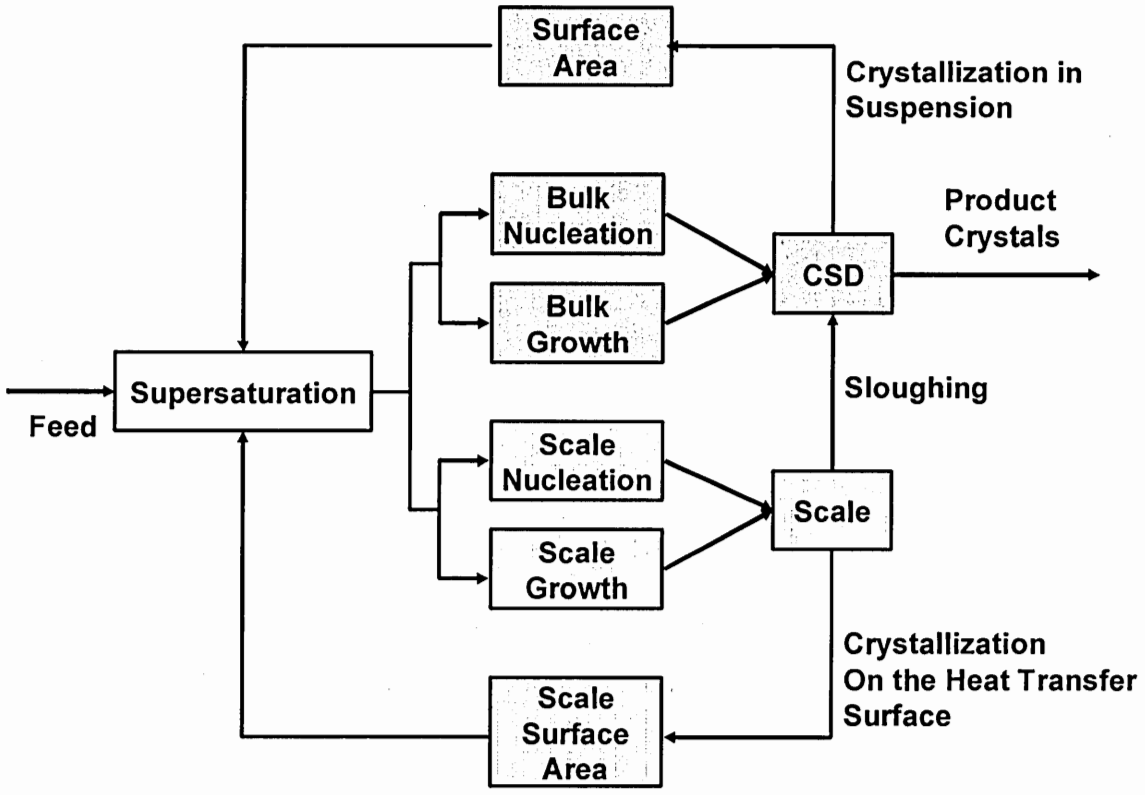

Figure 2.4: Diagram of crystallization phenomena that occur in suspension and on surfaces, as scale.

While crystals are removed from the system as product, scale is not removed unless it sloughs off from the heat-transfer surface and becomes a part of the crystal population (shown as the Crystal Size Distribution, CSD). In an evaporative process, if the supersaturation is raised above the metastable limit, the result will be primary nucleation. If supersaturation remains below that limit, any existing crystals will grow. The key to addressing fouling as a crystallization problem is then to control where and how that growth occurs, and to avoid primary nucleation.

With this understanding of supersaturation and its relationship to fouling, it is important to understand from a crystallization perspective what happens during the

fouling process. Hasson discussed two mechanisms for the initiation of surface scale for inorganic salts with inverse solubility behavior [7]. The first is direct nucleation. This process is similar to primary nucleation of crystals on the heat-transfer surface. In the second mechanism existing crystals adhere to the heat-transfer surface. Adhesion could occur when particles in the flow stream move into contact with the plate (where the no-slip condition indicates the flow velocity is 0). Growth of the crystal into the microscopic roughness of the heat transfer surface will hold the crystal in place. This adhered crystal becomes a surface nucleus and growth can occur in any direction from this crystal.

Hasson presents a model for the initiation rate of surface scale of the form,

$$J_0 = n^0 / \theta_D, \tag{2.16}$$

where n^0 is the number of surface nucleation sites per unit heat-transfer surface area and θ_D is the induction time [7]. Hasson substituted Equation 2.16 into a form of Equation 2.13, to obtain an estimation of n^0 given θ_D, which is valid, but may not be appropriate for heterogeneous nucleation on a heat-transfer surface where classical nucleation theory may not apply.

Hedrick and Kent [41] attempted to model crystallization during black-liquor evaporation by using a combination of material balances and empirical equations to describe nucleation and growth kinetics. They recognized that supersaturation occurs through two different mechanisms. They refer to the first mechanism as residual carry-over. Essentially, this is supersaturation caused by evaporation either in a previous effect or in the current effect that has not been reduced through crystal nucleation or growth via one of the mechanisms in Figure 2.4. Hendrick and Kent refer to the second mechanism as developed supersaturation. More accurately, it is the supersaturation due to the inverse

solubility of the crystallizing species and the elevated temperature at the heat-transfer surface. The actual supersaturation at the heat-transfer surface is the combination of the residual supersaturation and the developed supersaturation. The validity of this model at higher solids contents, when burkeite may not be the only salt species crystallizing, has not been determined.

It is only recently that experimental measurements of crystal nucleation and growth kinetics on exogenous surfaces have been published. This work has been limited to calcium scales, often referred to as hard-water scales.

Linnikov [42-44] used optical techniques to measure calcium sulfate nucleation and growth kinetics on a heat-transfer surface. His most important conclusion was that calcium sulfate scale formed through direct nucleation on the surface. This conclusion was based on his measurements of nucleation time, which he defined to be the time it takes for a crystal having a radius of 0 to nucleate on the surface. This value was obtained by linearly extrapolating measured diameters of crystals versus time back to 0. Negative nucleation times would be an indication that pre-existing particles are adhering to the surface. Because negative nucleation times accounted for less than 10% of his data, Linnikov stated that his determination of the initiation mechanism was justified [42]. One final observation from Linnikov's work is what he terms "crystal splitting." From his discussion it is apparent that what he is referring to is actually additional direct nucleation on an already growing crystal surface. This may actually have been dendritic growth [40]. Linnikov observed this phenomenon particularly at higher temperatures (higher supersaturations). This indicates an inability of the existing crystal surface area

in conjunction with the growth rate to reduce the supersaturation below the metastable limit.

Work of a similar nature, but conducted outside of a crystallization framework was undertaken by Kim et al. [45, 46]. They also used an optical method, this time to observe $CaCO_3$ crystallization induced by heated surfaces. The material published provides tantalizing potential for the development of a model for fouling of heat-transfer surfaces based solely on nucleation, growth and physical property data. However, such a model was not presented and could not be developed from the presented data. While this is unfortunate, it also highlights the disconnection between work conducted by heat-transfer researchers and crystallization researchers, and the need for multidisciplinary efforts in this area. This work does provide a useful discussion of the experimental apparatus used to microscopically observe a heat-transfer surface during initiation of fouling on the surface.

2.8. Crystal Species

The recognition of a transition in crystallization from one burkeite to another species as black liquor is concentrated led to significant speculation in the industry. Mill awareness of, and subsequently developed operational strategies to avoid operating in the region where the nucleation of a new salt species might occur alleviated fouling problems at some mills. No one had conducted any research to confirm the identity of the species crystallizing in this transition region. NAELS is limited to the salt species in its database. An experimental study of the crystals formed during the evaporative concentration of

black liquor was required to determine if NAELS contained all the salt species that might crystallize during the concentration of black liquor.

Such a study had been previously undertaken. In his Ph.D. dissertation, Novak [9] proposed that a number of different double salts could crystallize as black liquor is concentrated. He interpreted the XRD spectra of scale deposits from black liquor to show that burkeite was not the only double salt formed during evaporation. However, his scale samples were not pure enough to yield XRD spectra that defined clearly the different double salts. In the subsequent paper based on his thesis research [37], Novak backed away from his assertion of multiple double salts. This was unfortunate as it may have delayed for two decades the recognition of the importance of a double salt other than burkeite in fouling of black liquor evaporators.

Shi [12] conducted a fundamental study of the salts crystallized from black liquor and aqueous model solutions of black liquor. He determined that a second double salt composed of approximately two moles of Na_2CO_3 per mole of Na_2SO_4 crystallized from solution when the molar ratio of dissolved carbonate to dissolved sulfate in black liquor reached a value of about 7 to 1. After separating and cleaning these crystals, Shi used powder x-ray diffraction to determine that the crystal structure of this new "dicarbonate" salt crystal was different from either burkeite or any of the hydrated or anhydrous forms of pure sodium carbonate. It is likely that this is the same crystalline species that Novak observed but backed away from identifying.

Shi [12] also determined that calcium ions act as nucleation inhibitors for crystallization of burkeite from aqueous model solutions. His experiments indicated that substitution of sodium ions in the lattice structure is the mechanism by which this

happens. As calcium is a significant contaminant in most industrial black liquors, understanding this role it plays may be crucial in addressing black liquor fouling.

2.9. Summary

This review presented the significant steps taken in achieving the current understanding of issues in fouling of heat-transfer surfaces in black liquor evaporators. In summary, while considerable work has been conducted into fouling of heat transfer surfaces in black liquor evaporators, there is remaining work to be accomplished. Two key areas stand out from the literature reviewed here. The first area is in the modeling of heat-transfer fouling as a crystallization process. As this literature review indicates, there are models available for the dependence of fouling on growth and for the dependence of growth on supersaturation. One apparently novel development of the research presented in this thesis is combining the two models. Second, a better qualitative and quantitative understanding of the initiation mechanisms for surface fouling are required as little work has been accomplished in this area.

2.10. Variables

A Heat-transfer surface area, m^2

A' Adherence parameter, Equation 2.7

a Fouling rate fitting parameter, $m^4K^2W^{-2}s^{-1}$, Equation 2.8

a' Fouling rate fitting parameter, $m^2K{\cdot}W^{-1}s^{-1}$, Equation 2.9

a Chemical activity

b Fouling rate fitting parameter, $m^4K^2W^{-2}$, Equation 2.8

b' Fouling rate fitting parameter, $m^2K \cdot W^{-1}$, Equation 2.9

C Concentration, $mol \cdot m^{-3}$

ΔG_v Free energy change for the transformation from dissolved solute to crystal per unit volume, $J \cdot m^{-3}$

G Growth rate, $m \cdot s^{-1}$

J_O Nucleation rate, $m^{-3}s^{-1}$ (Volume) or $m^{-2}s^{-1}$ (Surface)

k Boltzmann constant, 1.380658E-23 $J \cdot molecule^{-1}K^{-1}$

k_F Effective thermal conductivity of fouling deposit, $W \cdot m^{-1}K^{-1}$

k_G Growth rate parameter, $m \cdot s^{-1}$

k_N Nucleation rate parameter, $m^{-3}s^{-1}$

$\dot{m}_T$ Mass transfer rate, $kg \cdot s^{-1}$

n^O Surface nucleation site count, m^{-2}

q Heat transfer rate, W

r_c Critical radius, m

R Thermal Resistance – subscript indicates what the resistance is measured through, $m^2K \cdot W^{-1}$

R Gas Constant, 8.31451 $J \cdot mol^{-1}K^{-1}$ (Equation 2.10 only)

S Supersaturation

T Temperature, K

t Time, s

U Overall heat transfer coefficient, $W \cdot m^{-2}K^{-1}$

v Crystal molar volume, m^3mol^{-1}

x Thickness, m

ε_{Surf} Interfacial surface energy, $J \cdot m^{-2}$

γ Activity coefficient

μ Chemical potential, $J \cdot mol^{-1}$

σ Relative Supersaturation

θ_D Induction time, s

Φ_D Fouling deposition rate, $m \cdot s^{-1}$

Φ_R Fouling removal rate, $m \cdot s^{-1}$

ρ Density, $kg \cdot m^{-2}$

τ Shear rate, s^{-1}

Superscripts and Subscripts

0 Clean plate conditions

i Chemical species

F Fouling

g Growth rate order, typically equals 1

L Liquor

i Nucleation order

S Steam condensate

W Wall, stainless steel heat transfer surface

$*$ Chemical equilibrium

2.11. Bibliography

1. Green, R.P., Hough, G, *Chemical Recovery in the Alkaline Pulping Processes Revised Edition*, TAPPI Press, Atlanta, 1992
2. Adams, T.N., Frederick, W.J., Grace, T.M., Hupa, M., Iisa, K., Jones, A.K., Tran, H., *Kraft Recovery Boilers*, TAPPI Press, Atlanta, 1997
3. Grace, T.M., *Pulp and Paper Manufacture Series Volume 5: Alkaline Pulping: Chapter 18, Overview of Kraft Recovery*, Edited by Kocurek, M.J., Grace, T.M., and Malcolm, E., Joint Textbook Committee of the Paper Industry, 1989
4. Grace, T.M., *Pulp and Paper Manufacture Series Volume 5: Alkaline Pulping: Chapter 19, Black Liquor Evaporation*, Edited by Kocurek, M.J., Grace, T.M., and Malcolm, E., Joint Textbook Committee of the Paper Industry, 1989
5. Somerscales, E.F.C., Knudsen, J.G., *Fouling of Heat Transfer Equipment*, Hemisphere Publishing Corporation, New York, 1981
6. Incropera, F.P., DeWitt, D.P., *Introduction to Heat Transfer, Third Edition*, John Wiley & Sons, 1996
7. Hasson, D., "Precipitation Fouling," *Fouling of Heat Transfer Equipment*, 527-568, Hemisphere Publishing Corporation, New York, 1981
8. Kern, D.Q., Seaton, R.E., "A theoretical analysis of thermal surface fouling," British Chemical Engineering, 4:5, pp. 258-262 (1959)
9. Novak, L., "Sodium Salt Scaling in Connection with Evaporation of Black Liquors and Pure Model Solutions," *Ph.D. Thesis*, Chalmers University of Technology, 1979
10. Berry, L.R., "Black Liquor Scaling in Multiple Effect Evaporators," *TAPPI Journal*, 49(4): 68A-71A (1966)

11. Green, S. and Frattali, F., "The System Sodium Carbonate-Sodium Sulfate-Sodium Hydroxide-Water at 100°C," *Journal of American Chemistry Society*, 68: 1789-1794 (1946)

12. Shi, B., "Crystallization of Solutes that Lead to Scale Formation in Black Liquor Evaporation," *Ph.D. Thesis*, Georgia Institute of Technology, 2002

13. Seidell, A. and W. Linke, *Solubility of Inorganic and Metal Organic Compounds*, Vol. II, 4th ed.: 1121, Van Nostrand, Princeton (1965)

14. Grace, T.M., *Solubility Limits in Black Liquor Project 3136*, Institute of Paper Chemistry (February 22, 1974)

15. Grace, T.M., "Solubility Limits in Black Liquors," *AIChE Symposium Series*, 72(157): 73-82 (1976)

16. Sinquefield, S.A, A Microcomputer Software Package for Simulation of Non-Ideal Aqueous Electrolyte Systems at Equilibrium, *M.S. Thesis*, Oregon State University, 1991

17. Pitzer, K.S., *Theory: Ion interaction Approach. Activity Coefficients in Electrolyte Solutions*, vol. 1 R.M. Pytkowicz, ed., CRC Press, 1979

18. Frederick, W.J., B. Kelly, H.C. Kim, M.J. McIntyre, and J.P. Danko, "Modeling Electrolyte Behavior in Pulp and Paper Processes," in *Chemical Engineering Technology in Forest Products Processing*, B. Crowell, editor, AIChE Forest Products Division, Tacoma, WA (1988), pp. 87-96.

19. Harvie, Charles E.; Weare, John H. The prediction of mineral solubilities in natural waters: the sodium-potassium-magnesium-calcium-chlorine-sulfate-water system

from zero to high concentration at 25° *Geochimica et Cosmochimica Acta* (1980), 44(7), 981-97.

20. Harvie, Charles E.; Eugster, Hans P.; Weare, John H. Mineral equilibriums in the six-component seawater system, sodium-potassium-magnesium-calcium-sulfate-chloride-water at 25°C. II: Compositions of the saturated solutions. *Geochimica et Cosmochimica Acta* (1982), 46(9), 1603-18.
21. Golike, G.P., Q. Pu, K.L. Holman, K.R. Carlson, P.C. Wollwage, H.G. Folster and S. Rankin, "NAELS: A New Method for Calculating Equilibrium Solubility of Burkeite and Sodium Carbonate in Black Liquor," *Proceedings of the 1998 International Chemical Recovery Conference. Part 1 (of 3)*: 403-418, TAPPI Press (Tampa, FL. Jun 1-4, 1998)
22. Verrill, C.L., Schmidl, W., Ball, A.R., Frederick Jr., W.J., DeMartini, N., Experimental Determination and Modeling of Sodium Salt Solubilities in High Solids Kraft Black Liquor – Accepted for Presentation at the *2003 TAPPI Fall Technical Conference*
23. Arhippainen, B. and Jungerstam, B., "Operating Experience of Black Liquor Evaporation to High Dry Solids Content," TAPPI Journal, 52(6): 1095-1099 (1969)
24. Grace, T.M., *A Survey of Evaporator Scaling in the Alkaline Pulp Industry Project 3234 Report 2*, Institute of Paper Chemistry (September 22, 1975)
25. Grace, T.M. and B.D. Andrews, *Study of Evaporator Scaling: Soluble Carbonate-Sulfate Scales Project 3234 Report 2*, Institute of Paper Chemistry (January 25, 1977)
26. Grace, T.M., "Evaporator Scaling," *Southern Pulp and Paper Manufacturer*, 42(8): 16-23 (1977)

27. Westervelt, H.H., W.J. Frederick, E.W. Malcolm, and D.B. Easty, "The Determination and Temperature Dependence of the Stability Constant of the Calcium - Catechol-4-Sulfonate Complex in Alkaline, Aqueous Media", *Analytica Chimica Acta*, 138, pp. 237-243. (1982)

28. Westervelt, H.H., W.J. Frederick, E.W. Malcolm, and D.B. Easty, "New Evidence Concerning the Role of Black Liquor Organics in Calcium Carbonate Scale Formation," *TAPPI*, 65(5):179-80 (1982).

29. Lamy, E.J., "Process changes reduce mill's concentrator fouling problems," *Pulp and Paper*, December: 92-95, 1979

30. Harrison, R., "New operating strategies for kraft evaporators can reduce scale," *Pulp and Paper*, March: 156-159, 1980

31. Rieke, J., Drone, K., Cox, D., Clark, C., "Willamette uses enhanced forced circulation to reach 80% solids," *Pulp and Paper*, 74(7): 37-41, (2000)

32. Osborne, D.M., "Evaporation to High Solids," *1993 Kraft Recovery Operations Short Course Notes*: 119-128, TAPPI (Orlando, Jan. 3-8, 1993)

33. Golike, G.P., Nakamura, N., "Global Evaporator: New Technology for Black Liquor Heating and High-Solids Evaporation," *1989 CPPA/TAPPI Int. Chem. Recovery Conf. Preprints*: 183-189, (Ottawa, April 3-6, 1989)

34. Makela, A., "TUBEL – a new black liquor concentrator technology for modern mill demands," *Proceedings of the 1998 International Chemical Recovery Conference. Part 1 (of 3)*: 393-401, TAPPI Press (Tampa, FL. Jun 1-4, 1998)

35. Branch, C.A., "Heat Transfer and Heat Transfer Fouling in Evaporators with Kraft Pulp Black Liquor," *Ph.D. Thesis*, University of Auckland, 1991

36. Branch, Craig A. and Hans M. Müller-Steinhagen, "Fouling during heat transfer to kraft liquor. Part 1: Experimental results," *Appita* 48:1 pp. 45-50 (1995)

37. Novak, L., "Sodium Salt Scaling in Connection with Evaporation of Black Liquors and Pure Model Solutions," *Swedish Paper Journal*, 8: 240-245 (1979)

38. Schmidl, Wolfgang and Frederick, Wm. James, "Current Trends in Evaporator Fouling," *Proceedings of the 1998 International Chemical Recovery Conference. Part 1 (of 3)*: 367-377, TAPPI Press (Tampa, FL. Jun 1-4, 1998)

39. Rousseau, R.W., "Crystallization Processes," *Encyclopedia of Physical Science and Technology, Third Edition, Volume 4*, Academic Press, 2002

40. Mullin, J.W., *Crystallization 3rd Edition*, Butterworth-Heinemann, 1997

41. Hedrick, R.H., Kent, J.S., "Crystallizing sodium salts from black liquor," *TAPPI Journal*, 75:12, 107-111 (1992)

42. Linnikov, Oleg D., "Investigation of the initial period of sulphate scale formation Part 1. Kinetics and mechanism of calcium sulphate surface nucleation at its crystallization on a heat-exchange surface," *Desalination*, 122:1-14 (1999)

43. Linnikov, Oleg D., "Investigation of the initial period of sulphate scale formation Part 2. Kinetics of calcium sulphate crystal growth at its crystallization on a heat-exchange surface," *Desalination*, 128:35-46 (2000)

44. Linnikov, Oleg D., "Investigation of the initial period of sulphate scale formation Part 2. Variations of calcium sulphate crystal growth rates at its crystallization on a heat-exchange surface," *Desalination*, 128:35-46 (2000)

45. Kim, W.T., Bai, C., Cho, Y.I., "A study of $CaCO_3$ fouling with a microscopic imaging technique," *International Journal of Heat and Mass Transfer*, 45:597-607 (2002)

46. Kim, W.T., Cho, Y.I., "Experimental Study of the Crystal Growth Behavior of $CaCO_3$ Fouling Using a Microscope," *Experimental Heat Transfer*, 13:153-161 (2002)

Chapter III: Experimental Apparatus

3.1. Introduction

The equipment used to examine the crystallization process as it occurs simultaneously in suspension and on the heat-transfer surface for black liquor and aqueous solutions of sodium carbonate and sodium sulfate is described in this chapter. Two pieces of equipment were used. The first was a pilot-scale falling-film evaporator with an FBRM (Focused Beam Reflectance Measurement) probe. This unit provided the capability to measure fouling of heat-transfer surfaces and bulk crystallization behavior under conditions similar to those in an industrial black liquor evaporator. The second was a unit designed to simulate a heat-transfer surface on which nucleation and growth rates and heat-transfer coefficients could be measured.

3.2. Pilot-Scale Falling Film Evaporator

A state of the art, pilot-scale dimple-plate, falling-film evaporator at the Institute of Paper Science and Technology was used for the evaporation experiments. The equipment, as configured for the experimental work presented in this thesis, is described here. Experimental details such as the composition of the solutions concentrated and the operating conditions are given in Chapters 5 and 6. Figure 3.1 presents a schematic of the pilot evaporator. Figure 3.2a and 3.2b show pictures of the vessel an example of the dimple-plate heat-transfer surface, respectively.

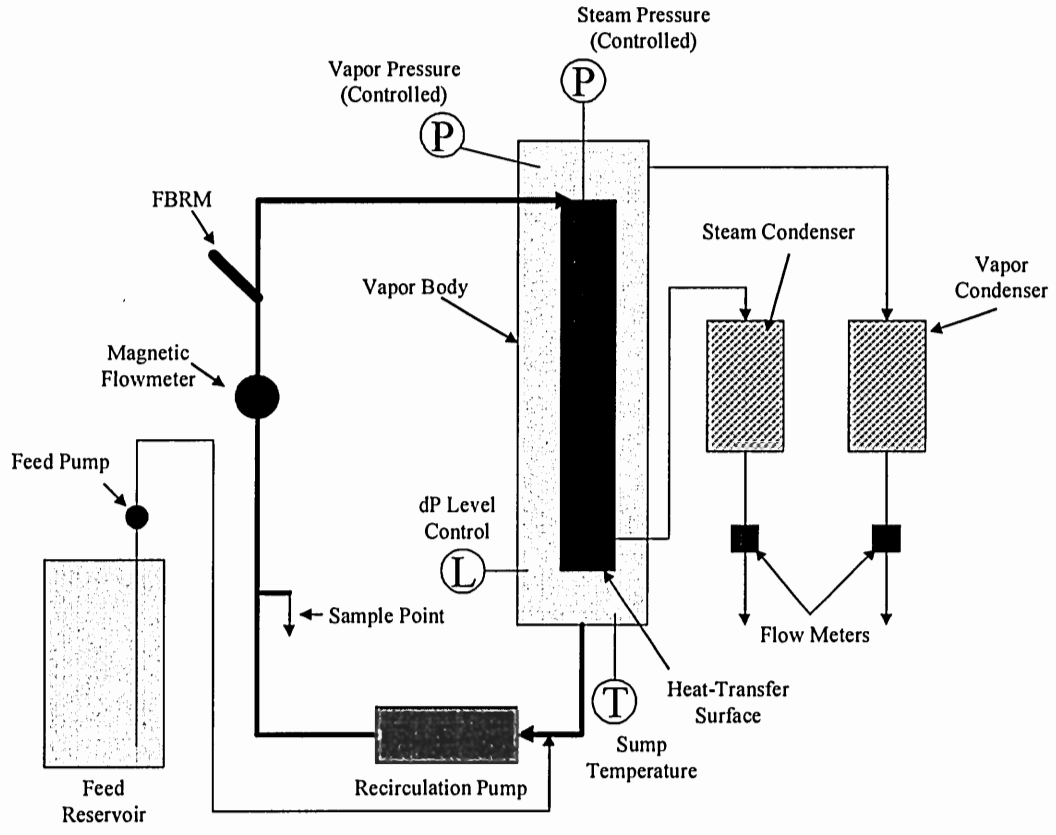

Figure 3.1: Schematic of the pilot-scale dimple-plate falling-film evaporator

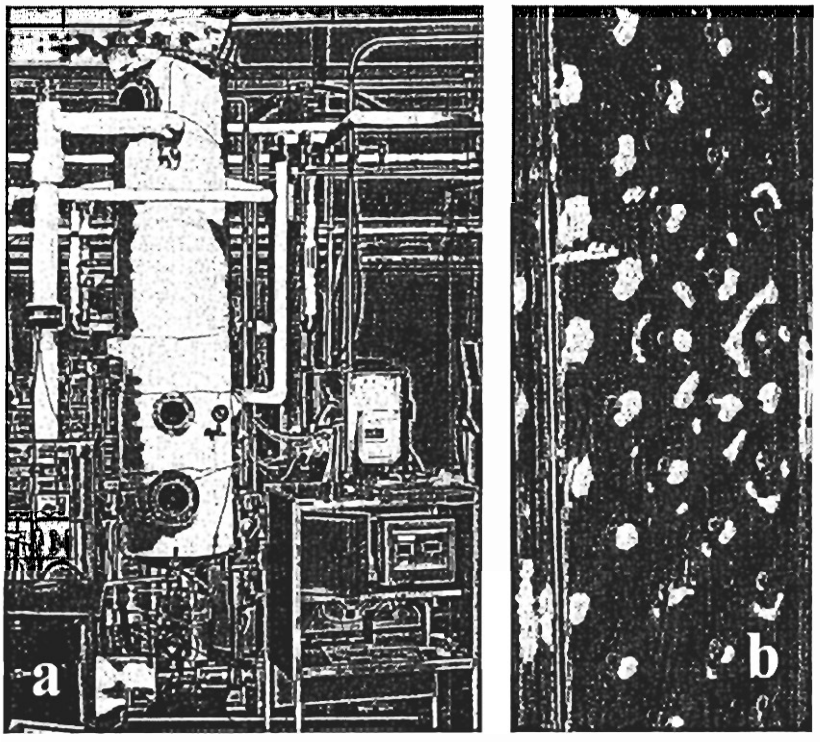

Figure 3.2: (a) Pilot evaporator vessel and (b) an example of a dimple-plate heat-transfer surface

3.2.1. Theory and Design

The evaporator was a pilot-scale, dimple-plate, falling-film unit obtained from Ahlstrom Recovery Incorporated (now Andritz Incorporated). The unit was originally equipped with 6 vertical, dimple-plate, heating elements, each 1.83 m (6.0 ft) by 0.30 m (1.0 ft). Five of them were removed to reduce the capacity of the unit and thus the amount of black liquor required when operating it. The liquor distribution system within the evaporator body was modified for operation with a single dimple plate panel, using the original Ahlstrom design. The flow rate of liquor to each side of the heat transfer panel was measured and the liquor distribution system adjusted until the flow rates were equal on both sides of the panel.

The ratio of sump volume to area of the heat-transfer surface is therefore an important design parameter for crystallizing evaporators. The ratio of the sump volume to the area of the heat-transfer surface for this evaporator as operated was approximately 0.10 m^3/m^2. For industrial black liquor evaporators, the ratio is often between 0.02 m^3/m^2 and 0.03 m^3/m^2.

3.2.2. Circulation Equipment and Issues

Circulation was accomplished with a Moyno pump designed for viscous, corrosive fluids such as black liquor. A Moyno pump operates more like a polymer extruder than a centrifugal pump. However, the stainless steel stator is analogous to the impeller and the Viton cavity is analogous to the pump body in a centrifugal pump.

The most significant difference between a centrifugal pump used industrially and the Moyno pump is the substantially smaller flow gap between the cavity and the stator.

Although Moyno pumps are designed for low shear rates, the smaller flow gap can potentially cause more crystal-crystal contacting and subsequent fracture of the crystals when a suspension of crystals is pumped. One indication of the likely occurrence of crystal contacting was excessive pitting in the Viton portion of the pump where crystals had apparently been forced into the Viton by the stainless steel stator.

The circulation pump had an upper pump speed of 1500 rpm, corresponding to 0.057 m^3/min (15 gpm). In each experiment, the pump speed was set to obtain the desired flow rate, which was actually measured with a magnetic flow meter and recorded by computer.

The Reynolds number (Re_Γ) was controlled by controlling the flow down the heat-transfer surface. The Reynolds number is defined as the mass flow rate divided by the wetted perimeter (twice the width) of the heat-transfer surface, and divided by the viscosity, as shown in Equation 3.1.

$$Re_\Gamma = \frac{4\left(\dot{m}_L / WP\right)}{\mu} \tag{3.1}$$

3.2.3. Measurement of Temperature, Pressure and Flow Rate of Condensates

The pilot unit was well instrumented for the measurement of temperature, pressure and flow rate of condensate. A computer-based data acquisition system recorded all temperature, pressure and condensate flow rate measurements for offline analysis.

The temperature of the black liquor was measured continuously at (a) the plate surface, with thermocouples oriented perpendicular to the heat transfer surface and

welded directly to it, (b) the evaporator sump, where bulk liquor temperature was measured with an RTD, and (c) the circulation line, also measured with an RTD. The thermocouples welded to the heat-transfer surface did not provide accurate measurements of the surface temperature; instead, the temperatures measured were identical to the bulk liquor temperature in the sump. For this reason, the temperature driving force used to estimate the heat transfer coefficients was the difference between the saturated steam temperature, evaluated at the steam pressure within the dimple-plate heat-transfer panel, and the liquor temperature measured in the sump. Thus all heat-transfer coefficients presented in this thesis are overall heat-transfer coefficients, U.

The pressures in the heat-transfer panel and vapor body were measured using pressure transducers. The saturated steam and vapor temperatures were calculated from a 5^{th}-order polynomial fit to saturated steam temperature versus pressure taken from the steam tables in Felder and Rousseau [1]. The boiling temperatures of the salt solutions and black liquor are the sum of the saturation temperature of steam at the pressure in the vapor body and the boiling point rise associated with the salt solution or black liquor. However, because the boiling point rise cannot be predicted accurately, the temperature of the bulk liquor temperature along the heat transfer surface was assumed to be the same as the liquor in the evaporator sump.

The pressures in both the heat-transfer panel and vapor body were controlled by self-tuning PID controllers. The set point for the steam pressure could be adjusted manually in an attempt to control the thermal driving force (ΔT).

Flow rates of condensate were measured to estimate the heat flux. Both the steam and vapor from the liquor were condensed using heat exchangers. Their flow rates were

measured continuously with turbine-type flow meters. The computer recorded a 4-20 mA signal from each flow meter and converted the signal into a flow rate based on a set of calibration data for each meter. For aqueous salt solutions, an energy balance around the evaporator closed well (-15% to 5%)[1] for the entire experiment. For black liquor, the energy balance closure was good prior to fouling (-5% - 20%). However, after fouling began, the closure dropped significantly (-100% - -20%). The main reason for this appeared to be the time lag between the thermal driving force and the evaporation rate when steam pressure was increased. The effect of this response time was particularly evident for changes in steam pressure or fouling. Thus, either condensate flow rate provided accurate heat transfer rates for aqueous salt solutions but for black liquor only the flow rate for steam condensate did so. For consistency, the steam condensate rate was used for all estimations of heat-transfer rate in this thesis.

3.2.4. Estimation of Fouling Rates

In order to analyze the experimental data collected from the pilot evaporator, several data reduction steps were used. A 10-point (1-minute) moving average of the data stream was used at each point to eliminate outlying data. In the pilot evaporator experiments, measured values of three process variables, steam pressure, sump temperature (T_{Sump}), and steam condensate mass flow rate ($\dot{m}_S$), were collected at intervals of 10 seconds. The saturated steam temperature, (T_S), was determined from the steam pressure using the polynomial regression equation mentioned previously.

Using these data, the rate of heat-transfer, $\dot{q}$, is equal to,

[1] The percent closure was determined from $(Q_S-Q_V)/Q_V$.

$$\dot{q} = \dot{m}_S \times \Delta H_V = UA\left(T_S - T_{\text{Sump}}\right), \tag{3.2}$$

where U is the overall heat-transfer coefficient which can be estimated from,

$$U = \frac{\dot{m}_S \times \Delta H_V}{A \times (T_S - T_{\text{Sump}})}, \tag{3.3}$$

where A, the evaporative surface area is the total plate surface area, 1.11 m^2 (12 ft^2).

The overall resistance ($1/U$) is composed of the resistances to heat-transfer through the steam condensate, the stainless steel plate, any surface deposit (fouling) and finally the resistance through the vaporizing liquor. Summing the resistances in series gives,

$$\frac{1}{U} = \frac{1}{h_S} + \frac{\Delta x_W}{k_W} + \frac{\Delta x_F}{k_F \frac{A_F}{A}} + \frac{1}{h_L}, \tag{3.4}$$

if the surface area through which the heat transfer occurs remains constant. The ratio A_F/A represents the ratio of heat-transfer surface area covered by fouling to the total surface area for heat-transfer. The dimple plate has been assumed to be flat in this research. If fouling occurs via a one-dimensional mechanism which nucleation occurs over the entire surface followed by growth away from the surface, then $A_F/A = 1$.

The first term on the right-hand side of Equation 3.4 is the resistance to heat transfer through the steam condensate to the heat-transfer surface, as represented by the reciprocal of the condensate-film heat transfer coefficient $1/h_S$. The heat-transfer resistance due to the condensate film is usually very small in comparison to the resistance due to fouling and the resistance through the liquor, and changes in it with condensation rate have a negligible impact on the overall resistance, $1/U$.

The second resistance is that of the heat-transfer surface, represented by the thickness of the wall divided by its thermal conductivity (k_W). This resistance is small, and the thermal conductivity of stainless steel changes very little with temperature. As a result, its time derivative can be assumed to be zero.

The third resistance occurs through any liquor-side scale that has been deposited. This resistance is expressed in a similar manner to that of the wall of the heat-transfer surface. However, it is not negligible, and can be the largest of the resistances. The thermal conductivity of the scale (k_F) may be one or more orders of magnitude less than that of stainless steel, so even small increases in thickness could produce significant increases in the thermal resistance. The thickness of scale can change with time, and the change is evidenced as an increase in $d(1/U)/dt$.

The final resistance occurs through the liquor film. In steady-state operation this term is normally assumed to be constant. In the semi-batch evaporation experiments with aqueous salt solutions presented in Chapter 5, the liquor-film resistance can also be assumed to be constant. However, for the semi-batch or batch evaporation of black liquor in Chapter 6 this is a bad assumption. The viscosity of black liquor increases substantially, often by 1 or 2 orders of magnitude, during the concentration process.

In the case of black liquor, a number of models or correlations for predicting convective and convective boiling heat transfer coefficients have been developed [e.g. 2, 3, 4, and 5]. In these models, the liquid-film heat transfer coefficient is proportional to the reciprocal of viscosity to a power that is usually between 0.3 and 0.4. A doubling of the viscosity would therefore reduce the liquid-film heat transfer coefficient by 20 to 25%.

When the process-side film Reynolds number is constant and the heat-transfer resistances on the steam condensate side are constant, the surface fouling rate (*SFR*), d(1/*U*)/dt, can be estimated from,

$$SFR = \frac{d\left(\frac{1}{U}\right)}{dt} = \frac{1}{k_F}\frac{d\Delta x_F}{dt} \tag{3.5}$$

In Equation 3.5, *SFR* has units of $m^2K \cdot W^{-1}s^{-1}$. The term $d\Delta x_F/dt$ on the right hand side of Equation 3.5 is essentially the one-dimensional growth rate of the scale on the heat-transfer surface, G_S.

All pilot scale runs were conducted in a semi-batch or batch mode. This means that either:

a. all of the liquor was added to the evaporator at the beginning of a run (batch mode), or
b. a batch of liquor was charged to the evaporator at the beginning of the run, and then liquor was added throughout the run to maintain a constant liquor volume within the evaporator as water was removed by evaporation (semi-batch mode).

Batch or semi-batch operation limited the volume of liquor required to conduct each experiment so that liquor recycling during the experiment was not required.

When concentrating black liquor in either of these modes, the total solids content of the liquor increased gradually with time. One result of this was concomitant increases in viscosity and density. For example, for an experiment where total solids content for the black liquor was raised from 50% to 70% solids, the liquor density was estimated to

increase by 9.4% and the viscosity by a factor of 23. The estimations were made using correlations found in Adams et al. [6].

Because of these changes in black liquor properties with time, the liquor film heat transfer coefficient, h_L, decreased with time. As a result, the rate of change of the overall heat-transfer coefficient depended on both the changes due to fouling and those due to the changing liquor film resistance term, $1/h_L$:

$$\frac{d\left(\frac{1}{U}\right)}{dt} = \frac{d\left(\frac{\Delta x_F}{k_F}\right)}{dt} + \frac{d\left(\frac{1}{h_L}\right)}{dt}. \tag{3.6}$$

It was necessary to account for the changes in the heat-transfer resistance through the liquor in order to estimate changes in the resistance due to fouling.

Convective and convective boiling heat transfer coefficients for liquid films are proportional to the film Reynolds number to a power less than 1, so that

$$h_L \sim \mathrm{Re}_\Gamma{}^{\alpha}. \tag{3.7}$$

In the black-liquor evaporation experiments, fouling occurred only after the liquor had been concentrated to a total solids content significantly higher than the initial value. Using Equation 3.1 and the previously mentioned influence of increased total solids concentrations on the liquor properties, Equation 3.7 can be reduced to,

$$h_{L,C} = C_o\left(\frac{1}{\mu}\right)^{\alpha}, \tag{3.8}$$

where C_O is a constant determined under non-fouling heat transfer conditions. Thus, for any given viscosity[2], a predicted clean-plate heat-transfer coefficient, $h_{L,C}$, can be estimated.

By combining Equations 3.4 and 3.6, an overall heat-transfer resistance when the heat-transfer surface is scale-free can be estimated for any given time, t,

$$\frac{1}{U_C(t)} = \frac{1}{h_S} + \frac{\Delta x_W}{k_W} + \frac{1}{C_o\left(\frac{1}{\mu(t)}\right)^{\alpha}}, \tag{3.10}$$

where the fouling term has been dropped since Δx_F is by definition 0 for a clean heat transfer surface.

This leaves only the determination of the value of α to obtain a useful predictive clean plate model for U_C. This value was found by assuming that for a given region where slow, but steady, reduction of the heat-transfer coefficient was observed, the observed reduction was due to the effect of increasing viscosity. After applying this assumption, a best-fit regression line for the data set $1/U$ - $1/U_C$ under clean-plate conditions (represented by the data in Figure 3.3 between 120 and 220 minutes) was determined. The parameter α was then adjusted so that the slope of the regression line was equal to zero for a variety of data sets using a given liquor sample. Over the wide range of operating conditions, the liquors used in this research consistently indicated that $\alpha = 0.3$.

[2] For the research in this thesis, the Adams et al. [6] correlation for viscosity was used to estimate black liquor viscosities.

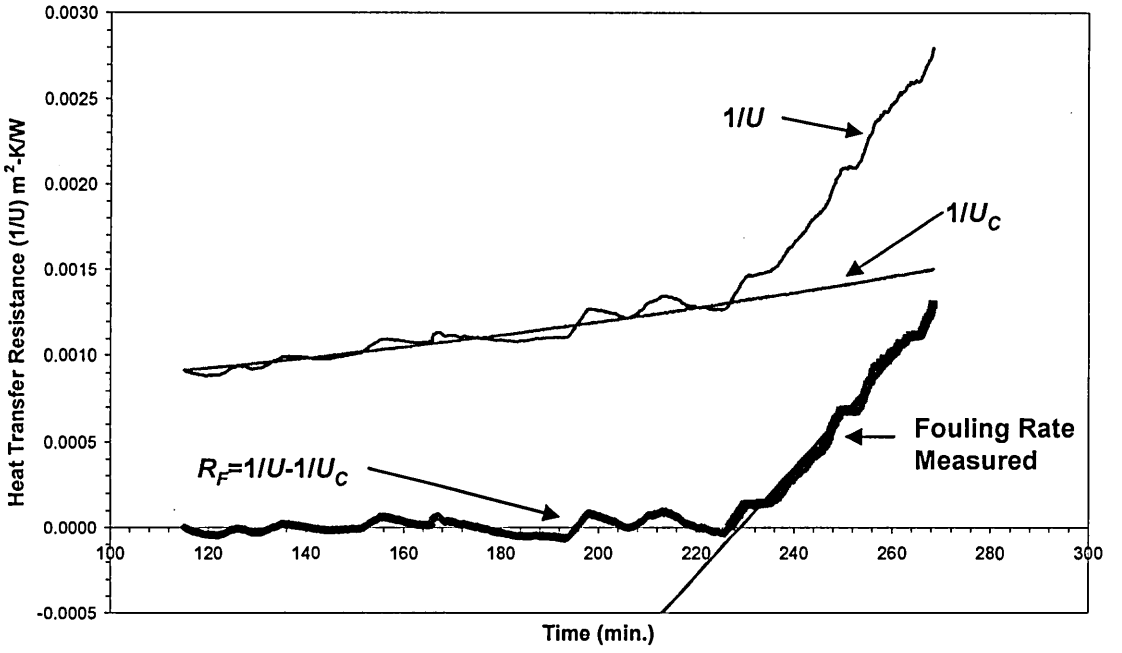

Figure 3.3: Heat-transfer resistance before and after removing the influence of changes in the liquor viscosity from the overall heat-transfer resistance to obtain the heat-transfer resistance due to fouling

Figure 3.3 shows the process graphically. The surface-fouling rate (*SFR*) was obtained by linear regression of the resistance due to fouling, R_F, versus time. The resistance due to fouling is equal to $1/U - 1/U_C$.

3.2.5. Measurement of the Crystal Population

Chapter 4 of this thesis presents an extensive discussion of the Focused Beam Reflectance Measurement equipment. In this section, only issues related to the location and settings on the instrument will be discussed.

The FBRM probe was inserted into the recirculation line downstream of inlet for feed during semi-batch experiments. The probe was inserted into the circulation line at a 45 degree angle on the recommendation of Lasentec, the manufacturer of the FBRM probe used. The feed rate of solution during semi-batch mode was not great enough to

cause dissolution of existing crystals in the circulation line. The circulation to feed ratio during the semi-batch experiments was between 50:1 and 200:1.

Calibration of the FBRM probe was conducted using a slurry of PVC particles provided as a standard with the equipment by Lasentec. At the completion of the research, the calibration had not changed.

The coarse/fine adjustment setting for the FBRM instrument allows the user limited input into its data-filtering algorithm. While the exact filtering algorithm is proprietary, fine filtering provides better recognition of small particle (nuclei) while coarse filtering allows for better recognition of larger particles. The filtering, in part, adjusts the amplitude required for a return signal to be recognized as a reflection from a particle.

3.3. Bench Scale Surface Crystallizer

A bench-scale surface crystallizer was designed and constructed for the purpose of microscopically observing the initiation and growth of crystals on the heat-transfer surface. The apparatus was designed to have flow characteristics similar to those in a falling-film evaporator, but the required system conditions made operation quite difficult. This section describes the final design of the flow cell and other components of the experimental apparatus. Issues that arose during the design and construction of the test cell are discussed in this section unless they are related to experimental results.

3.3.1. Materials of Construction

Because of the opaque nature of black liquor, a solution of aqueous sodium carbonate and sodium sulfate was used to represent black liquor for all bench-scale surface crystallization work. The combination of the high alkalinity of the solutions employed and high operating temperatures required a careful selection of materials of construction for the equipment.

For the bench scale experimental apparatus, nearly all wetted parts, aside from the test cell, were composed of 316-stainless steel or Teflon. A few flow measurement and control parts were composed of 304-stainless steel, as they were not available in 316-SS. Both grades of stainless steel are highly corrosion resistant for the environment under which the experiments were conducted.

The wetted parts in the test cell were: (a) 316-stainless steel for the heat transfer surface, (b) Teflon with Viton seals for the actual flow chamber, and (c) Borosilicate (Pyrex) glass for the viewing window. Of these three materials, borosilicate glass showed a tendency to etch at seal contact points during the experiment. However, it was less expensive to replace the borosilicate glass several times during the experimental work than to use a glass that was more corrosion resistant since there was no apparent effect on experimental results.

3.3.2. Flow Cell Design and Construction

Flow in the test cell was designed to approximate that in a falling-film evaporator. To accomplish this, the flow width (thickness) needed to be determined. For black liquor evaporators, this width depends on a number of physical and design parameters including mass flow rate, wetted perimeter, temperature and composition (the last two also

influence viscosity and density). After discussions with Andritz and initial estimations based on computational fluid dynamics from Frederick et al. [7], it was determined that flow thickness could vary between 2 and 10 mm with 3-5 mm being a representative range for most evaporators.

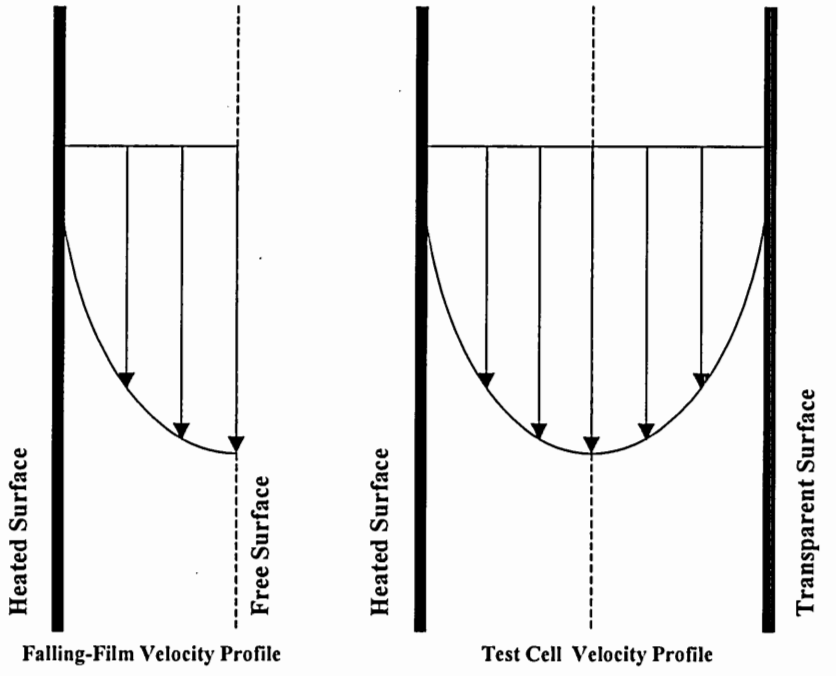

Figure 3.4: Falling-film velocity profile illustration for the test cell

The reasoned assumption was made that the surface flow profile for a falling-film evaporator could be modeled by laminar, one-dimensional flow with twice the flow width of the falling film. Figure 3.4 provides an illustration of this analogy. Essentially, if the duct gap width was twice the estimated falling-film flow width, assuming that Re_Γ was the same, the velocity profiles would be the same. The actual flow gap was created using 6.35 mm (0.25 in.) Teflon due to its availability in this specific thickness. Thus, the test cell reflected a falling-film flow width of approximately 3.2 mm.

The next step was to determine a typical Re_Γ for falling-film black liquor evaporators and derive the required flow rate for the salt solution experiments. Based on

estimations from several operating falling-film black liquor evaporators and standard proprietary designs, using Equation 3.1, the Reynolds number for black liquor flowing down the heat transfer surface was estimated to be approximately 150, indicating a laminar flow.

To estimate the required flow rates necessary, and to make sure that the Reynolds number remained in the laminar regime, the aqueous salt solutions were assumed to exhibit the same physical properties as water at the operating temperatures. Using these assumptions, the required circulation rate for the aqueous salt solution was determined to be 600 ml/min, producing a Re_Γ of 155 and a Re of 310 assuming that L>>d, where L is the width across the cell and d is the gap width.

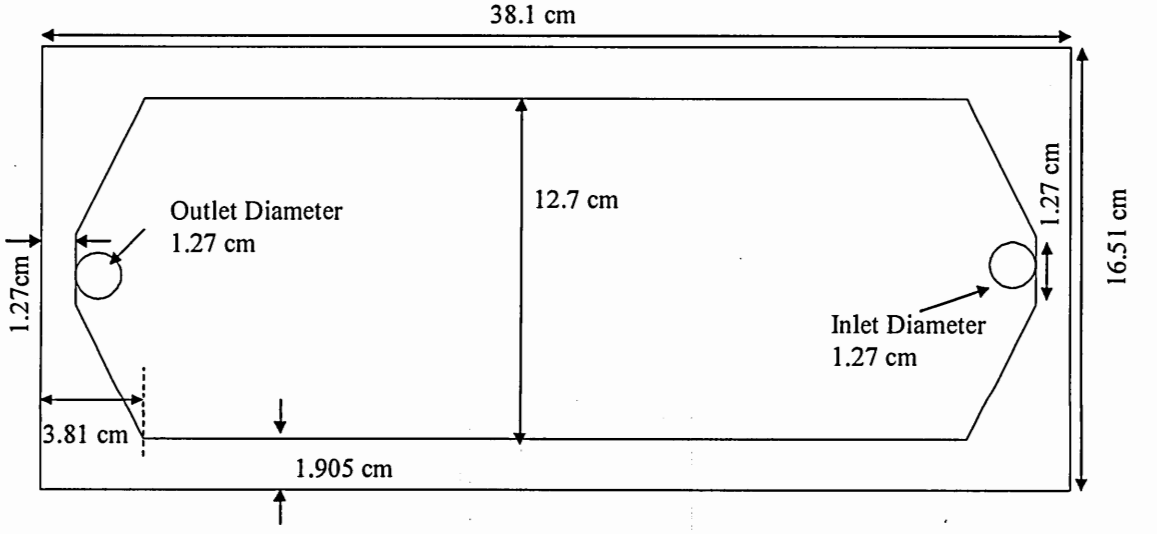

Figure 3.5: Dimensional sketch of the bench-scale surface crystallizer test cell with length and width indications. This part was custom machined from a 0.635 cm thick piece of Teflon

For flow in a duct, L>>d was assumed true for L/d = 20. Using this ratio, the width of the flow cell was set at 12.7 cm (5 in.). To avoid entry and exit length effects, the test cell length was set to 30.48 cm (12 in.). A 2.54 cm (1 in.) long, trapezoidal flow

distribution region was included at the entrance and the exit to the test cell. The completed test cell dimensions are illustrated in Figure 3.5.

The Teflon blank, machined to the exact specifications of the designed test cell, was also machined for two custom Viton seals. One of these seals was placed on each side of the Teflon, to provide a seal with the stainless steel and with the borosilicate glass.

The actual heat-transfer surface was composed of a stainless steal blank that was machined with a Fadal VMC 2016L milling machine. The surface was finished using a Valenite 539.62.650-facing mill with carbide grade TN450 Valenite SNMT 43531 inserts. At either end of the test cell, an NPT threaded hole was drilled to meet a hole that had been drilled perpendicular to it from the interior surface of the flow cell, as pictured in Figure 3.6. This figure also shows how sandwiching the machined Teflon flow region between the flat borosilicate glass surface and the heated stainless steel surface formed the test cell.

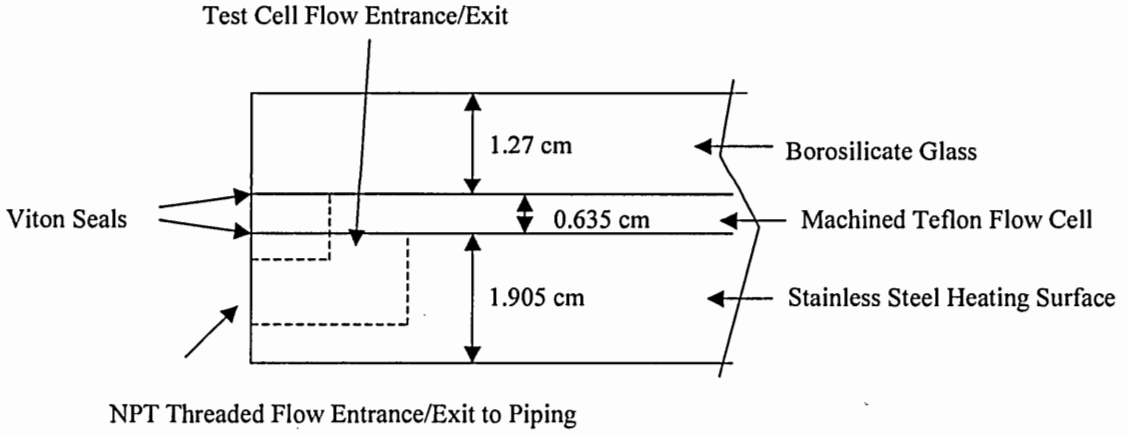

Figure 3.6: Schematic of the bench-scale test cell showing components and flow entry

The cell was heated using a 1.55 W/cm^2 silicon resistive-heating pad, adhered to the bottom side of the 1.905 cm thick stainless steel heating surface. With the cell in an experimental position, the 10.16 cm x 30.48 cm heating pad is positioned as shown in

Figure 3.7. The pad was placed in this position to resist overheating at the edges of the test cell flow region and to avoid high temperatures in the outlet region of the stainless steel. The energy input to the heating pad was controlled using a variable voltage transformer with a digital voltage display.

Due to viscosity reductions in the solution as the plate was heated, flow separation occurred from the glass surface. It was quickly determined that the test cell would not operate in a downflow configuration. For this reason, the test cell was operated in an up-flow configuration. While this changed the flow dynamics slightly due to the change in the flow direction relative to gravity, it was a better solution than operating in a horizontal flow configuration where gravity could cause settling on the heat-transfer surface.

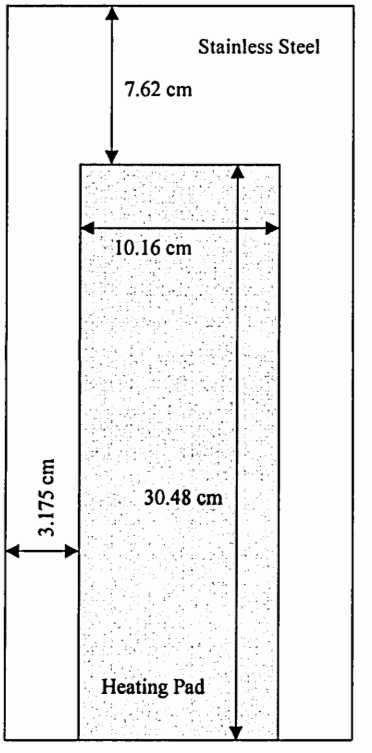

Figure 3.7: Placement of the resistive heating pad on the bottom of the stainless steel heating surface

Figure 3.8 shows a picture of the constructed flow cell. The cell itself was nested inside of a machined piece of Teflon that was bolted into a vertical position. Two stainless steel plates (the front one is pictured) acted as a compressing support frame for the flow cell. To reduce tension in the glass, a 1.27 cm thick polycarbonate frame with its center cut out was placed between the stainless steel and the borosilicate glass. Originally, polycarbonate was tried as the actual transparent surface material for the flow cell, but it was etched badly by the alkaline solutions at the operating temperatures. It proved useful in absorbing the slight tension that the stainless steel applied to the glass at operating temperatures due to thermal expansion. One new piece of glass was broken learning this valuable lesson.

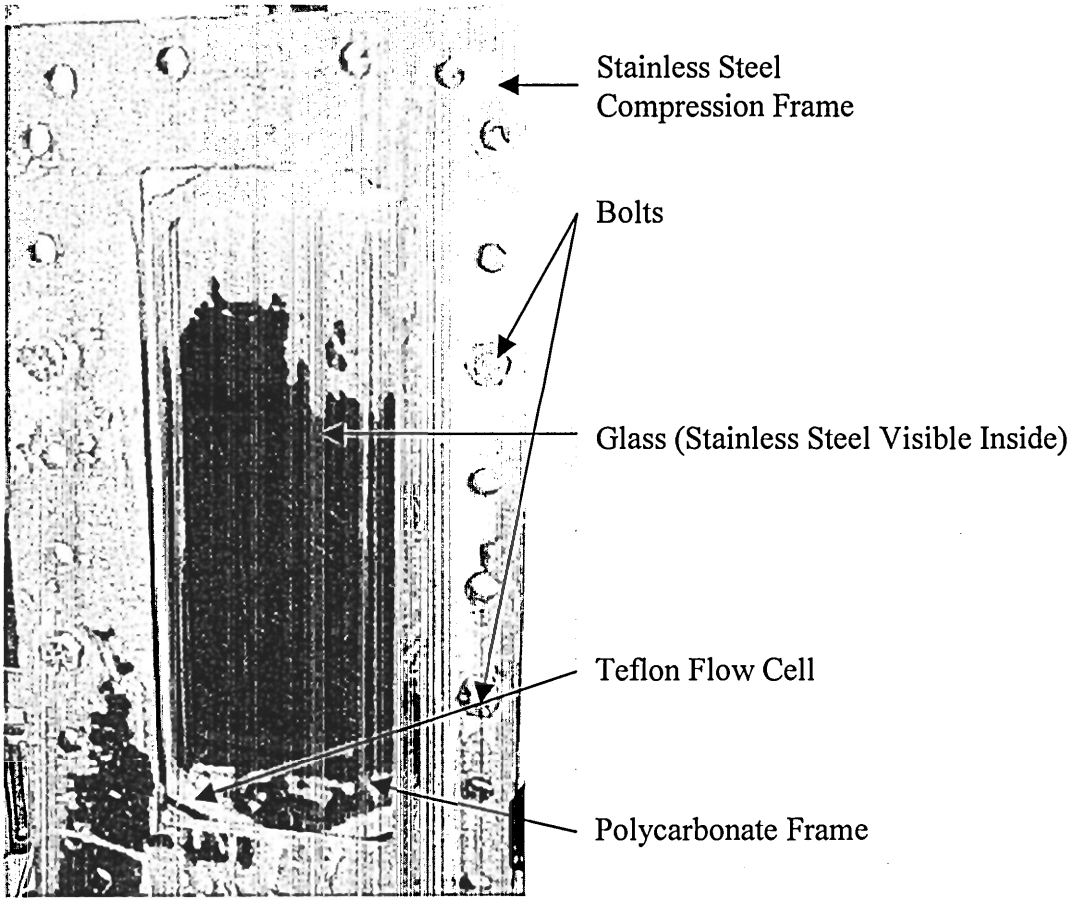

Figure 3.8: Front view of bench-scale surface crystallizer indicating individual parts which composed the test cell and support structure

3.3.3. Measurement, Control, and Supporting Equipment

In addition to the test cell, a number of additional pieces of equipment were necessary to store, control and measure the aqueous alkaline solution and any surface crystallization.

Circulation Tank

A circulation tank, fabricated from a piece of 45.72 cm long, 12" 316-SS Schedule 40 pipe with a welded 316-SS bottom and welded top flange, acted as combination feed reservoir, temperature-control vessel, and location for evaporation. Pictured in Figure 3.9, the feed tank was heated by a combination of two 1200 W and one 600 W silicon resistive-heating pads. A self-tuning PID controller was used to control the temperature of the solution in the reservoir by regulating the power input to the 600 W heating pad. A type-T thermocouple was inserted into the center of the tank to measure this temperature. A variable transformer was used to adjust the voltage input to one of the 1200 W heaters. The second 1200 W heater was only used to heat cold DI water more rapidly when preparing a solution for an experiment. The tank was well insulated except for the base. The base was on top of a large magnetic mixer. The magnetic mixer was used to turn a large Teflon stirring bar inside the tank.

The rate of evaporation from the tank was accomplished by a needle valve on the top of the tank. A pressure relief safety valve with a 30-psig rating was also located on the top of the vessel.

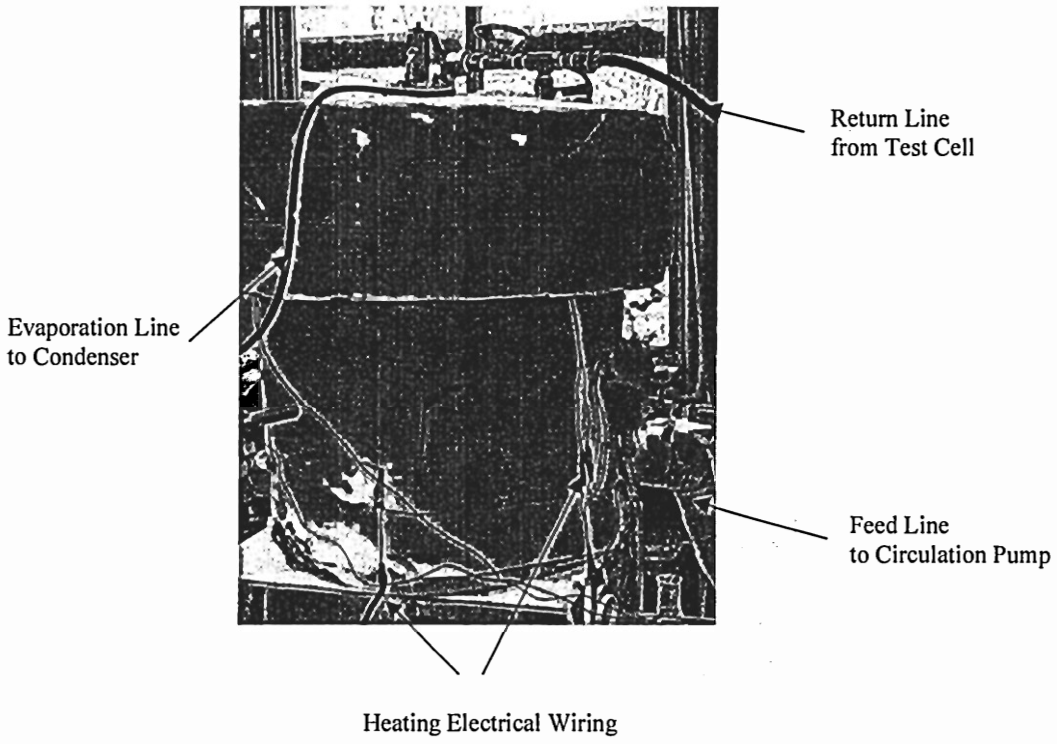

Figure 3.9: Bench-scale surface crystallizer feed tank

Solution Circulation

Pumping the experimental solution proved to be challenging due to the experimental conditions. The pump needed to: (a) not cause a net negative suction head, (b) be able to handle a low concentration of suspended particles in the solution, (c) not use mechanical seals, (d) not appreciably heat the solution, and (e) withstand the conditions of pH and temperature encountered with the sodium salt solutions . Also, the pump needed to pump between 500 and 1000 ml/min. There are few pumps that meet these requirements, and a significant number of pumps were tried in a variety of configurations before a satisfactory pump was identified.

A Micropump® miniature magnetically driven centrifugal pump was determined to meet the experimental requirements. Experimentally, the Micropump resolved each of the issues previously raised. First, once 1" feed lines from the tank into the 3/8" pump

inlet were installed, there was a net positive suction head at the inlet to the pump. This was very important as the solution is exiting the tank as a saturated solution (vapor/liquid) or even a supersaturated solution (solid/liquid). Any reduction in pressure due to suction could cause flashing and potentially crystal nucleation. Second, suspended particles were a possibility in these crystallization experiments, and while centrifugal pumps are not appropriate for handling slurries with high suspended particle concentrations, they can pump dilute suspensions. Third, mechanical seals were tried briefly, but they did not work due to the sealing mechanism. In a mechanical seal, the two surfaces are in close contact, but allow a very small amount of material to pass through the seal as a vapor. The heating of the solution between the contact points, as they rotate against each other, causes this vaporization. It is this vapor that actually seals the pump. In the experimental solutions, the dissolved salts crystallized across the seal and effectively destroyed the mechanical seal. The elevated pH and temperature requirements eliminated a number of standard laboratory-scale pumps. Finally, the combination of the flow rate and no appreciable heating disallowed the use of a larger industrial pump operated inefficiently.

Flow Measurement and Control

The flow was measured using an Omega model FTB9505 low flow turbine meter with a flow range of 65-1,400 ml/min. A flow-signal conditioner and digital indicator were also installed and calibrated using the manufacturer's nonlinear calibration curve. Measurements of water flow rates indicated that the manufacturer's calibration was accurate within ~6 ml/min. This was slightly higher than the manufacturer's guaranteed

accuracy but may represent pump variability from the centrifugal pump which varied ± 3-5 ml/min during the experiments.

Optical Microscopy

The stainless steel heat-transfer surface was viewed at high magnification through an Edmund Industrial Optics VZM-1000 lens with attached fiber optic light ring. The surface was imaged with a Roper Scientific CoolSNAP-Pro*cf* color digital microscopy camera. Image capture and analysis was performed using Image Pro Plus version 4.5 software. The imaging area viewed using this setup was approximately 2.7 mm by 2.0 mm.

Temperature Measurement

Thermocouples were inserted into the stainless steel heat transfer surface at six locations along the length of the plate. Figure 2.12 indicates the position for each of the 6 probes. Each probe was a Type T, 1/8" diameter probe. Probe positions 1 and 3-6, indicated by the black dots in Figure 3.10, were drilled 8.255 cm (3.25") deep, approximately the center of the plate. Position 2, the gray dot in Figure 3.10, was drilled 4.13 cm (1.625") into the stainless steel. The centers for thermocouple locations 1 and 3-6 were each positioned 5.08 cm (2") apart with 4 equidistant from each end of the plate. Thermocouple positions 1, 4 and 6 were centered in the plate, or 0.9525 cm from the heated surface. Positions 2, 3 and 5 were 1.43 cm from the heated surface.

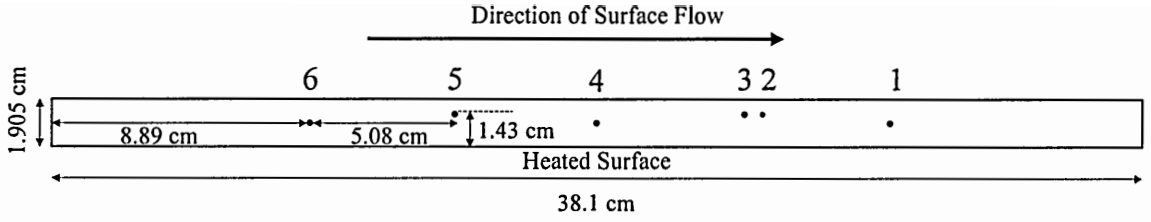

Figure 3.10: Schematic indicating the thermocouple positions in the stainless steel used as the heating surface in the test cell of the bench-scale surface crystallizer

3.3.4. Flow Diagram and Picture of the Physical Apparatus

Figure 3.11 shows a schematic of the bench-scale surface crystallizer, with the primary equipment and flow lines. Figure 3.12 is a photograph of the apparatus.

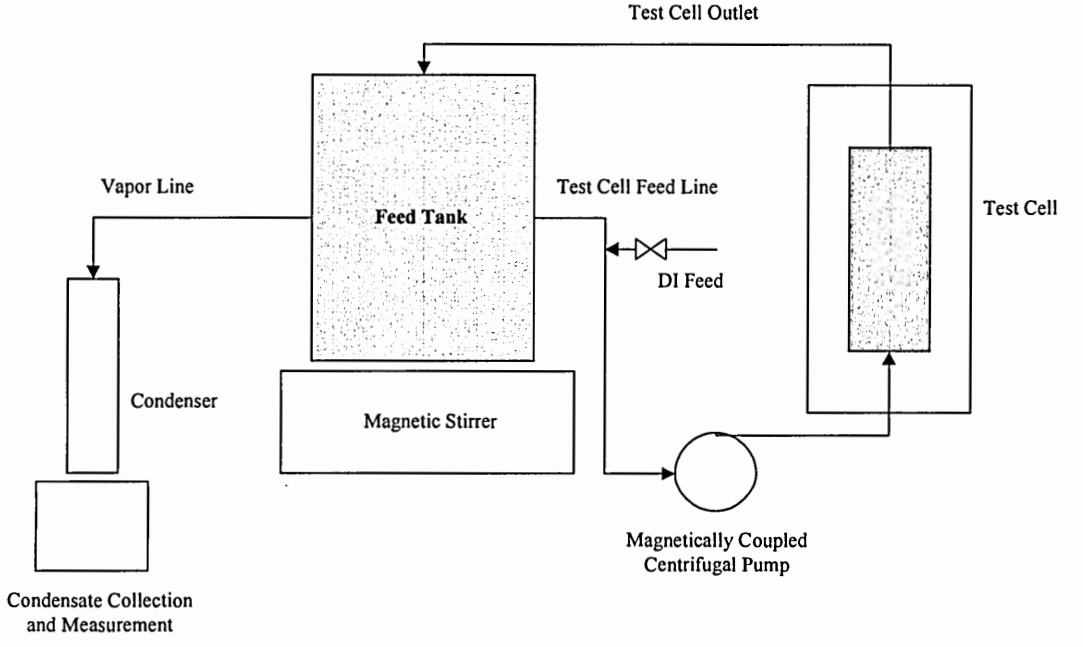

Figure 3.11: Operational flow schematic for the bench-scale surface crystallizer

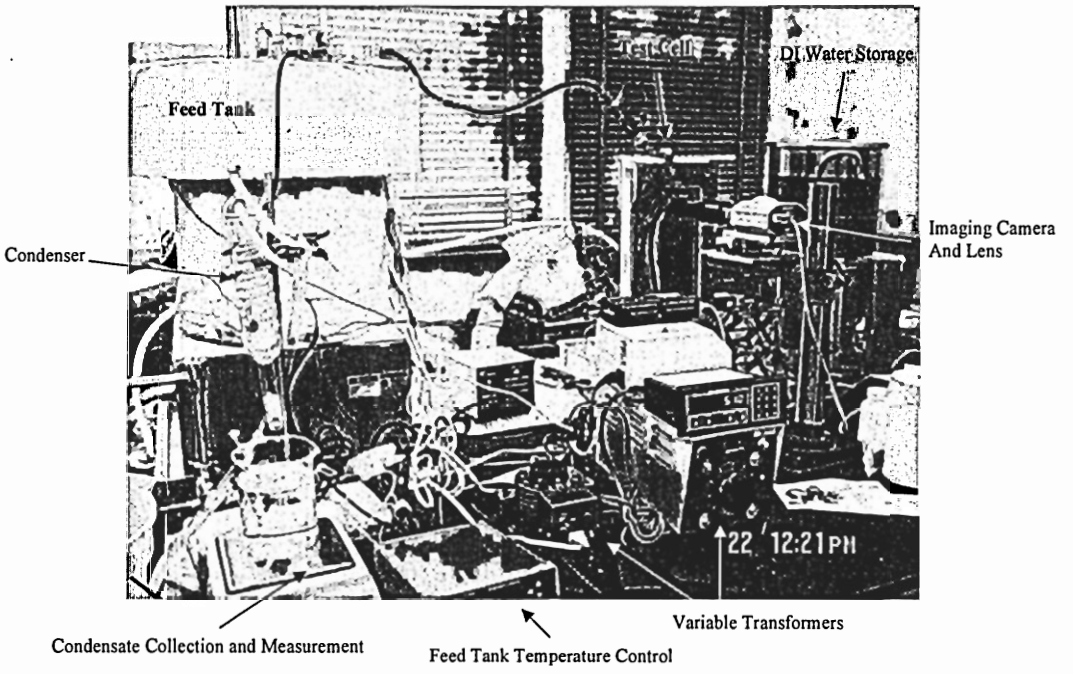

Figure 3.12: Apparatus composing the bench-scale surface crystallizer in the lab

3.4. Conclusions

For the experimental work in this thesis, two pieces of experimental equipment were utilized. A well-instrumented pilot-scale dimple-plate falling-film evaporator provided a source of fouling data. An FBRM device was added to this pilot unit, to allow quantitative measurement of bulk crystallization behavior[3]. While data from the pilot-scale evaporator provided an initial understanding of the phenomena of surface crystallization, these data were not sufficient to address the objectives of this research. To determine the initiation mechanism for surface fouling, a bench-scale surface crystallizer was constructed. While this apparatus required significant development, the equipment outlined in this chapter was suitable to study the initiation mechanism.

[3] Additional background and insight into FBRM measurements are located in Chapter 4 of this thesis.

3.5. Variables

A Heat transfer surface area, m^2

C_O Clean plate viscosity constant

G_S Growth rate of scale on the heat-transfer surface, $m \cdot s^{-1}$

h Heat transfer coefficient, $W \cdot m^{-2} K^{-1}$

ΔH_V Heat of vaporization, $J \cdot kg^{-1}$

k Thermal Conductivity, $W \cdot m^{-1} K^{-1}$

$\dot{m}$ Mass flow rate, $kg \cdot s^{-1}$

Q Heat, J

R Thermal resistance – subscript indicates what the resistance is measured through, $m^2 K \cdot W^{-1}$

Re Reynolds number

SFR Surface fouling rate, $m^2 K \cdot W^{-1} s^{-1}$

T Temperature, K

t Time, s

U Overall heat transfer coefficient, $W \cdot m^{-2} K^{-1}$

WP Wetted perimeter, m

Δx Thickness, m

α Fitting parameter

μ Viscosity, $kg \cdot m^{-1} s^{-1}$

Super and Subscripts

c Clean plate condition

$_F$ Fouling

$_L$ Liquor

$_S$ Steam or steam side condensate

$_V$ Vapor or vapor side condensate

$_W$ Wall, stainless steel heat transfer surface

* Chemical equilibrium

$_\Gamma$ Plate (Reynolds number)

3.6. Bibliography

1. Felder, R.M., Rousseau, R.W., *Elementary Principles of Chemical Processes, 3rd Edition*, John Wiley & Sons, New York, 2000
2. Harvin, Richard L. Thermal and physical properties and heat-transfer coefficients of sulfate paper mill black liquor. Ph.D. dissertation, Univ. of Florida (1955), 154 pp.
3. Lavery, H.P., Grace, T.M., Frederick, W.J., "Slug and Churn Flow Heat Transfer in the Long Tube Vertical Evaporator," *Svensk Papperstidning*, Research Section, pp.R72-80 (1983).
4. Stenuf, T.J., Liu, H.-S., "Heat Transfer to Black Liquor in a Falling-Film Evaporator," *ESPRI Research Reports*, 79:IX SUNY College of Environmental Science and Forestry (Syracuse) (NY) 80 October 15, 1983
5. Gao, S.-X., C.-B. Gu, Z.-L. Jiao, Y.-C. Li, D. Luo, L. Niu, D.-B. Shi and J.-S. Wang, "Falling-Film Flow on Vertical Plate and Evaporating Test Reseearch as well as Primary Test on the Concentration of Black Liquor from Wheat-Straw Pulp," *Int.*

Nonwood Fiber Pulping & Pmkg. Conf. (Beijing) Proc. Vol. 2: 865-876 (July 11-14, 1988)

6. Adams, T.N., Frederick, W.J., Grace, T.M., Hupa, M., Iisa, K., Jones, A.K., Tran, H., *Kraft Recovery Boilers*, TAPPI Press, Atlanta, 1997
7. Frederick Jr., W.J., Schmidl, G.W., Verrill, C.L., Rousseau, R.W., Shi, B., Euhus, D.D., Chen, F.C., Gao, Z., *Control of Soluble Scale Fouling in High-Solids Black Liquor Concentrators: Final Technical Report*, DOE Contract DE-FC36-99-GO10387,A003, April 28, 2003

Chapter IV – Methods for Estimating Bulk Nucleation and Growth Rates Using Moments of FBRM Chord Length Distributions

4.1. Objective

A method to obtain estimations of bulk nucleation rates from chord count densities measured with an FBRM will be presented in this chapter. *In situ* measurements of these rates provide an important analytical tool both for this research and for future crystallization work. In addition, a method for estimating growth rates of crystals from chord count densities measured with an FBRM will be presented in this chapter. These methods will be applied to FBRM experimental results in Chapters 5 and 6.

4.2. Introduction

There are few options for obtaining real-time, online measurements of crystal size distributions. This limitation has inhibited the implementation of schemes that would enable the control of crystal size so as to meet product or downstream-processing requirements [1]. A growing number of applications are being found for Focused Beam Reflectance Measurement (FBRM) technology in crystallization and particulate processes. FBRM is based on laser backscattering principles. It is reported to provide fast *in situ* particle dimension analysis at any concentration of solids without sampling, diluting or recirculating the stream being monitored. These features render FBRM appropriate for real-time process monitoring and control.

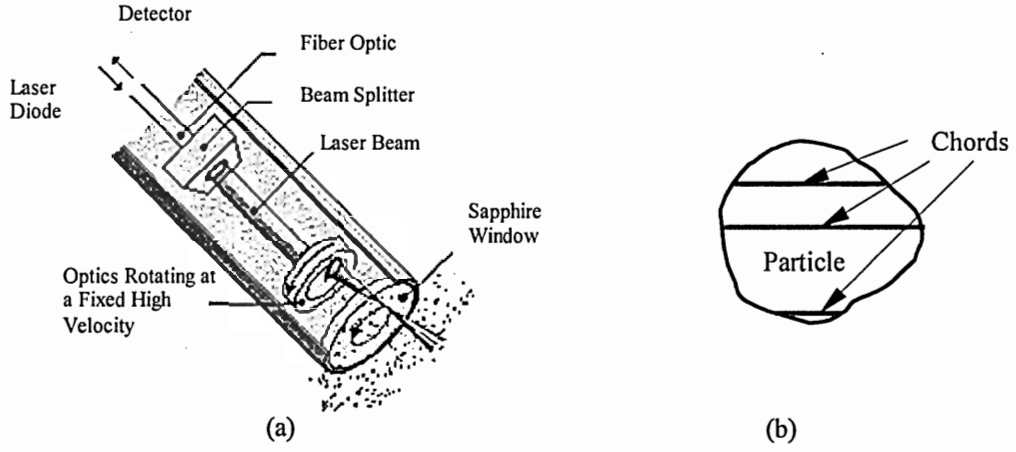

Figure 4.1: Schematic of the Lasentec® FBRM and an example of three possible chords measured from one particle

The FBRM probe (shown in Figure 4.1a) utilizes a focused laser beam rotating at a constant velocity. As the laser beam scans across a particle passing through the measurement zone, the time duration of detected reflectance from a particle is determined and related to the chord length. The chord length is calculated by multiplying the velocity of the scanning laser beam and the duration of reflection. The measured chord length is not necessarily equivalent to the characteristic particle length (for example the diameter of a spherical particle). A chord (illustrated in Figure 4.1b) is a line connecting two points on different edges of a 2D projection of a 3D particle. Typically, thousands of chord lengths per second are measured by an FBRM probe, with the counts of chord lengths stored in a maximum of 1000 channels. The Lasentec® FBRM probe (Lasentec Inc., USA) measures particles ranging from 0.5 to 1000 μm in chord length, and can be employed in the temperature range -20°C to 150°C. A more complete description of the FBRM probe can be found elsewhere [1, 2]. The application of FBRM technology has been shown to provide useful information regarding the size distribution of particulates in slurries, and it has been used in harsh environments [2, 3, 4, 5]. Additional applications are given in a number of references [6, 7, 8].

4.3. Chord Length and Particle Size Distributions

Current applications of FBRM are promising, but the instrument is limited by the nature of the data it generates. Namely, FBRM provides measurements of chord lengths sampled randomly from a particle population. As shown in Figure 4.1, the measured chord length can be anywhere on a crystal. Thus the chord length is bounded by $0 \leq l_i \leq d_i$, where l_i is the measured chord length of the i^{th} crystal and d_i is the largest particle dimension; e.g., should the particles being analyzed have a spherical geometry, d_i is the particle diameter.

For a given crystal population, the size distribution may be characterized by the population density function,

$$n(L) = \lim_{\Delta L \to 0} \frac{\Delta N(L)}{V_S \Delta L}, \tag{4.1}$$

where L is a characteristic dimension and $\Delta N(L)$ is the number of crystals with characteristic length between L and $L + \Delta L$ in a volume of slurry or liquid sampled, V_S. The relationship of the characteristic dimension to an actual dimension of the crystal depends on the technique by which the dimension is determined and on crystal shape. If the shape is spherical, for example, it may be appropriate to define $L = d$. Equation 4.1 also assumes that all crystal geometric properties can be defined in terms of L, which means that crystals of all sizes have the same shape.

In a fashion similar to the development of Equation 4.1, it is possible to define a chord-count density (CCD) function $c(l)$, as,

$$c(l) = \lim_{\Delta l \to 0} \frac{\Delta C(l)}{\overline{V}_S \Delta l}, \tag{4.2}$$

where $\Delta C(l)$ is the number of chord counts with lengths between l and $l + \Delta l$ in the volume of slurry or liquid sampled by the FBRM probe, $\overline{V}_S$.

Procedures for relating the population density function to nucleation and growth kinetics are well-developed for a perfectly mixed, steady-state crystallizer. Such relationships lend themselves to implementation of procedures to control crystal size distributions. Unfortunately, relationships between the chord-count density function and nucleation and growth kinetics do not exist, even though a number of researchers have attempted to relate crystal (or particle) size distributions to measured chord distribution functions [9, 10, 11, 12].

In the present work, a methodology has been developed to obtain nucleation and growth rates from FBRM data. The approach was to use moments of the chord-count density in a manner analogous to methods using moments of population density.

4.3.1. Moments of the Chord-Count Density Function

Moments of population density functions can have both physical significance and great utility in analyzing crystallizer performance. The j^{th} moment of the population density function, for example, is,

$$m_j = \int_0^\infty L^j n dL . \tag{4.3}$$

Randolph and Larson [13], among others, have shown that the following relationships apply:

$$m_0 = N_{\text{total}} \equiv \text{total number of particles per unit volume} \tag{4.4}$$

$$m_1 = L_{\text{total}} \equiv \text{total length of crystals per unit volume} \tag{4.5}$$

$$k_A m_2 = A_{\text{total}} \equiv \text{total surface area of particles per unit volume} \tag{4.6}$$

$$\rho_C k_V m_3 = M_{\text{total}} \equiv \text{total mass of particles per unit volume} \tag{4.7}$$

where kA and kV are area and volume shape factors defined for a specific crystal geometry such that, $k_A=A(L)/L$ and $k_V=V(L)/L$.

By analogy to Equation 4.3, moments of the CCD function can also be defined,

$$\overline{m}_j = \int_0^\infty l^j c dl \,. \tag{4.8}$$

However, since the chord length measured for a given crystal varies depending upon the portion of the crystal scanned, it is not possible to relate chord moments to properties of the crystal population, with one apparent exception. If chord-counting irregularities, which will be dealt with later, can be ignored, then the total number of crystals and the total number of chords should be identical. Therefore,

$$\overline{m}_0 = \int_0^\infty c dl \equiv \text{total number of particles per unit volume,} \tag{4.9}$$

and,

$$N_{total} = \int_0^\infty c dl = \int_0^\infty n dL \,. \tag{4.10}$$

Therefore, any application requiring an estimate of the total number of particles per unit volume can be performed by direct substitution of the 0^{th} moment of the CCD function as determined using the above procedures. For example, it is recognized that the nucleation rate, J_0, in a batch, perfectly mixed crystallizer, in which there is insignificant breakage and agglomeration, is given by the expression

$$J_0 = \frac{dN_{total}}{dt} = \frac{d\overline{m}_0}{dt} \,. \tag{4.11}$$

However, to obtain a meaningful nucleation rate from the chord-counts density function, an accurate estimate of the effective (sampled) control volume must be determined.

4.3.2. Control Volume Estimation

Definition of the control volume is arbitrary, but important. When defining a specific population density, as in Equation 4.1, the volume usually chosen is either that of the slurry or of the clear liquid. The slurry volume was chosen in the current work. Most often, the volume can be obtained by a simple direct measurement. However, it is much more difficult to get an estimate of the effective volume scanned by the laser in the FBRM apparatus.

An estimate of the scanned volume can be obtained by recognizing that the laser effectively penetrates the slurry sample by distance λ, has width b, and moves along its path at a velocity (scan speed) $\dot{v}_S$. Then, the volume scanned over any period of time Δt can be approximated by the equation,

$$\overline{V}_S = \dot{v}_S \lambda b \Delta t \,. \tag{4.12}$$

Substituting these results into Equation 4.2 gives,

$$c(l) = \lim_{\Delta l \to 0} \frac{\Delta C(l)}{\dot{v}_S \lambda b \Delta t \Delta l} \,. \tag{4.13}$$

The major uncertainty in this measurement is the value of λ, which is highly dependent on the solution and crystals. Specifically, the solution may absorb the laser light and the crystals may not reflect the laser light back to the probe so that it can be measured.

4.3.3. Growth Rate Measurements

Randolph and Larson [13] show that the mean growth rate can be calculated from moments of the population density function and the crystal growth rate, $G = dL/dt$, by the equation

$$\frac{dm_3}{dt} = \frac{1}{2} G m_2 . \tag{4.14}$$

It is not known whether this equation holds for moments of the chord-count density function, and there is no clear justification for assuming that it does, as was the case in using the 0^{th} moment to represent the total number of crystals counted.

Ratios of moments of the CCD function have been used to define growth rates using FBRM data [6]. The methodology used was to define some weighted-average mean chord length, $\bar{l}$, using specified moments of the population [9]. For example, if the 2^{nd} and 3^{rd} moments of the CCD function are used, then the growth rate, is defined as,

$$G = \frac{d\bar{l}}{2dt} = \frac{d\left(\overline{m}_3 / \overline{m}_2\right)}{2dt} . \tag{4.15}$$

This would be the growth rate estimated from the area-weighted mean chord length. This estimation of the growth rate is valid if the particles are of uniform shape and exhibit size-independent growth. Also, it is assumed that the chords counted are an accurate characterization of the entire slurry. The last assumption is important because if enough particles are sampled, even though the actual chord lengths sampled are not representative of the fundamental particle length, the change in the mean chord length should be indicative of the change in the fundamental length. However, this estimation of the growth rate is highly susceptible to chord-counting irregularities.

4.3.4. Irregularities in Determining the CCD

Irregularities in determining chord length and, subsequently, the CCD are best described as aberrations due to the back-scattering measurement. Two irregularities, (a) particle screening and (b) effects due to particle curvature are considered especially important and will be discussed more extensively here.

As previously mentioned, the measurement is dependant on the laser light reaching a particle, and then scattering back from the particle surface with enough intensity to be detected by the FBRM probe. Particle screening occurs when the laser penetrates far enough into the solution that overlapping crystals are observed as, represented in Figure 4.2. This generally will lead to shorter chord-length measurements, and significant undercounting of the longer chord lengths for the relative few large particles in the sampled volume. Screening can occur in any slurry with distribution of particle sizes. Screening is also more likely in systems with greater laser penetration depths, λ, as the likelihood of observing crystal overlap increases with λ. Thus, the relative importance of this aberration is dependant on the particle-solution system.

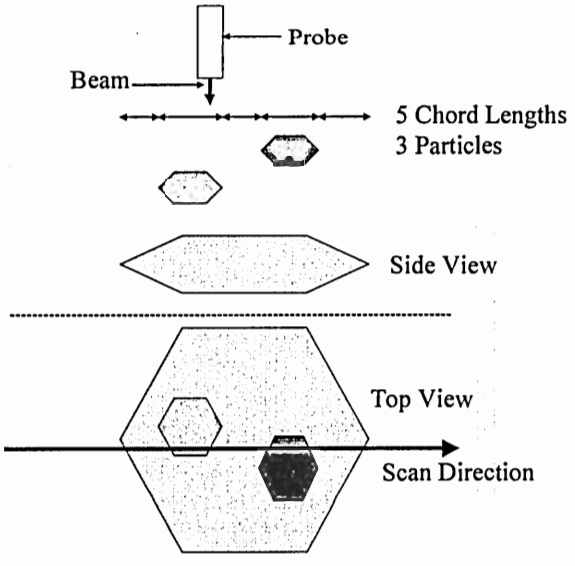

Figure 4.2: Example of Possible Measurement Irregularities Due to Screening

Because the FBRM filtering algorithm is proprietary and complex, it is impossible to determine exactly how many chords would be recognized in a situation such as that shown in Figure 4.2. However, a potential filtering algorithm is one in which both the length of time for a reflected intensity of the required magnitude and the derivative of the intensity are considered when identifying separate particles. While this filtering algorithm is speculative, it would lead to shorter chord lengths as well as significant undercounting of longer chord lengths from larger particles.

Increasing particle curvature decreases the reflectance to the FBRM probe from a particle surface. Rather than observing a sharp drop in intensity as the laser passes off a crystal edge, a gradual decay in backscattering intensity might be expected if curvature and its impact on angle of reflection are important. Curvature will also tend to decrease the measured chord lengths as the requisite backscattering intensity is only observed from a portion of the particle.

Curvature does not have any impact on the 0^{th} moment, since all of the particles are still counted. Screening may significantly affect the 0^{th} moment, and irregularities can significantly impact higher moments. For this reason, it may not be appropriate to use the growth rates estimated from Equations 4.14 and 4.15.

4.4. Equipment and Procedures

The experimental work presented here was conducted on a bench-scale crystallizer designed for evaporative crystallization. The crystallizer was constructed from a temperature-controlled, stirred, 1-L Parr reactor from which a measured vapor flow was continuously withdrawn. Figure 4.3 presents a schematic of the bench-scale

crystallizer. The initial solution placed in the crystallizer was prepared from 300 grams of ACS grade Na_2CO_3 and Na_2SO_4 in 700 grams of DI water. During the experiment, evaporation rate and chord-length data were collected. Additional details can be found in Shi [12].

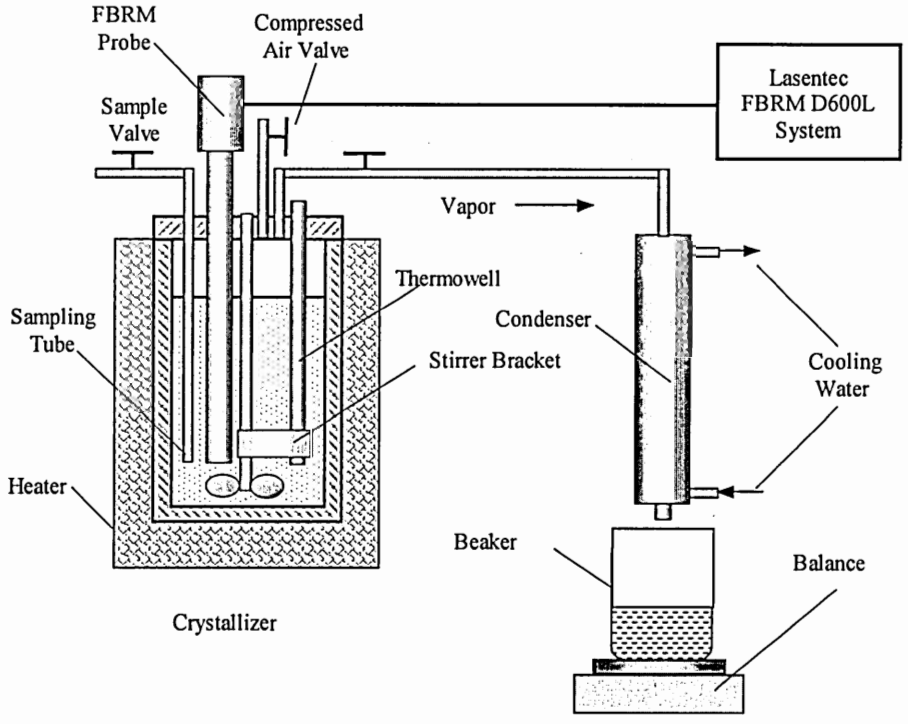

Figure 4.3: Schematic of bench-scale crystallizer with FBRM (Courtesy of Shi, [12]).

One critical assumption was made in this work based on the work of Ruf et al. [11]. The value of λ was fixed at 1500 μm. In Ruf et al., this value provided the most accurate measurement of the dimension of the ceramic bead that was used in that work. At lengths greater than 1500 μm, the dimension of the bead was significantly underestimated in many cases. The ceramic bead used by Ruf et al. was 600 μm in diameter, larger than the majority of particles being studied here. It has not been determined exactly how this difference might affect λ. However, as λ is being used

essentially as a fitting parameter in order to develop specific nucleation rates, a difference in λ only changes the accuracy of the number, not the precision.

4.5. Results and Analysis

Results from a bench-scale evaporative crystallization experiment, were analyzed to determine whether using moments of the CCD might provide nucleation and growth kinetics. The bench-scale experiments were conducted at 107°C with a 1:1 molar, Na_2CO_3:Na_2SO_4 solution.

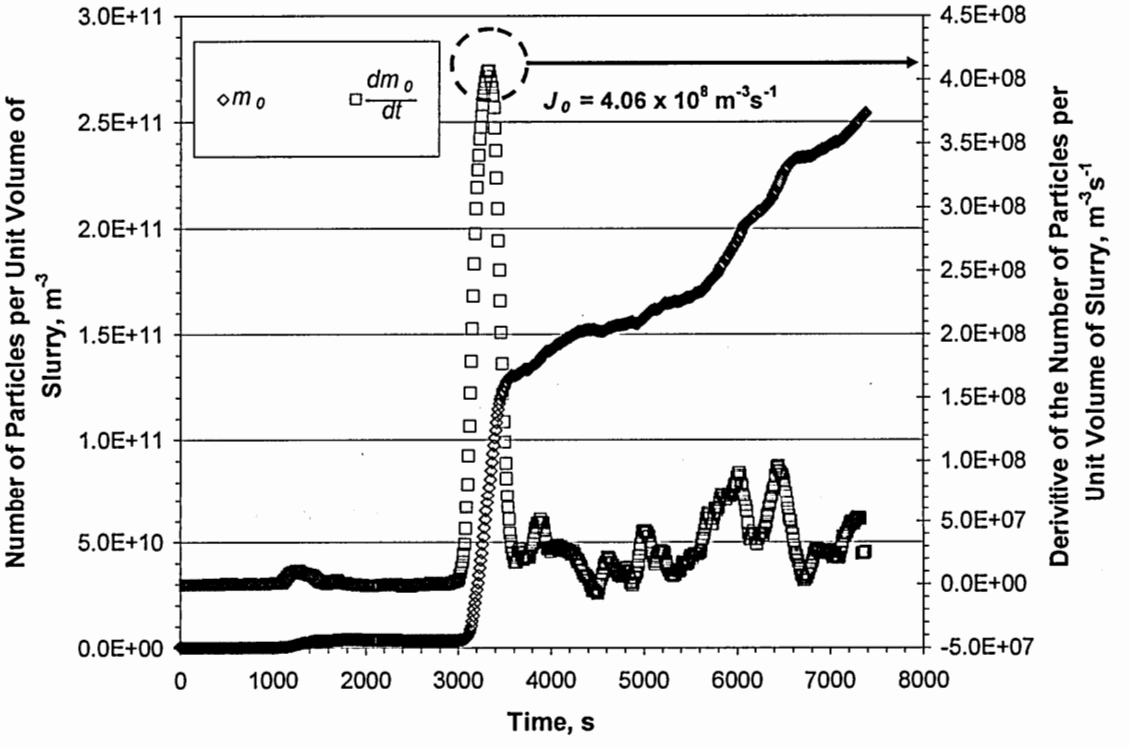

Figure 4.4: 0^{th} Moment of the CCD from bench-scale evaporation of a 1:1 mole ratio aqueous solution of Na_2CO_3:Na_2SO_4 at 107°C.

The specific 0^{th} moment, which represents the total number of particles detected per unit scanned volume, and its derivative with time are presented in Figure 4.4. The data can be interpreted to show that primary nucleation at approximately 3000 s and

agglomeration combined with secondary nucleation took place after approximately 4000 s. Secondary nucleation was identified from the continued positive derivative of the 0^{th} moment. Agglomeration was identified by the multiple locations where the derivative of the 0^{th} moment was negative. One example of this was seen at approximately 4500 s. The apparent primary nucleation rate, J_0, was determined from Figure 4.4 using Equation 4.11. The nucleation rate was 4.06×10^8 $m^{-3}s^{-1}$ at the peak of primary nucleation, observed about 3330 s into the run.

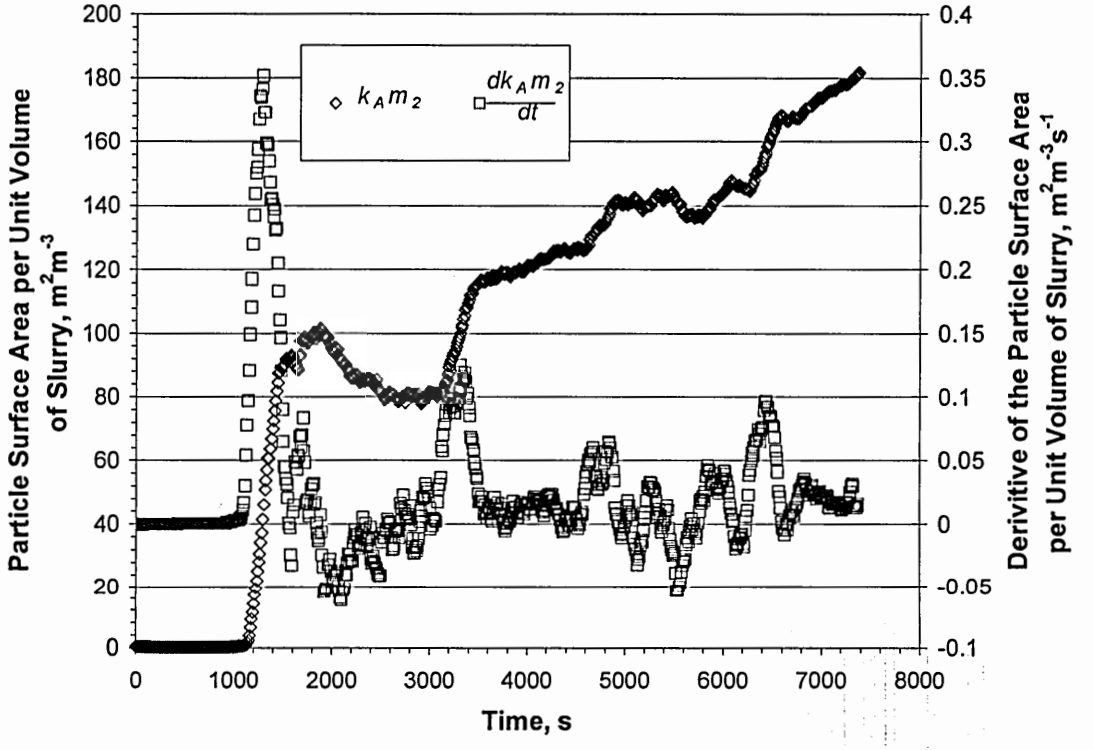

Figure 4.5: 2^{nd} Moment of the CCD from bench-scale evaporation of a 1:1 mole ratio aqueous solution of Na_2CO_3:Na_2SO_4 at 107°C.

Second and third moments of the CCD, which are shown in Figures 4.5 and 4.6 respectively, provide an interpretive challenge. The data in Figures 4.5 and 4.6 are from the same experiment as Figure 4.4. In Figure 4.5, based solely on peaks in the derivative of the 2^{nd} moment with time, evidence for 3 separate significant nucleation events can be

found. These are indicated by large values of the derivative at 1290 s, 3310 s, and 6440 s.

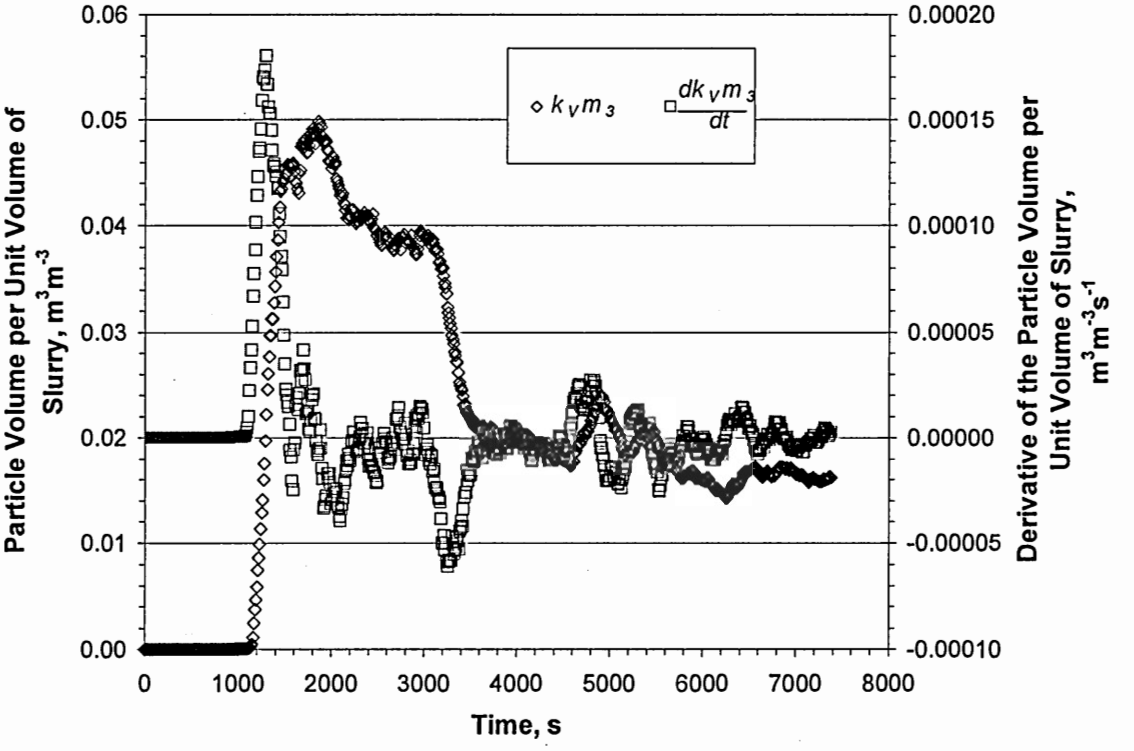

Figure 4.6: 3rd Moment of the CCD from bench-scale evaporation of a 1:1 mole ratio aqueous solution of Na_2CO_3:Na_2SO_4 at 107°C.

The specific 3rd moment data in Figure 4.6 is troubling theoretically. During batch evaporation of an aqueous solution, the mass of crystals (represented in Figure 4.6 by the volume) should not decrease. Yet in Figure 4.6, at 1290 s, the third moment reaches a maximum and then decreases. These data imply that as evaporation progressed past this maximum, the crystal mass in the system decreased.

A closer examination of Figure 4.4 reveals a small increase in the particle population density at 1290 s, but, the increase is insignificant when compared to the primary nucleation point at 3300 s.

Shi [12] and Ruf et. al. [11] provided the foundation for an explanation of the observed behavior in Figures 4.5 and 4.6. Shi found that for aqueous solutions of Na_2CO_3 and Na_2SO_4 in this composition range, a small number of burkeite ($2Na_2SO_4 \cdot Na_2CO_3$) crystals nucleated and grew to large sizes due to the relatively high supersaturation prior to primary bulk nucleation. A specific explanation for this phenomenon was not identified, but it was suggested this might be due to an unidentified trace contaminant in the reagent grade make-up chemicals used. If the evaporation experiment was stopped after the formation of these large crystals in Region I, and the solution was filtered to remove these crystals, then no additional crystals nucleated or grew until the primary bulk nucleation event [12]. Ruf et. al. showed that the addition of 80 ppm of titanium dioxide ($d_P \approx 10$ μm) provided a significant screening effect for the water/ceramic bead system studied. This effect was significant enough that λ decreased over 50% [11].

Based on the previous discussion, early increases in the 2nd and 3rd moments, seen in Figures 4.5 and 4.6, likely were due to a limited number of crystals that nucleated prior to 1290 s. These particles grew rapidly in the supersaturated solution. Then as primary nucleation occurred, the small nuclei formed began to screen the large existing crystals. This hypothesis was confirmed by chord-length distributions (CLD) at several significant points during the experiment.

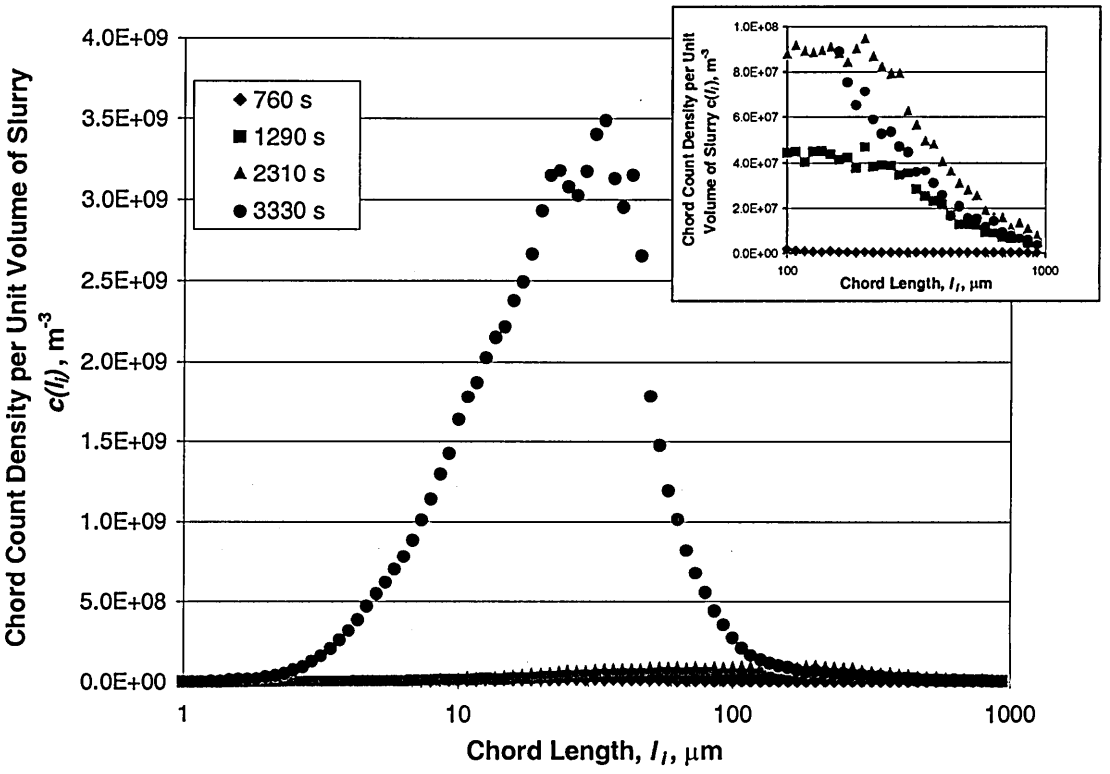

Figure 4.7: Chord Length Distributions for the evaporation experiment shown in Figures 4.4, 4.5 and 4.6 at t=760 s, 1290 s, 2310 s, and 3330 s.

Figure 4.7 presents the CLD at four different times: (a) 760 s, before the initial nucleation; (b) 1290 s, just after the initial nucleation; (c) 2310 s, between the initial nucleation and primary bulk nucleation; and (d) 3330 s, at the peak of primary bulk nucleation. The main plot shows each complete CLD, clearly showing that the CLD at 3330 s has increased by at least an order of magnitude. However, the inset plot of particle chord lengths from 100 μm to 1000 μm shows that the longest chord lengths measured actually decreased at 3330 s. This decrease confirms that the larger particles were screened by the small nuclei after primary bulk nucleation.

Because of these screening effects, any approach using weighted average chord-lengths to determine growth rates may not be valid. However, applying Equation 4.15 to particle data in the region between 4650 and 4900 s produced a growth rate of 1.81×10^{-8}

ms^{-1}. This growth rate falls between $1x10^{-8}$ ms^{-1} and $5x10^{-7}$ ms^{-1}, the reported range for growth rates for a number of inorganic salts [17, Table 6.1]. But, because the ratio of $\overline{m}_3/\overline{m}_2$ is affected by particle screening issues, a non-FBRM based growth rate calculation would be required to determine the validity of FBRM growth rate estimations. No secondary estimation method was used in this work for the reasons discussed in the introduction.

4.6. Conclusions

Bench-scale evaporation/crystallization work confirmed the capability of the FBRM system to estimate the bulk crystal nucleation rate, J_0. If no counting irregularities affect the measurement, this value should be accurate if $\overline{V}_S$ is determined appropriately. No alternative population measurement technique could be used for comparative purposes.

This work applied traditional particle population principles to FBRM chord-count densities with limited success. The FBRM measurement violated a primary underlying principle of population balances, namely that all of the particles in the test volume are properly sized. This issue remains one of the key challenges in applying FBRM technology to fundamental research. The 0^{th} moment does not have issues with accurate sizing of particles as it only measures the total number of particles counted. Thus, if no chord-counting irregularities occur, the nucleation rates estimated from FBRM data should be precise. Improving accuracy would require a more accurate, slurry specific, measure of λ.

As Braatz et al. note in their review article, online particle population tracking technology is a critical limitation in industrial crystallization control [1]. Counting irregularities not withstanding, this work shows that the FBRM can be used to provide an estimation of nucleation and possibly growth kinetics. Additional work is necessary to determine the accuracy of this estimation method. By correlating off-line size distributions in a less experimentally demanding particle slurry with online FBRM chord-count densities, it may be possible to determine the precision and accuracy of this methodology.

4.7. Acknowledgements

The author wishes to thank Bing Shi who conducted a number of bench-scale evaporative crystallization experiments as a part of his thesis work. While Dr. Shi did not develop the FBRM results in his thesis as this chapter has done, without his insight and his assistance operating the equipment, this work may not have been possible.

4.8. Variables

b FBRM laser width, m

$c(l)$ Chord-count density, m^{-3}

$C(l)$ Chord count, s^{-1}

ΔC_i Number of chords measured in the i^{th} channel, s^{-1}

d_i Diameter of i^{th} particle, m

d_P Particle diameter, m

G Growth rate, $m \cdot s^{-1}$

J_0 Nucleation rate, $m^{-3}s^{-1}$

k_S Shape factor, $_V$ indicates volume, $_A$ indicates surface area

l_i Chord length at the start of the i^{th} channel

$\bar{l}$ Square-weighted mean chord length, m

L Characteristic particle length, m

m_j j^{th} moment of the particle population, m^{j-3}

$n(L)$ Particle population density, m^{-3}

$N(L)$ Particle population, s^{-1}

V_S Sample volume, m^3

$\dot{v}_S$ FBRM laser rotation speed

$\bar{V}_S$ Volume scan rate of the solution by the FBRM, m^3s^{-1}

λ Effective laser penetration depth, m

ρ_C Crystal density, $kg \cdot m^{-3}$

4.9. Bibliography

1. Braatz, R.D., Fujiwara, M., Ma, D.L., Togkalidou, T., Tafti, D.K., "Simulation and New Sensor Technologies for Industrial Crystallization: A Review," International Journal of Modern Physics B, Vol 16, Nos 1 & 2 pp. 346-353 (2002)
2. Euhus, D.D., Shi, B., Rousseau, R.W., Frederick Jr., W.J., "Control of Soluble Scale in Black Liquor Evaporators and Concentrators: Part 1. Pilot Plant Studies," Proceedings of the 2002 TAPPI Fall Technical Conference, TAPPI Press, Atlanta, 2002

3. Frederick Jr., W.J., Euhus, D.D., Shi, B., Rousseau, R.W., "Control of Soluble Scale in Black Liquor Evaporators and Concentrators: Part 2. Interpretation of Crystallization Results," Proceedings of the 2002 TAPPI Fall Technical Conference, TAPPI Press, Atlanta, 2002
4. Euhus, D.D., Rousseau, R.W., Frederick Jr., W.J., Lien, S.J., "Black Liquor Evaporation: Links between Nucleation in the Bulk and Fouling of Heat Transfer Surfaces," Separations Technology Topical Conference, AIChE, New York, 2001, pp. 236-241.
5. Euhus, D.D., Rousseau, R.W., Frederick Jr., W.J., Lien, S.J., "Sodium Salt Fouling of Falling-Film Evaporators: A Pilot Study," International Chemical Recovery Conference, Oral Presentations, PAPTAC, Montreal, 2001, pp. 183-193.
6. Dowding, P.J., Goodwin, J.W., Vincent, B., "Factors governing emulsion droplet and solid particle size measurement performed using the focused beam reflectance technique," Colloids and Surfaces A: Physicochemical and Engineering Aspects 192 (2001) 5-13.
7. Custers, J.P.A., Hersmis, M.C., Meuldijk, J., Vekemans, J.A.J.M., Hulshof, L.A., "3,4,5-Tri-Dodecyloxybenzoic Acid: Combining Reaction Engineering and Chemistry in the Development of an Attractive Tool to Assist in Scaling Up Solid-Liquid Reactions," Organic Process Research & Development, 2002, 6, 645-651.
8. Hukkanen, E.J., Braatz, R.D., "Measurement of Particle Size Distribution in Suspension Polymerization Using In Situ Laser Backscattering," Submitted Article provided by the Authors.

9. Tadayyon, A., Rohani, S., "Determination of Particle Size Distribution by Par-Tec ® 100: Modelling and Experimental Results," Part. Part. Syst. Charact. 15 (1998) 127-135.

10. Barrett, P., Glennon, B., "In-line FBRM Monitoring of Particle Size in Dilute Agitated Suspensions," Part. Part. Syst. Charact. 16 (1999) 207-211.

11. Ruf, A., Worlitschek, J., Mazzotti, M., "Modeling and Experimental Analysis of PSD Measurements through FBRM," Part. Part. Syst. Charact. 17 (2000) 167-179.

12. Shi, B., Crystallization of Solutes that Lead to Scale Formation in Black Liquor Evaporation, Ph.D. Thesis, Georgia Institute of Technology, 2002.

13. Randolph, A.D., M.A. Larson, Theory of Particulate Processes, 2nd ed., Academic Press, 1988

14. Mullin, J.W., Crystallization 3rd Edition, Butterworth-Heinemann, Oxford, 1997

Chapter V: Pilot Evaporation Studies with Aqueous Solutions of Sodium Carbonate and Sodium Sulfate

5.1. Objectives

A methodology for the estimation of primary nucleation and growth rates in bulk solutions and of the growth rate of crystals on a heat-transfer surface will be developed in this chapter. This methodology will provide an analytical tool for modeling and for comparative analysis of experimental heat-transfer and bulk crystallization results from pilot-scale falling-film evaporation of aqueous solutions of sodium carbonate and sodium sulfate. The influence of the Reynolds number, the thermal driving force, and the composition of the dissolved salts on the rate processes will be determined. The influence of calcium on the crystallization behavior of burkeite and dicarbonate in the bulk solution and on the heat-transfer surface will also be investigated.

5.2. Introduction

Pilot-scale evaporation of aqueous solutions of sodium carbonate and sodium sulfate was used to simulate the evaporation of black liquor. Two different series of experiments were conducted using the pilot apparatus. The first series was conducted to determine the influence of ΔT, Re_Γ, and the molar ratio of Na_2CO_3:Na_2SO_4 on the nucleation process for primary bulk nucleation and the growth process for crystals on the heat-transfer surface. The second series was conducted to determine the influence of removing calcium from the system. These experiments were analyzed using the methods developed in this chapter. The present work appears to be the first in which the

fundamental phenomena leading to bulk crystallization and surface fouling have been measured simultaneously.

5.3. Procedure

The pilot-scale studies with aqueous sodium carbonate and sodium sulfate solutions were performed with the falling-film, dimple-plate, pilot evaporator described in Chapter 3 of this thesis. Only operational details and the experimental design will be discussed here.

In both series of experiments, samples of salt crystals were scraped from a 15 mm mesh inline filter for identification of the crystalline species using powder X-ray diffraction (XRD). Sampling in this fashion sought to avoid formation of additional crystals due to cooling.

5.3.1. Statistically Designed Experiments

Smith conducted a set of statistically designed experiments similar to those conducted in this study [1]. This research is a substantial advancement over Smith's work for three reasons. First, upgrades in the control structure of the pilot falling-film apparatus have resulted in more accurate continuous measurements and better control of the vessel pressure and condensate flow rates. This resulted in more accurate heat-transfer data. Second, this work was conducted using an FBRM to obtain real-time data on the particle population. Third, new methodologies were developed and used to analyze the results of the statistically designed experiments conducted.

The statistically designed experiments were conducted in semi-batch mode, with a solution of dissolved Na_2CO_3 and Na_2SO_4 added continuously to maintain a constant volume of solution in the evaporator as vapor was withdrawn. The effects of steam pressure (temperature of the heat source), the rate of recirculation of the aqueous solution over the heat transfer surface, and solution composition on bulk and surface crystallization were evaluated. The initial thermal driving force, $\Delta T_{Initial}$, was determined by the temperature of the saturated steam and the boiling temperature of the aqueous solution. The initial thermal driving force was used because as each experiment progressed, the thermal driving force changed due to the rise in the boiling point caused by concentrating the dissolved salts. The Reynolds number, Re_Γ, of the solution flowing over the heat-transfer surface was determined by the rate of recirculation of liquor over the plate and the properties of the black liquor. The composition of the aqueous solutions was described by the ratio of sodium carbonate to sodium sulfate initially in the solution. The experiments were conducted at each possible combination of Re_Γ {7300, 14600}, $\Delta T_{Initial}$ {2.8°C, 8.3°C}, and Na_2CO_3:Na_2SO_4 {1, 6.7}. In addition, three replicate center-point experiments were run at $Re_\Gamma = 10{,}000$, $\Delta T_{Initial} = 5.5$°C, and Na_2CO_3:$Na_2SO_4 = 3.9$. These last three experiments were run to determine repeatability and as a basis to determine the statistical significance of the results.

The solutions were composed of industrial-grade sodium carbonate and sodium sulfate fully dissolved in approximately 180 kg of deionized water. As calcium is known to inhibit the nucleation of burkeite [2], the calcium contents of these industrial-grade salts were also determined. The sodium carbonate used in the experimental solutions contained approximately 235 ppm by mass of calcium. The sodium sulfate used in the

experimental solutions contained approximately 140 ppm by mass of calcium. Table 5.1 presents the design variables and initial solution composition for the 11 statistically designed experiments and two additional experiments run at higher Na_2CO_3:Na_2SO_4 ratios.

Table 5.1: Values of the experimental variables, including the initial masses of Na_2CO_3, Na_2SO_4, and calcium that were dissolved in 180 kg of DI water

Experiment	ΔT (°C)	Re_Γ	Na_2CO_3:Na_2SO_4 (molar)	Mass of Na_2CO_3 (kg)	Mass of Na_2SO_4 (kg)	Calcium (ppm)
1	5.5	10900	3.9	39.89	13.88	202
2	8.3	14600	1.0	23.04	30.73	173
3	8.3	7300	6.7	44.81	8.96	210
4	8.3	7300	1.0	23.04	30.73	173
5	2.8	7300	1.0	23.04	30.73	173
6	8.3	14600	6.7	37.80	7.56	210
7	5.5	10900	3.9	39.89	13.88	202
8	2.8	14600	6.7	37.80	7.56	210
9	2.8	14600	1.0	23.04	30.73	173
10	5.5	10900	3.9	39.89	13.88	202
11	2.8	7300	6.7	44.81	8.96	210
13.4:1	5.5	10900	13.4	48.88	4.89	217
20.1:1	5.5	10900	20.1	50.41	3.36	220

During the experiments, the chord lengths of crystals suspended in the solutions were measured by FBRM to quantify the behavior of the crystal population. The FBRM filtering adjustment was placed on the coarse setting. The effective penetration depth for the FBRM laser was assumed to be 1500 μm as discussed in Chapter 4. Condensate flow rates and relevant temperatures were measured for estimation of overall heat-transfer coefficients, and subsequently surface fouling rates, as described in Chapter 3. The average flow rate of condensate after reaching the operating conditions but before crystallization was determined for each of the three center-point experiments in order to measure the repeatability of the experimental procedure. The standard deviation of these flow rates relative to the average flow rate for the three experiments was 7%.

Each experiment was conducted until one of two endpoints was reached. The first was marked by rapid bulk nucleation and growth followed by apparent settling of the salt crystals inside the evaporator body. Because the pilot unit did not have a conical bottom,

crystals were allowed to settle in regions where they could not be entrained. The second endpoint was marked by loss of thermal driving force, ΔT, due to surface fouling and/or boiling-point rise in the aqueous solution.

5.3.2. Calcium Inhibition Study

The influence of calcium ions on nucleation and crystal growth in suspension and on the heat-transfer surface was not specifically studied in the statistically designed experiments. However, Shi's work had identified calcium as a burkeite nucleation inhibitor [2]. For that reason, a second series of pilot experiments was conducted to determine the effect of calcium ions on nucleation and growth of crystals both in bulk and on the heat-transfer surface. One specific objective of these experiments was to determine the effect of calcium on the rate parameters for bulk nucleation and crystal growth on the heat-transfer surface.

All of the experiments in the calcium study were conducted under semi-batch conditions maintaining a constant volume of solution in the sump of the evaporator. The circulation rate corresponded to a Re_Γ of 11,600. The liquor-side vapor pressure was set at 1.758 bar (T_{Sat}=116°C) and the steam pressure was set at 2.275 bar (T_{Sat}=124°C). Taking into account the boiling point rise of approximately 4°C, the initial thermal driving force, ΔT, was 4°C. The FBRM filtering was changed to the fine setting to improve fine particle recognition and improve identification and measurement of primary bulk nucleation. The effective penetration depth for the FBRM laser was assumed to be 1500 μm as discussed in Chapter 4.

Like the solutions evaporated in the series of statistically designed experiments, the solutions used to study the effect of calcium on crystallization behavior were composed of deionized water and fully dissolved industrial grade sodium carbonate and sodium sulfate at approximately 25 wt % total solids content. The industrial grade sodium carbonate contained approximately 235 ppm by mass of calcium. The industrial grade sodium sulfate contained approximately 140 ppm by mass of calcium. Calcium was sequestered using EDTA (ethylene-diamine-tetraacetic sodium salt, dihydrate crystals, FW 372.24) dissolved in the solution.[1] The amount of each species present at the start of each experiment is given in Table 5.2.

Table 5.2: Initial masses of Na_2CO_3, Na_2SO_4, calcium, and additives per 180 kg of DI water

Run	Mass of Na_2CO_3 (kg)	Mass of Na_2SO_4 (kg)	Initial Calcium* (ppm)	Mass of Additive	Type of Additive
1	14.46	39.07	166		
1a	14.46	39.07	220	4.1 g	CaO
2	43.74	9.78	218		
3	44.92	8.59	220		
4	49.13	4.39	227		
5	14.46	39.07	166	97 g	EDTA
6	43.74	9.78	218	97 g	EDTA
7	44.92	8.59	220	97 g	EDTA
8	49.13	4.39	227	97 g	EDTA

*including additives

5.4 Results and Analysis

In this section, methods for analyzing experimental results for pilot-scale evaporation of aqueous solutions of Na_2CO_3 and Na_2SO_4 will be presented. Then, these methods will be used to obtain rate parameters for primary bulk nucleation and crystal growth on the heat transfer surface during evaporation experiments in the pilot apparatus.

[1] EDTA is a commonly available chelating agent which forms a metal-ligand complex with Ca^{2+}. When the molar concentration of EDTA is in excess of the molar calcium concentration, the free calcium level becomes negligible.

5.4.1. Development of Analytical Methodologies

Because crystallization in the bulk solution and on the heat-transfer surface are thought to be interconnected, methods to interpret and analyze data collected simultaneously for bulk crystallization and heat-transfer fouling are critical to examining the interdependencies of the two phenomena.

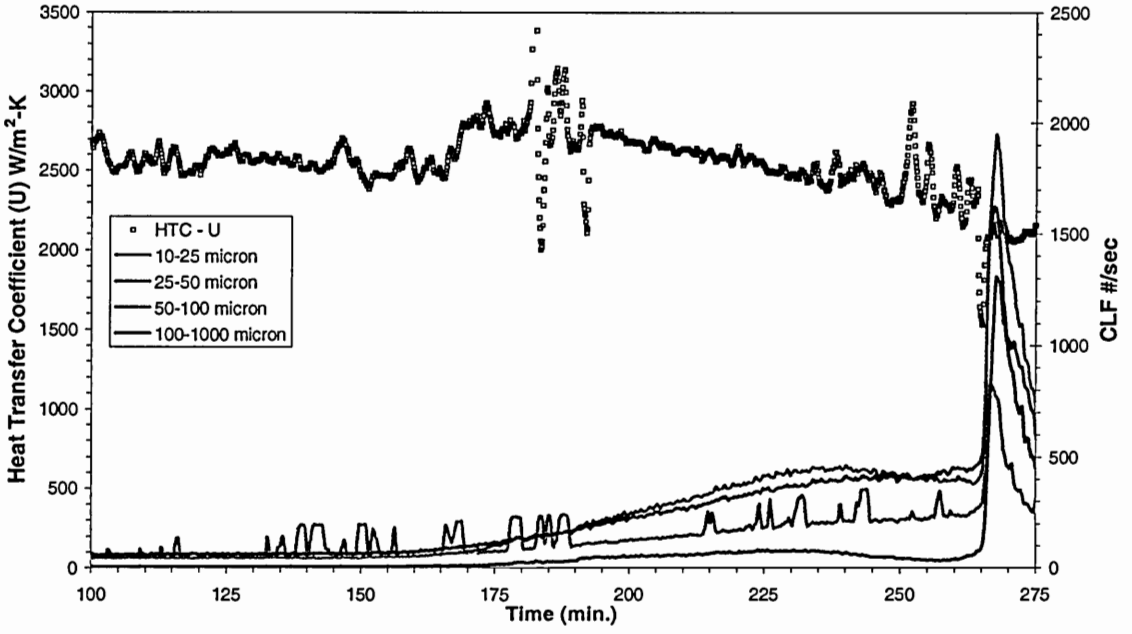

Figure 5.1: Heat-transfer coefficient and chord length frequency data versus time for Experiment 1 of the statistically designed series of experiments

Figure 5.1 provides an example of the changes in heat-transfer coefficient and chord-length frequency (CLF) observed during the evaporation process for one of the experiments in the statistically-designed study. Note that the heat-transfer coefficient remained relatively constant until approximately 165 minutes into the run, when it increased approximately 20%. This is indicative of an increase in surface area created by microscopic crystals on the heat-transfer surface. Also, the increased surface roughness due to the crystals can increase the local heat-transfer coefficient by disturbing the flow. After the initial increase, there was a steady decline in the heat-transfer coefficient until

primary bulk nucleation occurred. The fluctuations in the heat-transfer coefficient between 180 and 190 minutes were due to PID controller problems which were quickly corrected during the experiment. These fluctuations were only observed in three of the experiments in this study and each was directly connected to control of the vapor pressure in the vessel.

The CLF data are the total number of particles counted per second in a given size range through the entire experiment. Crystals were observed in solution early in the experiment between approximately 125 and 150 minutes. There were probably two sources of these particles. One source may have been early nucleation of crystals, prior to the solution reaching the metastable limit for primary bulk nucleation of Na_2CO_3 and Na_2SO_4. In burkeite-producing solutions where calcium is present as in the experiment in Figure 5.1, it had previously been reported that some early nucleation does occur prior to reaching the metastable limit [2]. Second, random sloughing of crystals off of the heat-transfer surface into solution may have occurred after crystallization occurred on the surface. This mechanism of nucleation is more likely after initiation of fouling on the heat-transfer surface, which occurred at 165 minutes. Early growth of nuclei occurred in the saturated solution, and is evidenced by increases in the CLFs for each of the ranges shown in Figure 5.1, beginning somewhere between 150 and 175 minutes. Finally, primary bulk nucleation is identified by the sharp spikes in CLFs at approximately 265 minutes.

Procedures for extraction of fouling rates (*SFR*) from pilot evaporator experiments were discussed in Section 3.2.4. Defining *SFR* to be proportional to the growth rate of crystal on the heat-transfer surface,

$$SFR = \frac{1}{k_F} G_S , \tag{5.1}$$

where k_F is the thermal conductivity of the fouling deposit. Furthermore, the crystal growth on the heat-transfer surface can be assumed to be given by the expression,

$$G_S = k_S \sigma . \tag{5.2}$$

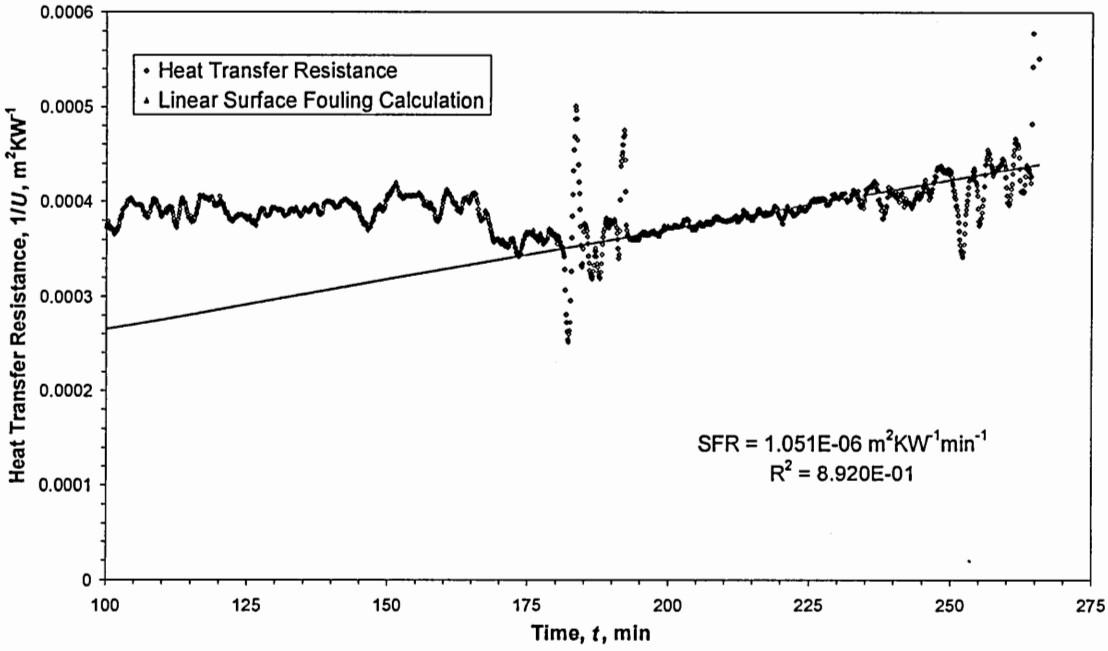

Figure 5.2: Linear regression of the heat-transfer coefficients in Figure 5.1 to determine the surface-fouling rate

Figure 5.2 shows an example of how linear regression of the heat-transfer resistance data was used to estimate the surface-fouling rate in an aqueous sodium carbonate and sodium sulfate experiment. Since burkeite was the crystallizing species, and the thermal conductivity, k_F, of burkeite scale was estimated by Smith to be approximately 1.73 $Wm^{-1}K^{-1}$, for this experiment G_S = 1.82 μm/min. This value is of the order of magnitude observed in aqueous crystallization of inorganic salts [3, Table 6.1].

An estimation of the supersaturation in the solution is required to obtain the growth rate parameter, k_S. It was assumed that the relative supersaturation, σ, was

$$\sigma = \frac{(C - C^*)}{C^*}, \tag{5.3}$$

where C is the total concentration of the dissolved sodium salts at nucleation while C^* is the total concentration of the dissolved sodium salts at chemical equilibrium. Primary bulk nucleation was identified through analysis of FBRM data. Samples of the solution in the pilot evaporator were taken approximately every 30 minutes and analyzed for total solids content. These measured compositions were fit to a polynomial expression for each experiment. After identifying the time at which primary bulk nucleation occurred, the concentration at which it occurred was estimated using the polynomial expression. The solubility limits for solutions composed of Na_2CO_3 and Na_2SO_4 were predicted using the NAELS chemical equilibrium software.

In Chapter 4, the development of chord count densities (CCD) from FBRM data and then determination of crystallization rates using the appropriate moments of the CCDs were discussed. In the experiments with aqueous solutions of Na_2CO_3 and Na_2SO_4, growth rates for crystals in the bulk solution during evaporation were estimated immediately before primary bulk nucleation. Just prior to primary bulk nucleation, a small number of particles were observed in suspension by the FBRM. Two possible sources for these crystals were (a) early nucleation and (b) crystallization on the heat-transfer surface and subsequent sloughing. However, the validity of the FBRM-derived growth rates was called into question by the work in Chapter 4.

Once the nucleation rate, J_0, was estimated, the rate parameter for primary bulk nucleation could be estimated from,

$$J_0 = k_N \sigma_{max}{}^{i}. \tag{5.4}$$

The best way to determine i so that k_N can be determined is to divide Equation 5.4 by an equation for the growth rate such as Equation 5.2. If this is done, the resulting equation can be rearranged to obtain,

$$\ln J_0 = i \ln G + (\ln k_N - i \ln k_G), \tag{5.5}$$

i can then be determined by linear regression of concurrently measured primary bulk nucleation rates and crystal growth rates. Once the value of i has been determined it can be used with the supersaturation at primary bulk nucleation (Equation 5.3) to determine k_N from Equation 5.4.

The rate of crystal growth in the bulk solution was estimated from Equation 5.6,

$$G = \frac{d\bar{l}}{2dt} = \frac{d\left(\overline{m}_3 / \overline{m}_2\right)}{dt}. \tag{5.6}$$

The term on the right side of this equation is the time derivative of the area-weighted mean chord length. This growth rate was then used to determine the growth rate parameter in the bulk solution, k_G, from,

$$G = k_G \sigma. \tag{5.7}$$

5.4.2. Results for the Statistically Designed Experimental Study

The study was designed to determine the influence of ΔT, Re_Γ and Na_2CO_3:Na_2SO_4 ratio on the crystallization of burkeite in the bulk solution and on the heat-transfer surface. The dependence of the surface-fouling rate, the bulk growth rate and the bulk nucleation rate on each independent variable was determined. In addition, the crystallization rates were analyzed using Equations 5.2, 5.4 and 5.7 to obtain rate

parameters for the bulk and heat-transfer surface crystallization phenomena studied. The rate parameters were correlated with the independent variables.

5.4.2.1. Heat Transfer and Surface Fouling Rates

Table 5.3 contains the heat fluxes and surface fouling rates for the 13 pilot-scale experiments conducted according to the experimental design and the two additional experiments conducted at higher sodium carbonate to sodium sulfate ratios (C:S). These data are plotted in Figure 5.3.

Table 5.3 : Initial heat flux and estimated surface-fouling rates for the statistically-designed, pilot-scale series of experiments and two additional experiments at high C:S ratio

Experiment	Initial q ($W \cdot m^{-2}$)	SFR x10^9 ($m^2K \cdot W^{-1}s^{-1}$)
1	10600	17.5
2	17100	18.1
3	16800	27.1
4	15900	30.4
5	4500	7.34
6	17000	9.86
7	9600	19.0
8	4100	14.7
9	5700	13.5
10	9700	19.3
11	3800	15.2
13.4:1	10800	21.4
20:1	11100	48.6

Although scattered, these data indicate a direct relationship between the initial heat flux[2] and the fouling rate, if the higher C:S ratio experiments are disregarded. That a relationship exists is not surprising as a greater heat flux should increase the temperature of the heat-transfer surface and consequently the supersaturation at the surface for an inversely soluble salt. The scatter of the data in Figure 5.3 indicates that either the experimental error was significant or that the independent variables have some

[2] The initial heat flux was the average heat flux measured after reaching the operating conditions but before crystallization occurred.

influence on fouling aside from how they impact the heat flux. Because the standard deviation of the surface fouling rate for the three repeat experiments was only 5% of the average value of those three experiments, the latter seems more likely.

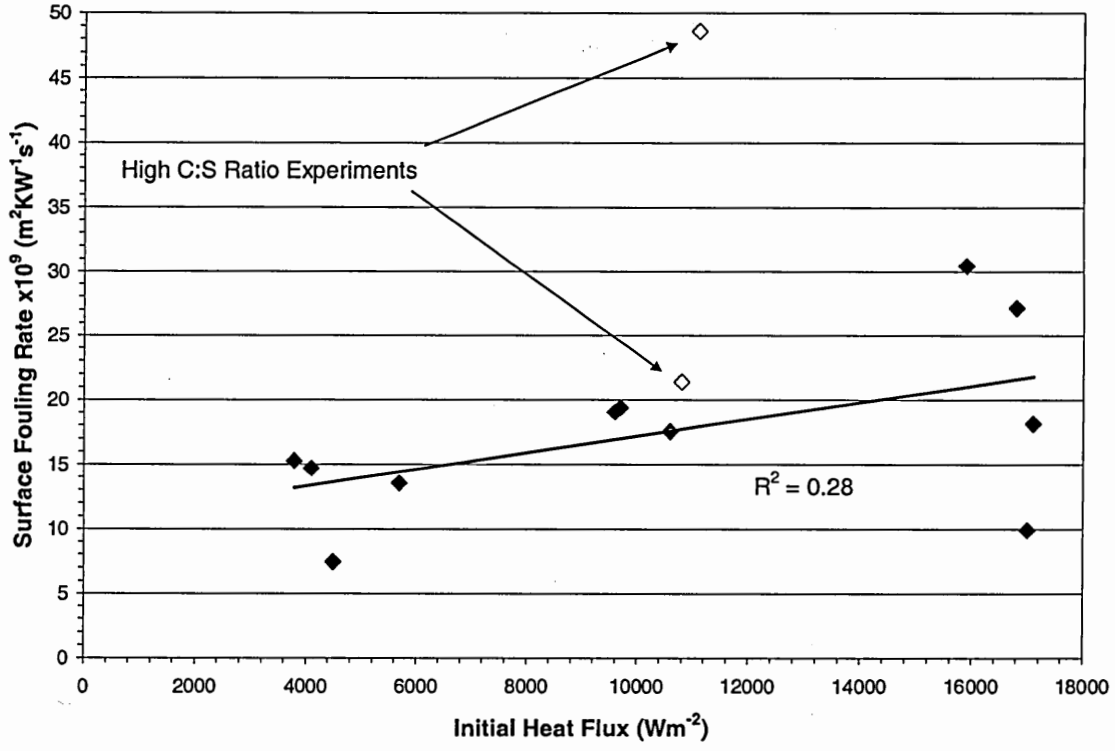

Figure 5.3: Dependence of surface-fouling rate of the heat flux during a semi-batch pilot evaporation of aqueous solutions of sodium carbonate and sodium sulfate.

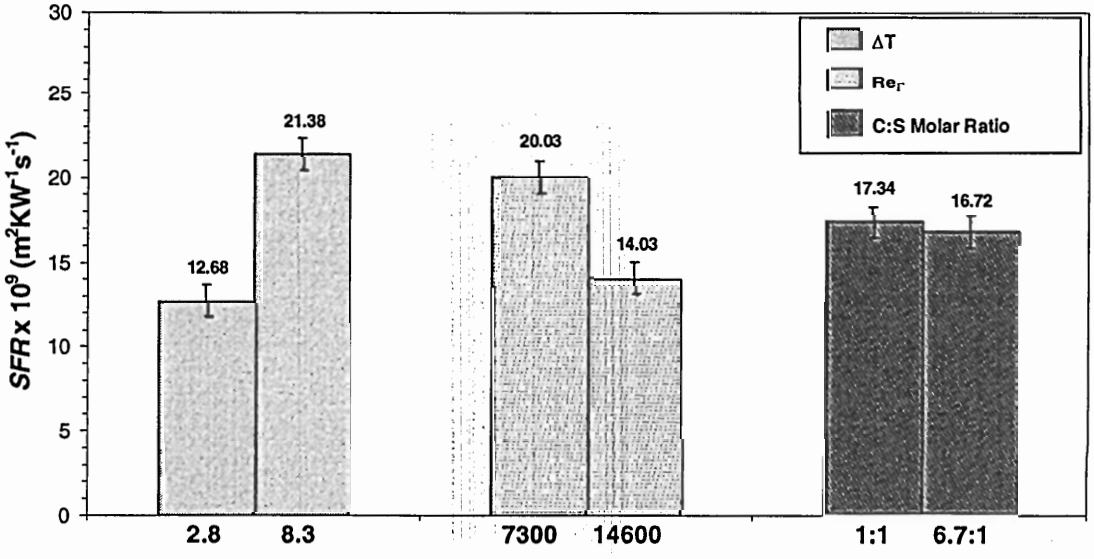

Figure 5.4: Influence of the experimental variables studied on the surface-fouling rate.

The surface-fouling rates were analyzed to determine the influence of the independent variables on the *SFR*. Figure 5.4 shows the influence of each of the experimental variables studied on the surface-fouling rate. Each bar represents the average fouling rate for the four experiments conducted at the specified condition (i.e. the first bar on the left of Figure 5.4 is the average of the four experiments conducted with $\Delta T = 2.8°C$). The error bars represent one standard deviation, as determined from the three replicate center-point experiments, on either side of the average value. The standard deviation of the *SFR* for the center-point experiments relative to the average for these experiments was 5.2%. If the error bars do not overlap for the high and the low operating condition, then that variable was considered to have a significant influence in this work. Both the Reynolds number and the thermal driving force have significant influence on the surface-fouling rate.

In principle, the influence of thermal driving force is straightforward. Increasing the thermal driving force will increase the supersaturation at the heat transfer surface for a solution of salts that exhibit inverse solubility. Increasing supersaturation in turn should increase the growth rate for the crystals on the heat-transfer surface.

The influence of the Reynolds number is more difficult to reconcile traditional crystallization theory developed for bulk solutions. In general, nucleation and growth of crystals in a bulk solution increase with mixing, so the rates of nucleation and growth on the heat transfer surface might be expected to increase with mixing. However, there can be two additional influences of the rate of recirculation of the aqueous solution over the fouling rate on the heat-transfer surface: (a) the impact of mixing on the thermal and supersaturation gradients and (b) mechanical removal of the scale (sloughing). In bulk

solutions, mixing tends to increase crystal growth because it reduces transport limitations. For growth on the heat-transfer surface, the primary driving force is the temperature difference and its influence on the supersaturation. An increase in Re_Γ increases the heat transfer coefficient, changing the temperature (and the supersaturation) gradient. Also, at higher Re_Γ, scale is more likely to slough off due to shear.

The ratio of sodium carbonate to sodium sulfate did not have a statistically significant influence on the surface fouling rate in Figure 5.4.

5.4.2.2. Bulk Crystallization

Table 5.4: Estimates of kinetic rates of bulk crystallization for the statistically-designed series of pilot-scale experiments and two additional experiments conducted at high C:S ratios

Experiment	J_0, ($m^{-3}s^{-1}$)	G ($m \cdot s^{-1}$)
1	8.88E+08	1.2E-07
2	1.82E+09	1.8E-07
3	4.12E+08	4.9E-07
4	6.36E+09	2.2E-07
5	2.86E+08	1.5E-07
6	3.11E+08	8.8E-07
7	2.05E+09	4.0E-07
8	2.65E+08	4.9E-08
9	1.11E+09	1.1E-07
10	1.38E+09	2.0E-07
11	1.51E+08	3.0E-07
13.4:1	6.05E+07	
20:1	1.32E+08	

Table 5.4 presents estimated primary nucleation and growth rates for crystals suspended in the bulk solutions of the experiments conducted in the statistically designed study. The primary nucleation and growth rates in bulk solutions were not completely independent. The growth rate of crystals present in the bulk slurry prior to the massive bulk nucleation event described earlier, should have influenced the rate at which supersaturation was developed prior to that nucleation event. The bulk growth rate was

averaged over the same time range as the surface fouling rate estimation. The nucleation rates for the high Na_2CO_3:Na_2SO_4 experiments are also included in Table 5.4.

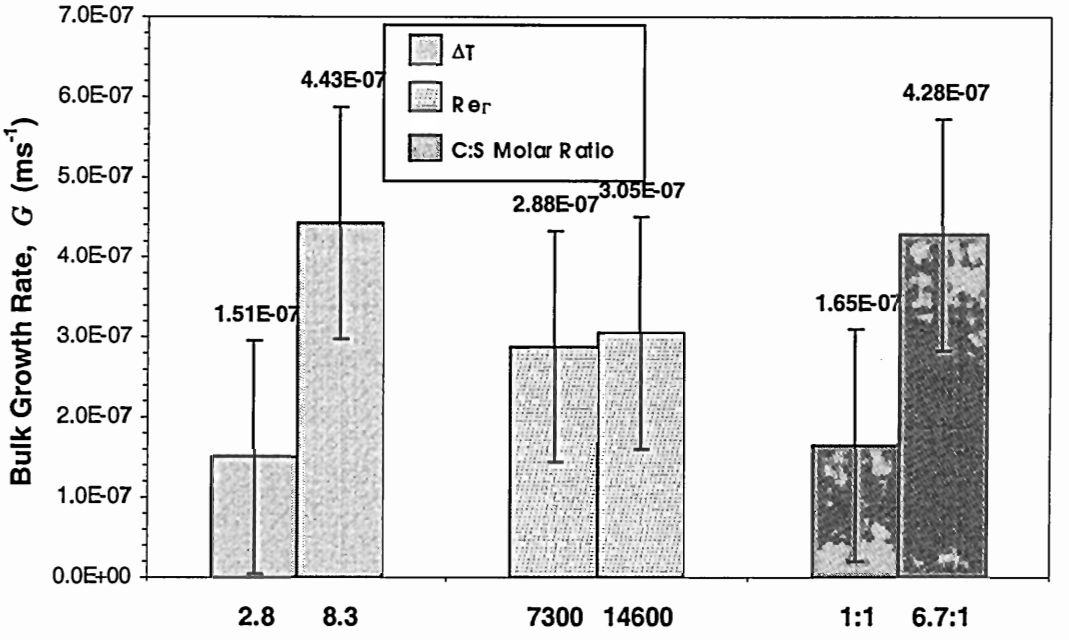

Figure 5.5: Influences of the experimental variables on the bulk growth rate, *G*

Figure 5.5 shows influence of the experimental variables on the estimated bulk growth rates for the statistically designed experimental data set. The variability in the bulk growth rates estimated was large, but the observed effects of all three experimental variables were clear. Both the thermal driving force and the Na_2CO_3:Na_2SO_4 ratio influenced the bulk crystal growth rate. The standard deviation of *G* for the center-point experiments relative to the average for these experiments was 61%.

An interesting observation can be made about the relationship between Na_2CO_3:Na_2SO_4 ratio, supersaturation, and fouling rate regarding the bulk growth rate analysis. In Figure 5.5, the bulk growth rate (*G*) increased over 150% when the molar ratio of Na_2CO_3:Na_2SO_4 was increased from 1:1 to 6.7:1. This increase in fouling rate is very difficult to account for in terms of increased supersaturation alone, since a relative supersaturation change of the magnitude required to cause this change in growth rate

should have caused primary bulk nucleation. One potential cause for this observed difference would be two different species crystallizing at the two different molar ratios of Na_2CO_3:Na_2SO_4.

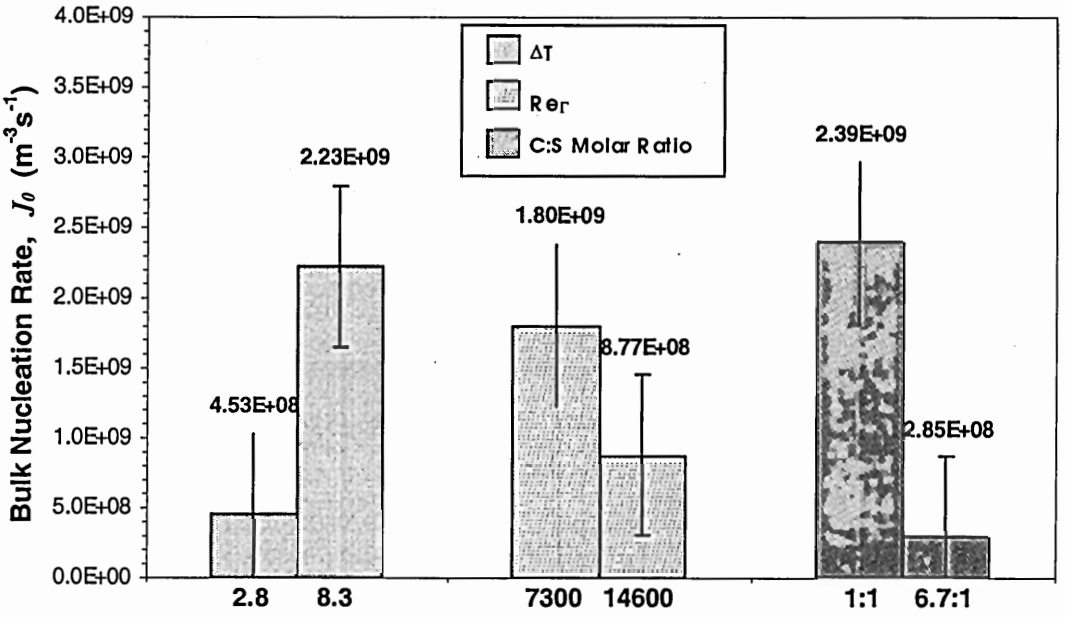

Figure 5.6: Influences of the experimental variables on the primary bulk nucleation rate, J_0

Figure 5.6 presents the influence of each of ΔT, Re_Γ, and Na_2CO_3:Na_2SO_4 ratio on the bulk nucleation rate. The most important influence was the nearly order of magnitude decrease in J_0 when the C:S ratio was increased from 1:1 to 6.7:1. This also suggests a change in the crystal species that is nucleating. The standard deviation of J_0 for the center-point experiments relative to the average for these experiments was 40%.

5.4.2.3. Crystal Species

It is possible that the influence of the ratio of Na_2CO_3:Na_2SO_4 lies in the fact that two different crystal species were nucleating and growing. Three crystalline species are known to exist in equilibrium with saturated solutions in the range of the compositions

and temperatures in this work. These are burkeite, a double salt with a nominal composition of 1 mole of sodium carbonate for every 2 moles of sodium sulfate, anhydrous sodium carbonate and sodium carbonate monohydrate (thermonatrite).

Chemical equilibrium calculations with the NAELS software predicted that the transition between thermonatrite and sodium carbonate occurs at approximately 103.4°C. However, some sources indicate that the transition may occur closer to 109°C [6]. At 106°C, which was the approximate solution temperature during evaporation in the present work, the transition from burkeite to sodium carbonate is predicted to occur when the C:S molar ratio is 13.5:1. If the equilibrium species is crystallized from solution, then scale taken from the heat-transfer surface and crystals in the bulk solution should contain only burkeite, except for the case when the C:S molar ratio was 20.1:1.

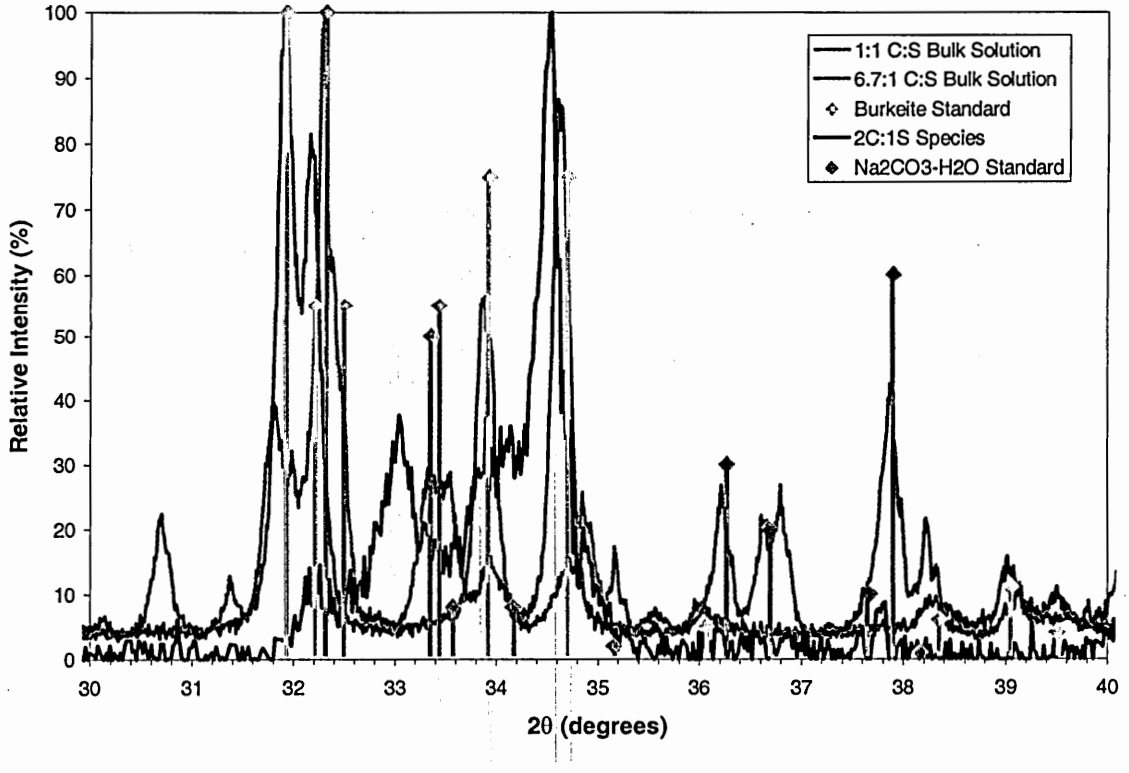

Figure 5.7: XRD spectra for crystals sampled from salt solutions where burkeite is the predicted species that crystallizes

Figure 5.7 shows XRD spectra for the salt samples collected from the pilot evaporation experiments. The peaks at approximately 31.9 and 34.7 in the spectra indicate that the crystals formed from the solution with a 1:1 molar ratio of C:S were burkeite. The peaks at approximately 32.3 and 37.9 in the spectra indicate that the crystals formed from the solution with a 6.7:1 molar ratio of C:S were thermonatrite. Dicarbonate was not identified as the crystallizing species for any of the statistically designed experiments as none of the spectra contained the primary peak at 34.5 or the key secondary peak at 33. This may have been due to operating at lower experimental temperatures than those used by Shi [2]. Also, none of the expected peaks for anhydrous sodium carbonate were observed in any XRD pattern for any experiment in this section.

Analysis of the XRD spectra indicate that either the aqueous solubility behavior predicted by NAELS was incorrect, or that kinetics dictated the solid species that crystallized. Essentially this would mean that thermonatrite is actually a metastable species at the experimental conditions that crystallizes instead of burkeite due to higher nucleation and growth rates.

5.4.2.4. Estimates for the Value of *i* and the Rate Parameters

Equation 5.5, which was presented previously, provides a method to estimate the value of i. The slope of the regression lines in Figures 5.8 and 5.9 indicate the estimated i-value for each crystal species relative to the growth rates in the bulk solution, G, and on the heat-transfer surface, G_S. For the purposes of estimating the rate parameters for primary bulk nucleation, an average of these i-values was used. The average i-value from

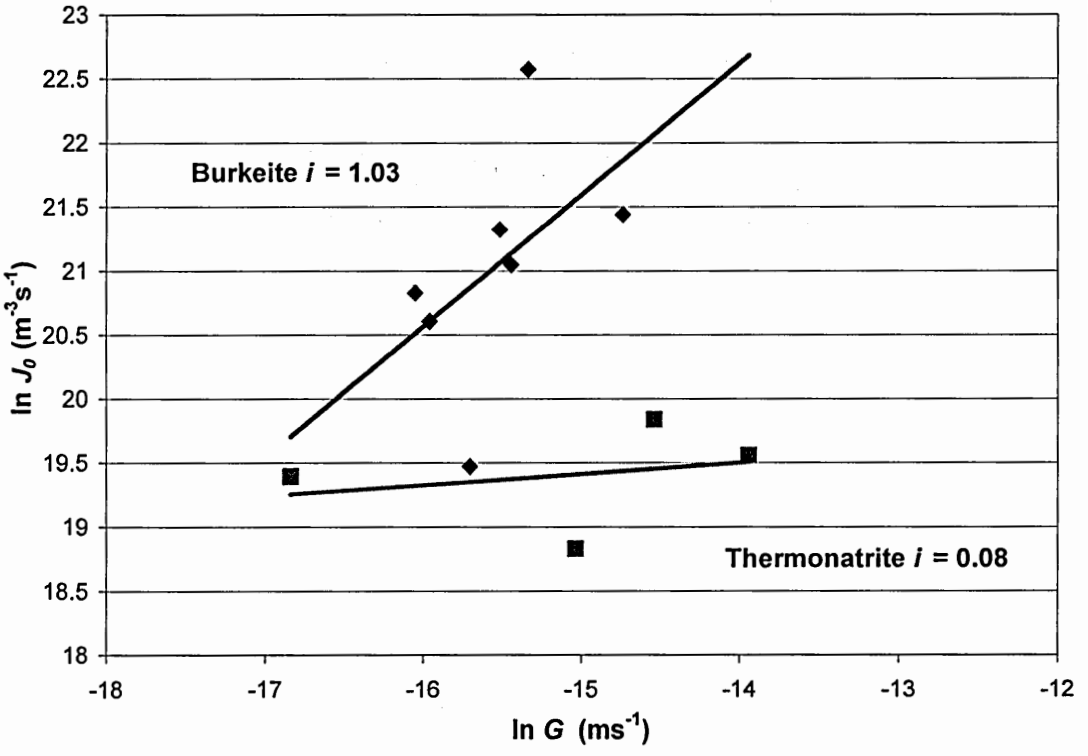

Figure 5.8: Determining the order of nucleation, *i*, from bulk growth rate data

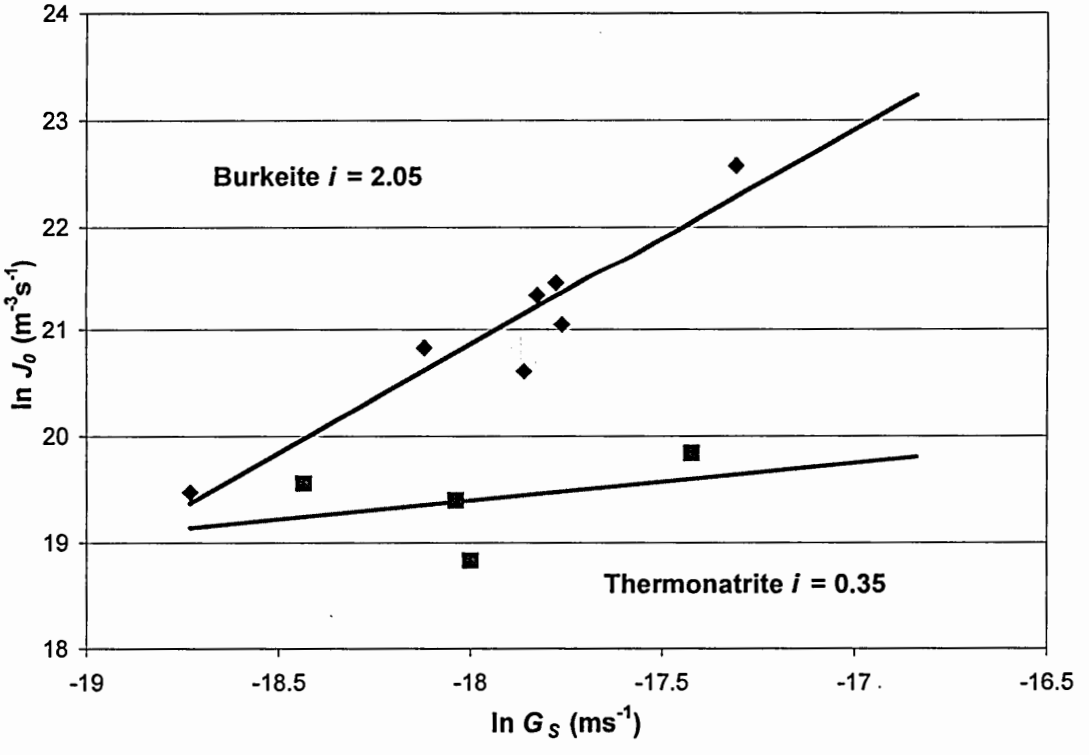

Figure 5.9: Determining the order of nucleation, *i*, from surface growth rate data.

Figures 5.8 and 5.9 for burkeite was 1.54. For thermonatrite, the average *i*-value from Figures 5.8 and 5.9 was 0.22.

Table 5.5: Estimations of the kinetic rate parameters for crystallization and the metastable supersaturation.

Experiment	k_N ($m^{-3}s^{-1}$)	k_G ($m \cdot s^{-1}$)	k_S ($m \cdot s^{-1}$)	$\sigma_{Nucleation}$
1	1.00E+10	5.65E-07	1.46E-07	0.207
2	5.83E+10	1.73E-06	2.98E-07	0.105
3	6.29E+08	3.30E-06	3.19E-07	0.147
4	1.28E+11	1.53E-06	3.69E-07	0.143
5	6.35E+10	5.06E-06	4.24E-07	0.030
6	4.62E+08	5.34E-06	1.03E-07	0.165
7	2.02E+10	1.76E-06	1.46E-07	0.226
8	4.04E+08	3.31E-07	1.72E-07	0.147
9	1.53E+10	5.88E-07	1.28E-07	0.182
10	1.11E+10	7.61E-07	1.30E-07	0.258
11	2.50E+08	2.96E-06	2.63E-07	0.100
13.4:1	1.10E+08		5.66E-07	0.065
20.1:1	2.58E+08		1.77E-06	0.047

In this work, the effective thermal conductivity of the fouling deposit was assumed to be constant and equal to 1.73 $Wm^{-1}K^{-1}$[1]. Using the values of *i* from Figures 5.8 and 5.9 and Equations 5.1, 5.2, 5.4 and 5.7, the rate parameters were determined for bulk nucleation (k_N), bulk growth (k_G), and surface growth (k_S). These rate parameters are presented in Table 5.5. Their standard deviations for the center-point experiments relative to the average for these experiments were 40%, 62% and 6.7% respectively. The supersaturation, σ, used to determine the rate parameters in Table 5.5 was estimated using Equation 5.3 and had a standard deviation for the center-point experiments relative to the average for these experiments of 11%.

5.4.2.5. Statistical Analysis of the Rate Parameters from the Designed Study

A rigorous statistical analysis was conducted using the rate parameters determined in the previous section. In a full-factorial design of the type used in this study, the P-

value is used to measure the probability that an independent variable had a statistically significant effect. A P-value of 0 implies that the variable studied has a 100% probability of being significant. A P-value of 1 implies that the variable studied has a 0% probability of being significant. Typically a P-value of 0.1 or less is considered statistically significant at a 90% confidence level. The P-value is dependant on both the experimental results for the factorial design and the results of the replicate experiments at the center-point. The variability in the measured results is determined from the values of the replicate experiments performed at the center-point conditions. This variability is used in assessing whether an experimental variable had a statistically significant effect. In this work, the Minitab13 software package was used for the statistical analysis. Further information about the P-value and its determination can be found in the Minitab13 guides [7, 8].

Table 5.6: P-values from the statistical analysis of the effects of single variables and combinations of variables.

Term	k_N ($m^{-3}s^{-1}$)	k_G ($m \cdot s^{-1}$)	k_S ($m \cdot s^{-1}$)	$\sigma_{Nucleation}$
Constant	0.004	0.007	0.000	0.001
ΔT	0.021	0.244	0.060	0.073
Re_Γ	0.018	0.115	0.001	0.316
Na_2CO_3:Na_2SO_4	0.004	0.237	0.005	0.008
$\Delta T \cdot Re_\Gamma$	0.302	0.036	0.062	0.006
$\Delta T \cdot Na_2CO_3$:Na_2SO_4	0.021	0.051	0.039	0.027
$Re_\Gamma \cdot Na_2CO_3$:Na_2SO_4	0.018	0.179	0.149	0.023
$\Delta T \cdot Re_\Gamma \cdot Na_2CO_3$:$Na_2SO_4$	0.313	0.999	0.006	0.702
Center Point	0.035	0.068	0.003	0.679

P-values from analysis of the pilot experimental data are presented in Table 5.6. The importance of each independent variable and combinations of independent variable is indicated for each of the rate parameters as well as the supersaturation at the metastable limit. The "constant" in Table 5.6 is a fitting parameter, and is nearly always significant.

Finally, the P-value for the center point is shown. This value indicates if nonlinearity in the relationship between the independent variables and dependant variable was significant

For this work, a P-value ≤ 0.1 (a 90% level of confidence) was used as the criterion for determining if an independent variable had a significant effect in determining the value of one of the rate parameters or supersaturation at the metastable limit. Using this criterion, all of the single variable interactions were significant for k_N. In addition, the 2-variable interactions of ΔT and Re_Γ with the ratio of Na_2CO_3:Na_2SO_4 were also significant. The influence of each of these variables or pairs of variables that had a statistically significant effect in determining k_N can be explained from crystallization theory.

The rate parameter for bulk growth, k_G, was influenced significantly by only two variables. These variables were the paired interactions of Re_Γ and the ratio of Na_2CO_3:Na_2SO_4 with ΔT.

The rate parameter for growth of a deposit on the heat-transfer surface, k_S, depended on all three single variables and on the same variable pairs as k_G.

5.4.2.6. Correlative Models for the Influence of Experimental Variables on k_N and k_S

Correlative models for k_N and k_S were determined from the experimental data. The models were developed with the assumption that the dependence of the rate parameter on the experimental variables followed a power law. These empirical models provided additional insight into the magnitude of the influence exhibited by each

variable. The criterion for an acceptable model was that the correlation maximized the R^2-value with the fewest additional parameters beyond the three independent variables.

This methodology did not produce a useful correlation for k_G. For k_N, the data was best fit using this method with an equation of the form,

$$k_N = \frac{C_1 \Delta T}{\mathrm{Re}_\Gamma SR}, \tag{5.5}$$

where C_1 is a constant. When $C_1=10^{14}$ ($m^{-3}s^{-1}$), the R^2-value was 0.94. The four lowest nucleation rates exhibited the poorest fit in the data set. The k_S data were correlated as,

$$k_S = \frac{C_2}{\mathrm{Re}_\Gamma SR^\alpha}, \tag{5.6}$$

where the R^2-value of 0.74 was obtained when $C_2=0.0029$ (ms^{-1}) and $\alpha=0.25$.

5.4.2.7. Conclusions for the Statistically Designed Study

Two conclusions were made based on the data from the pilot-scale experiments in the statistically designed study. First, it was possible to measure bulk and surface crystallization behavior simultaneously and to develop rate parameters for the important crystallization processes. Second, the dependence of these rate parameters on the experimental variables was modeled using a simple power law expression, and provided a good correlation of the experimental results.

In the process of conducting this study an important observation was made. The salt species crystallized on the heat-transfer surface or in the bulk solution is not always the species predicted by the NAELS chemical equilibrium software. It remains to be

determined whether incorrect prediction of the crystallizing species is due to errors in the thermodynamic model or database, or to kinetic effects determining the crystal species.

5.4.3. Influence of Calcium on Bulk Crystallization and Fouling

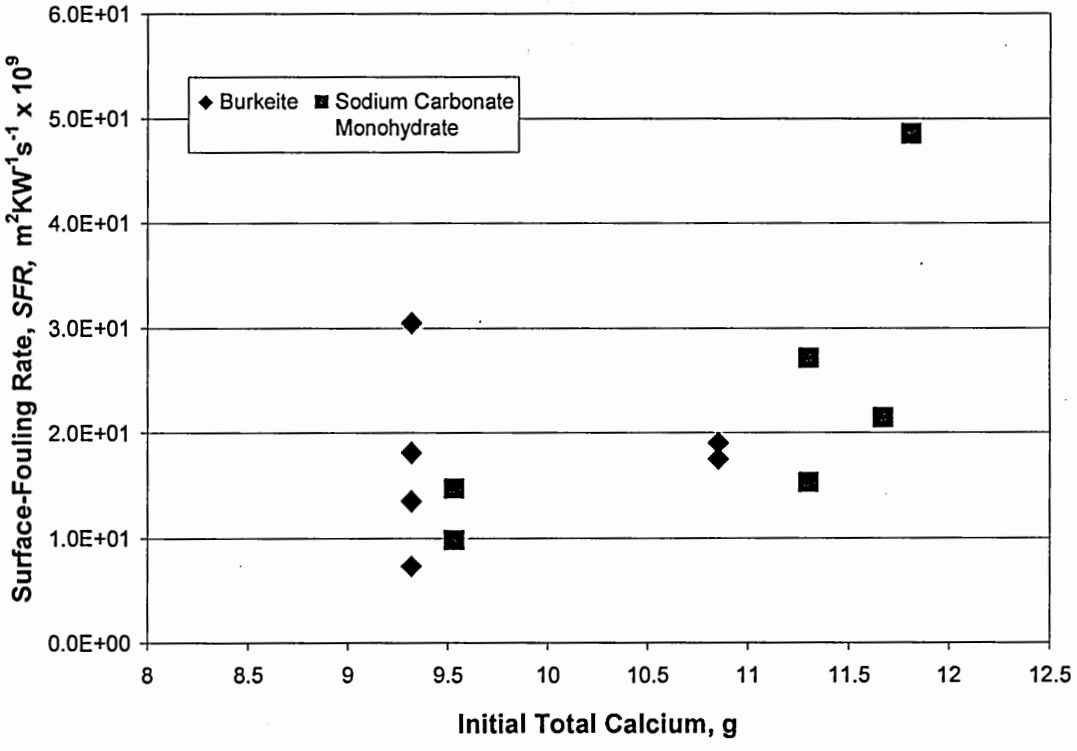

Figure 5.10: Surface-fouling rates for the different initial calcium contents from experiments in the statistically designed study.

Calcium ions act as nucleation inhibitors in burkeite crystallization [2], so determining the influence of calcium on the fouling process is important. The first step was to determine what, if any, influence calcium had on the crystallization in bulk and on the heat-transfer surface during the experiments in the statistically designed study.

Figure 5.10 shows the surface fouling rates measured during the experiments in the statistically designed study. The solutions happened to have different calcium concentrations due to differences in the calcium content of the make-up salts and changes

in the total mass of salts used in two of the experiments. Because of this, a number of different initial calcium levels were inadvertently studied. The overall trend in Figure 5.10 indicates that at higher initial calcium levels, the surface-fouling rate was greater. This held true for both burkeite and sodium carbonate monohydrate. However, because calcium content was not one of the variables specifically tested, it is possible for example that differences in the ratio of Na_2CO_3:Na_2SO_4 was responsible for the higher fouling rates.

Because of ambiguity that remained after examining the influence of calcium in the statistically designed study, it was clear that a second set of pilot evaporator experiments needed to be conducted. This study needed to answer the question of what effect calcium had on bulk crystallization and heat-transfer fouling during evaporation experiments.

5.4.3.1. Crystal Species Observed During Calcium Inhibition Experiments

The ratio of Na_2CO_3:Na_2SO_4 used in the calcium inhibition experiments (listed in Table 5.2) were purposefully chosen to encompass the range of solution compositions that would produce each of the three salts identified by Shi [2] during evaporation. Specifically, the low ratio was in the burkeite region. The high ratio was in the sodium carbonate region. The two middle ratios were where dicarbonate crystallization was expected. Crystal samples were collected after primary bulk nucleation to determine the salt species crystallized, and to determine if calcium influenced the crystallizing species. They were removed from the bulk suspension using a 15 μm filter. The molar ratios and crystal species identified through XRD are shown in Table 5.7.

Table 5.7: Analysis of Crystals Produced in the Calcium Inhibition Experiments

Experiment	Molar Ratio (C:S)	Expected Species	Species Identified by XRD Analysis	Analysis Time†
1	0.44	$2Na_2SO_4 \cdot Na_2CO_3$	$2Na_2SO_4 \cdot Na_2CO_3$	12 days
2	2.50	$2Na_2CO_3 \cdot Na_2SO_4$	$Na_2CO_3 \cdot H_2O + 2Na_2SO_4 \cdot Na_2CO_3$	20 days
2	2.20	$2Na_2CO_3 \cdot Na_2SO_4$	$Na_2CO_3 \cdot H_2O + 2Na_2SO_4 \cdot Na_2CO_3$	20 days
3	2.59	$2Na_2CO_3 \cdot Na_2SO_4$	$Na_2CO_3 + 2Na_2SO_4 \cdot Na_2CO_3$*	26 days
4	23.88	Na_2CO_3	Na_2CO_3	26 days
5	0.45	$2Na_2SO_4 \cdot Na_2CO_3$	$2Na_2SO_4 \cdot Na_2CO_3$	5 days
5	0.45	$2Na_2SO_4 \cdot Na_2CO_3$	$2Na_2SO_4 \cdot Na_2CO_3$	5 days
6	3.17	$2Na_2CO_3 \cdot Na_2SO_4$	$Na_2CO_3 + 2Na_2SO_4 \cdot Na_2CO_3$	2 days
6	3.00	$2Na_2CO_3 \cdot Na_2SO_4$	$Na_2CO_3 + 2Na_2SO_4 \cdot Na_2CO_3$	2 days
7	2.99	$2Na_2CO_3 \cdot Na_2SO_4$	$Na_2CO_3 \cdot H_2O + 2Na_2SO_4 \cdot Na_2CO_3$	3 days
7	3.14	$2Na_2CO_3 \cdot Na_2SO_4$	$Na_2CO_3 \cdot H_2O + 2Na_2SO_4 \cdot Na_2CO_3$	3 days
8	31.67	Na_2CO_3	-	-

*There was some indication that this sample also contained $2Na_2CO_3 \cdot Na_2SO_4$
†The length of time between sample collection and XRD

Table 5.7 presents the results of the analysis of the crystals recovered. It shows both the results from the XRD analysis and the analysis of carbonate and sulfate in the crystals. The mole ratios of Na_2CO_3:Na_2SO_4 in the crystals collected indicate that the salt species predicted by Shi are the ones that actually crystallized during the experiments. Perhaps the most interesting observation of the crystal composition data is that when EDTA was added, the ratio of Na_2CO_3:Na_2SO_4 for the dicarbonate species actually shifted toward a tricarbonate ratio. Based on Shi's Figure 5.12 [2], this ratio appears to actually be quite high. Unfortunately, the metastable dicarbonate species decomposed upon standing for several days to sodium carbonate and burkeite. Shi noted that the species appeared to be metastable. He stored a sample at room temperature in a sealed container for approximately 1 month and then reanalyzed by XRD, only to find that the dicarbonate species had changed to burkeite and sodium carbonate. In the present study, the first set of samples was analyzed after long delays due to unavailability of the XRD spectrometer. However, the samples from experiments where EDTA was added were performed after only 2-3 days. In both cases, the dicarbonate shifted to the stable salt

species. The only indicator that dicarbonate was crystallized was the overall ratios of carbonate to sulfate in the crystals.

5.4.3.2. Results of the Calcium Inhibition Study

The experimental results from the calcium inhibition study are grouped into two subsets, with EDTA and without EDTA. In the experiments with EDTA, enough EDTA was added to effectively bind all the calcium ions in the solution. At the lowest C:S ratio, two experiments were conducted without EDTA. In one, calcium was added to the solution so that the total calcium level would be similar to that at the other three C:S ratios. In the other, the calcium level was lower due to the differences in the calcium content of the two industrial-grade salts used in this study.

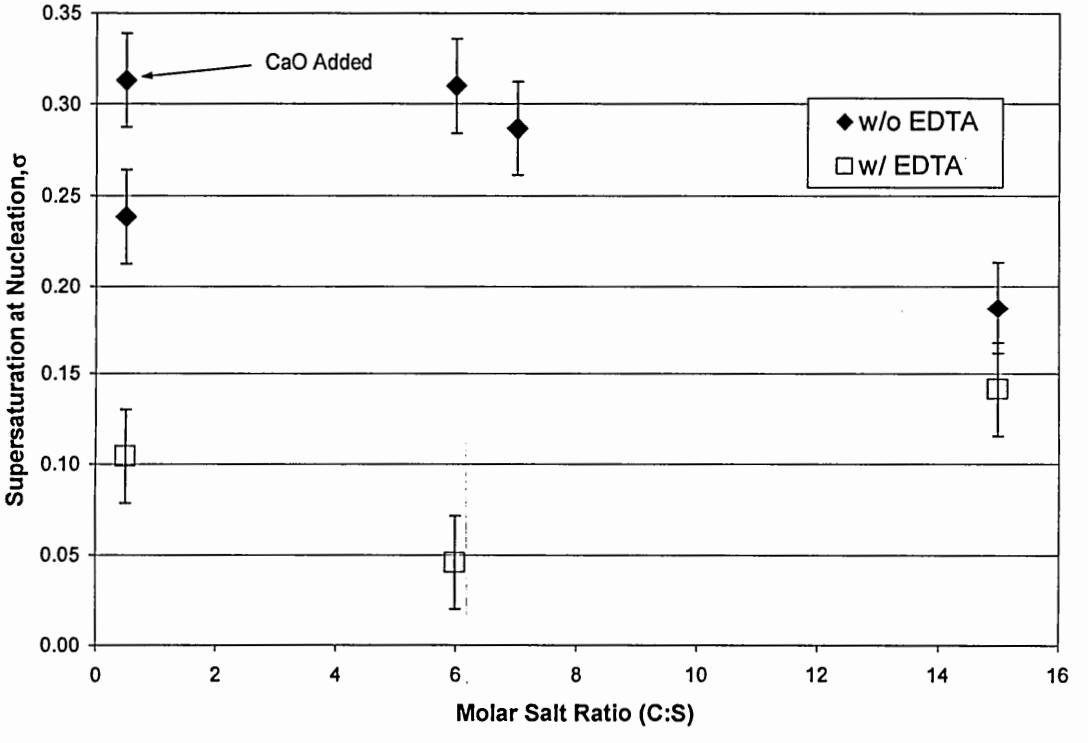

Figure 5.11: Influence of calcium on supersaturation at four different Na_2CO_3:Na_2SO_4 ratios

Figure 5.11 indicates that calcium inhibited primary bulk nucleation. Always at lower C:S ratios, where crystallization of a double salt was expected, the experiments conducted with EDTA added as a calcium scavenger exhibited lower supersaturation at primary bulk nucleation. For the data at the lowest ratio of Na_2CO_3:Na_2SO_4 data set where two experiments were conducted without EDTA, after a 33% increase in the calcium level, a 32% increase in σ was observed. This result corresponds well with Shi's observation that increasing calcium level increased the inhibition and consequently the metastable limit [2]. It should also be noted that this inhibition could be quite substantial. Relative supersaturation increased by more than a factor of 6 for the experiment with a C:S ratio of 6.0:1. The error bars shown are one standard deviation as determined by the center-point experiments in the statistically designed study.

The fact that the inhibiting effect of calcium was strong at Na_2CO_3:Na_2SO_4 mole ratios of 6.0 and 7.0 implies that calcium influenced the crystallization of the dicarbonate salt species, and not just burkeite. The data in Figure 5.11 suggest that the inhibition of dicarbonate may even be greater than it was for burkeite. However, that cannot be definitively concluded based on this experimental work.

Figure 5.12 indicates that calcium had little influence on the nucleation rate. The estimated nucleation rates are nearly identical for the experiments conducted with and without the addition of EDTA. This is interesting considering the significant differences in σ among the different experiments.

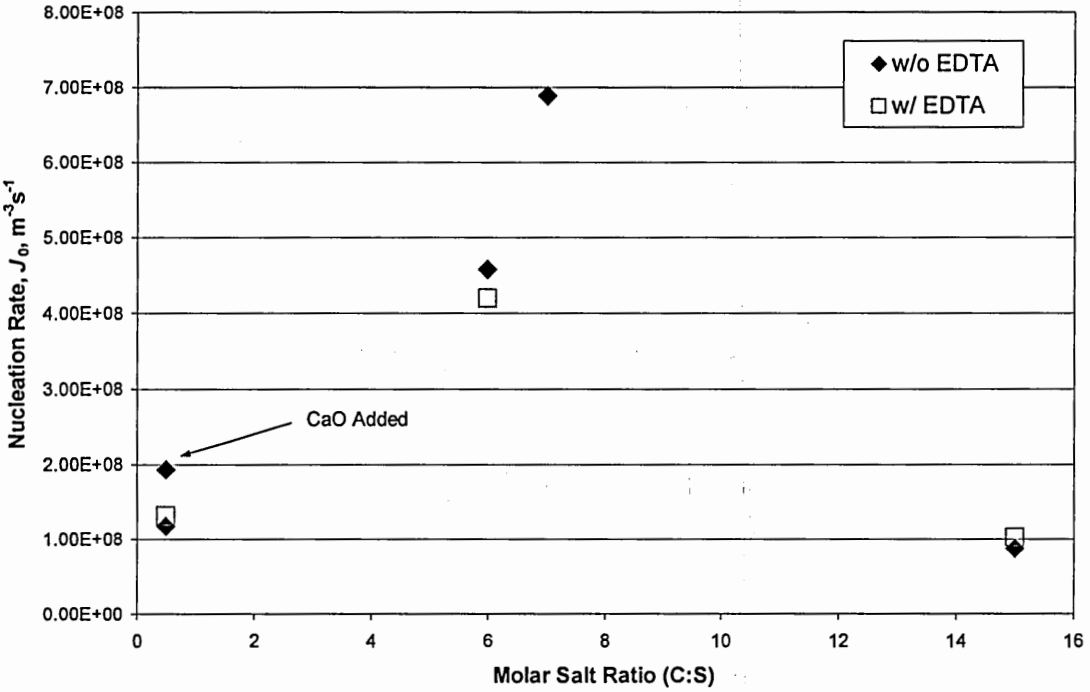

Figure 5.12: Influence of calcium on primary bulk nucleation at four different ratios of Na_2CO_3:Na_2SO_4

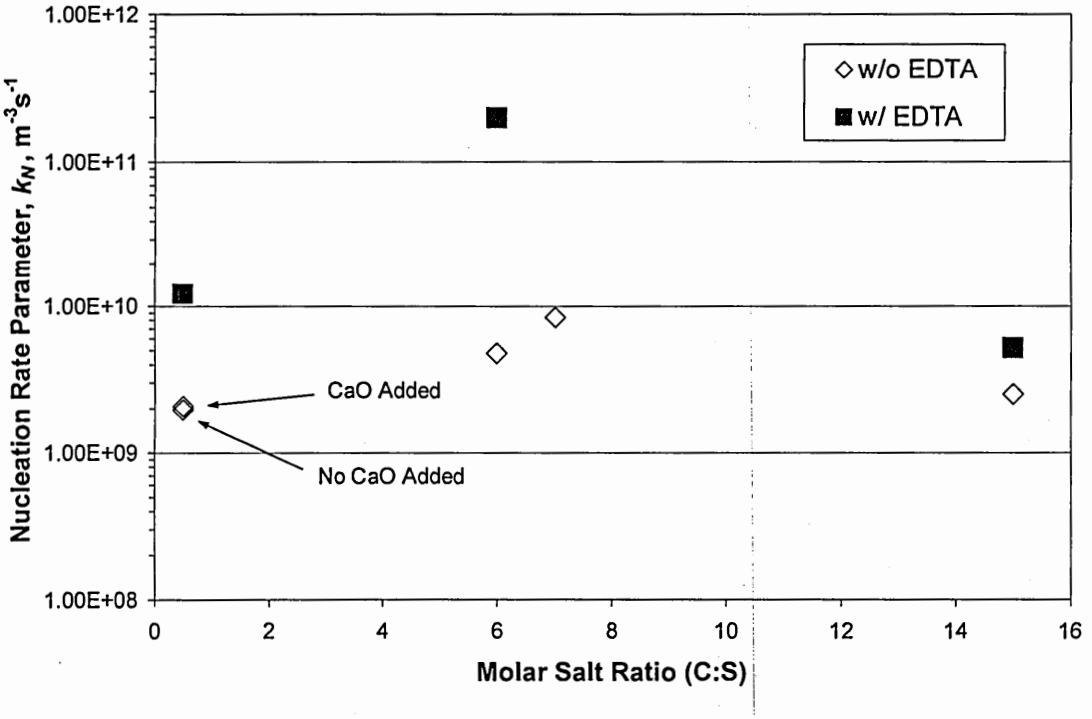

Figure 5.13: Influence of calcium on the rate parameter for primary bulk nucleation at four different ratios of Na_2CO_3:Na_2SO_4.

Figure 5.13 shows that the nucleation rate parameters are influenced by calcium. The values of k_N were always higher when calcium ions had been sequestered with EDTA. Another interesting observation is that the values of the rate parameter for nucleation were independent of the level of calcium in the system, as long as calcium was present (experiments with no EDTA). The two experiments conducted at a C:S ratio of 0.5:1 and at two different calcium levels but without the addition of EDTA, had different metastable limits and different nucleation rates, but their nucleation rate parameters were identical. Figure 5.13 also shows that the difference in the nucleation rate parameter between the two experiments conducted at high C:S ratios, with and without addition of EDTA , is significantly less than for similar experiments conducted at lower C:S ratios. This again suggests that the crystal structure of anhydrous sodium carbonate is more resistant to calcium inhibition than are those of the two double salt crystals.

Each of the conclusions drawn from Figures 5.11 – 5.13 is a confirmation of what should occur if calcium is indeed a nucleation inhibitor in the double salt systems under study, but not in anhydrous sodium carbonate.

The influence of calcium in the fouling process may be as simple as its inhibitive influence in the bulk solution, or it may be more complex. In the bulk solution, the calcium ions inhibit nucleation by complicating the formation of critical nuclei. The calcium ions incorporate themselves into the nuclei as lattice defects [2]. That this would occur on a heterogeneous substrate is not intuitively obvious. Due to changes in the geometry of the critical nucleus (a half sphere on the heat-transfer surface versus a sphere in the bulk solution), it is difficult to predict exactly what influence the calcium might have on surface fouling.

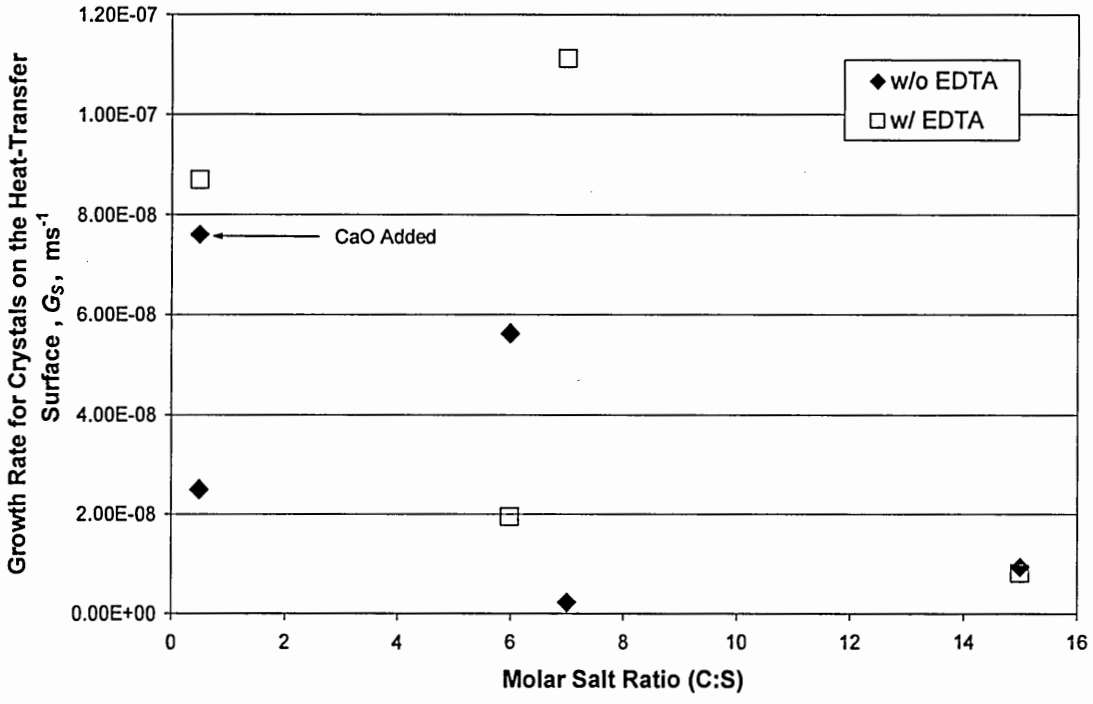

Figure 5.14: Influence of calcium on the growth rate for crystals on a heat-transfer surface at four different ratios of Na_2CO_3:Na_2SO_4.

Figure 5.14 compares the rate of growth of crystals on the heat transfer surface versus C:S ratio, for the experiments with and without addition of EDTA. The apparent lack of data trends in Figure 5.14, where the effect of supersaturation has not been eliminated, might suggest that calcium did not influence fouling. The rate parameters for surface growth, presented in Figure 5.15, clarify the influence of calcium on the fouling process. For crystal growth on the heat-transfer surface a behavior opposite that seen in the rate parameters for primary nucleation was observed. For crystal growth on the hot surface, the rate parameter for growth of crystals of double salts was increased by the addition of EDTA. For anhydrous sodium carbonate, the two parameters are identical. This is additional evidence that calcium did not influence anhydrous sodium carbonate.

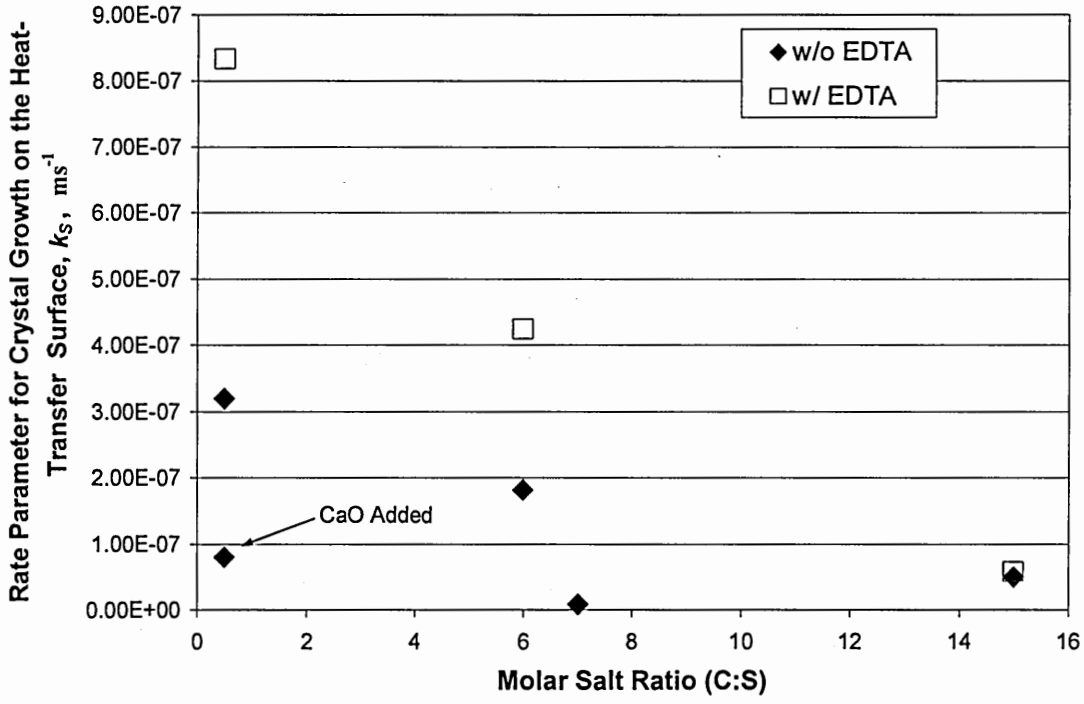

Figure 5.15: Influence of calcium on the rate parameter for crystal growth on a heat-transfer surface at four different ratios of Na_2CO_3:Na_2SO_4.

More important is the observation that the rate parameter for crystal growth on the heat-transfer surface was greater when calcium was not allowed to act as an inhibitor. This indicates that the inclusion of calcium as a lattice defect is not limited to nucleation. Rather, calcium acts as both a nucleation and a growth inhibitor.

5.4.3.3. Conclusions for the Calcium Inhibition Study

The most significant conclusion of this portion of this work is that calcium acts as both a nucleation and a growth inhibitor. Further work is required to determine the relative inhibition for bulk and surface nucleation and for bulk and surface growth. Without this additional data, no conclusions can be drawn regarding the possible benefit of operating at a given calcium concentration in black liquor.

One conclusion that can be drawn is that operating with a variable calcium level would be likely to lead to fouling conditions in industrial black liquor evaporators. This is because fluctuating calcium levels will cause the supersaturation to also fluctuate. When the level of calcium decreases, only nucleation or growth will reduce the supersaturation. If operating conditions are in a transition region where a new salt species might nucleate, then increasing and decreasing the supersaturation without a stable bulk crystal population may lead to heavy fouling as supersaturation is reduced by nucleation and growth on the heat-transfer surface when they are not inhibited by the calcium.

5.5. Conclusions for Experimental work Conducted with Aqueous Solutions on the Pilot-Scale Falling-Film Apparatus

The pilot-scale falling-film evaporator provided simultaneous data for crystallization in the bulk solution and on the heat-transfer surface. Analytical methods were developed to determine crystallization rate parameters from the results for semi-batch experiments. Models estimating the rate parameters for primary bulk nucleation and fouling of heat-transfer surfaces that are dependant on the studied variables were developed. The estimated rate parameters were used to confirm that calcium acts as both a nucleation and growth inhibitor for both burkeite and dicarbonate.

Several additional observations were made. One of these was that the dicarbonate species that can crystallize from aqueous solutions is not stable, and decomposes to burkeite and sodium carbonate. This finding is extremely significant in terms of developing a solution to the problem of fouling in black liquor evaporators. The standard

methodology for control of fouling during evaporative crystallization in black liquor evaporators for many years has been to maintain a crystal population in the bulk solution of any potential species that might scale out on the heat-transfer surface. The goal is to avoid conditions where primary nucleation might occur. Generally, seeding crystallizing evaporators with product liquor during start-up accomplishes this task. However, if the dicarbonate species is not stable, even for short time periods (days), then seed liquor may not contain any dicarbonate seed crystals. This could lead to conditions where primary nucleation of dicarbonate would occur, and fouling rapidly the heat-transfer surface in the black liquor concentrators.

5.6 Acknowledgements

Steve Lien and Gary Heedick from IPST deserve special thanks for conducting the calcium inhibition pilot-scale experiments that were presented in this chapter. At the author's suggestion, and after discussions with Steve Lien and Wolfgang Schmidl at IPST, these experiments were conducted. The raw data was provided to the author for analysis and inclusion in this thesis. Without these individual's help conducting the evaporation experiment, it would not have been possible to include these results in this thesis.

5.7. Variables

C Concentration, $kg \cdot m^{-3}$

C_1 Fitting parameter, Equation 5.5

C_2 Fitting parameter, Equation 5.6

G Bulk growth rate, $m \cdot s^{-1}$

G_S Surface growth rate, $m \cdot s^{-1}$

J_O Nucleation rate, $m^{-3}s^{-1}$ (Volume) or $m^{-2}s^{-1}$ (Surface)

k_G Growth rate parameter, $m \cdot s^{-1}$

k_N Nucleation rate parameter, $m^{-3}s^{-1}$

k_S Surface growth rate parameter, $m \cdot s^{-1}$

m_0 0^{th} Particle population moment, m^{-3}

R_F Thermal fouling, $m^2K \cdot W^{-1}$

Re_Γ Plate Reynolds number

T Temperature, K

t Time, s

U Overall heat transfer coefficient, $W \cdot m^{-2}K^{-1}$

α Fitting parameter, Equation 5.6

σ Relative supersaturation

Superscripts and Subscripts

^{i} Nucleation order

$_s$ Steam

$_{Sat}$ Saturated condition

* Equilibrium

5.8. Bibliography

1. Smith, J.B., Sodium Salt Scaling in Falling Film Black Liquor Evaporators, *Ph.D. Thesis*, Georgia Institute of Technology, 2000
2. Shi, B., Crystallization of Solutes that Lead to Scale Formation in Black Liquor Evaporation, *Ph.D. Thesis*, Georgia Institute of Technology, 2002.
3. Mullin, J.W., *Crystallization*, 3rd Edition, Butterworth Heinemann, Boston, 1997
4. Sinquefield, S.A, A Microcomputer Software Package for Simulation of Non-Ideal Aqueous Electrolyte Systems at Equilibrium, *M.S. Thesis*, Oregon State University, 1991
5. Golike, G.P., Q. Pu, K.L. Holman, K.R. Carlson, P.C. Wollwage, H.G. Folster and S. Rankin, NAELS: A New Method for Calculating Equilibrium Solubility of Burkeite and Sodium Carbonate in Black Liquor, *1998 International Chemical Recovery Conf.* pp. 403-418
6. Seidell, A. and W. Linke, *Solubility of Inorganic and Metal Organic Compounds*, Vol. II, 4th ed.: 1121, Van Nostrand, Princeton (1965)
7. *MINITAB User's Guide 1: Data, Graphics, and Macros*, Release 13, 1999
8. *MINITAB User's Guide 2: Data Analysis and Quality Tools*, Release 13, 1999

Chapter VI: Pilot Evaporation Studies with Black Liquor Solutions

6.1. Objectives

Crystallization in bulk black liquor and rates for fouling of the heat-transfer surface will be measured simultaneously during evaporation experiments using the falling-film pilot-scale apparatus with the objective of determining the crystallization events that lead to rapid fouling during the concentration of black liquor. The methodology developed in Chapter 5 for estimating rate parameters for primary nucleation and growth in bulk solutions and growth of crystals on a heat-transfer surface will be extended to black liquor in this chapter. Estimated rate parameters will be used to determine the influence of changes in the liquor composition, specifically the ratio of Na_2CO_3:Na_2SO_4, on the bulk crystallization and fouling of the heat-transfer surface. The rate parameters will also be used to evaluate a number of alternatives for reducing fouling in black-liquor evaporators

Another key objective of this work will be to determine the role played by the dicarbonate species identified by Shi [1] on fouling in the 65%-80% total solids content liquor composition range.

6.2. Introduction

Before Shi's work [1], no attempt to measure particle populations *in situ* for black liquor solutions had been published due to the inherent difficulties in conducting this

measurement. Simultaneous observation of crystallization in the bulk liquor and fouling on the heat-transfer surface has never been published previously.[1]

FBRM provided continuous monitoring of the particle population in black liquor as it did for the aqueous solutions studied in Chapters 5. However, there are several differences between aqueous solutions and black liquor. One significant difference is that black liquor is composed of both water and dissolved organic material. The dissolved organics adsorb infrared radiation. The adsorption of the FBRM laser changes as water is evaporated and the ratio of the mass of dissolved organic material to the mass of water increases. This was dealt with in this work using Beer's law. Another effect of the organic material is that laser penetration depth should be reduced. Thus, the sample volume would be significantly less. Also, the viscosity is much greater, and changes with total solids content and temperature, which should change the flow dynamics around the FBRM probe.

Of these differences, one calls for a significant assumption. Unlike the aqueous salt solution work for which an educated estimate could be made, there is no published work on the effective depth of laser penetration for the FBRM in black liquor. As this is outside of the scope of this work and the experimental equipment for obtaining this measurement was unavailable, an educated guess of 100 μm has used in this research. This was based on the observation that very few particles had chord lengths over 100 μm for CCDs measured in black liquor. Since many crystals observed in black liquor are roughly spherical agglomerates [1], geometric arguments would suggest that the effective

[1] Weyerhaeuser Company experimented with FBRM for particle population tracking at a mill location before suggesting the idea to the GIT/IPST evaporator consortium. However, none of their work has been published.

penetration depth would be 100 μm and any particle over 100 μm would have non-spherical geometry.

The work reported here covers three studies conducted using black liquors from two kraft pulp mills, identified as Mill A and Mill B. The first study characterized bulk crystallization and fouling of heat-transfer surfaces when evaporating black liquor. The second study examined liquor from Mill B to determine the effect on crystallization, both in the bulk solution and on the heat-transfer surface, caused by a change in the liquor composition. The third study was a joint research project between a sponsor company, the Institute of Paper Science and Technology and the Georgia Institute of Technology. A number of potential methods for controlling evaporator fouling at Mill A were evaluated, with the goal of reducing fouling at this mill. These methods have not been formally evaluated or presented previously.

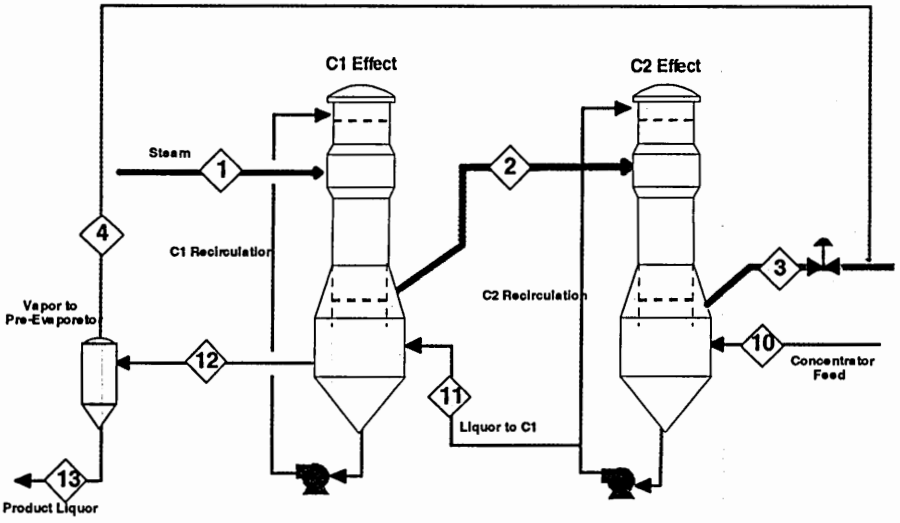

Figure 6.1: Process flow diagram of the black liquor concentrators at Mill A.

The evaporation capacity at Mill A is limited by fouling of the heat-transfer surface in the first effect (C1) of a two-effect, tube-type, falling-film, crystallizing

concentrator set. The concentration of the product liquor from effect C1 ranges from 66% to 72% total solids content. Figure 6.1 is a process diagram of the black liquor concentrators at Mill A.

Two major process streams are merged at the high solids concentrators. They are (a) the virgin black liquor from the low solids evaporator train, and (b) brine (an aqueous solution of Na_2SO_4 solution) from precipitator ash recovered from the exiting gas stream from the recovery boiler.

At the time of this study, the brine stream was being added to the feed tank for the C2 concentrator effect, along with black liquor at a total solids content of 50%. The C2 effect concentrated the liquor to ~55-60% total solids content. The product liquor from this effect was fed to the C1 effect, which produced black liquor at 66-72% total solids content. Under normal operating conditions, the heat-transfer surface of the C1 effect fouled rapidly, usually requiring cleaning[2] within one to seven days.

In this study, several options were evaluated for reducing the rate of fouling of the heat-transfer surface in the C1 concentrator effect at Mill A. The options evaluated were chosen because each had the potential to change the crystallization behavior in the C1 effect in a way that might reduce fouling of the heat-transfer surface in that effect. Also, each of the methods evaluated could be implemented at Mill A without a large capital investment.

[2] Regular cleaning of the C1 effect is performed by filling the effect with weak black liquor, boiling the liquor, and recirculating it until the Na_2CO_3-Na_2SO_4 scale has been dissolved completely.

6.3. Procedure

These pilot-scale evaporations of black liquor were performed on the falling-film dimple-plate evaporator located at the Institute of Paper Science and Technology. The physical apparatus has been previously described in Chapter 3 of this thesis so only experimental details are addressed here.

During the experiments, the pilot evaporator was operated in either batch or semi-batch mode. In the batch mode, black liquor was charged to the sump of the evaporator, and the total volume of black liquor within the evaporator was allowed to decrease as evaporation proceeded. In the semi-batch mode, black liquor was charged to the sump prior to the start of an experiment, and fresh liquor was fed continuously to the evaporator during the experiment, to maintain a constant total volume of black liquor within the evaporator. Evaporation rates of 3 to 12 ml/s were achieved. Except for small samples for chemical analysis, no black liquor was removed from the evaporator during the experiments.

The black liquors used in this work were obtained from two different kraft pulp mills. Both are located in the Southeastern United States and both produce softwood pulps. They are referred to here as Mills A and B. Other materials were obtained from Mill A for addition to the black liquors during the pilot evaporator experiments. The chemical compositions of the as-received black liquors and the other materials are given in Table 6.1. Analysis of these materials was performed at by the Chemical Analysis Laboratory of the Institute of Paper Science and Technology.

Table 6.1: Inorganic chemical constituents in the two virgin black liquors used in this study. The black liquor, lime mud solids, and ESP ash data are as wt% of dry solids. The ESP ash brine data are on a wet basis.

Analyte	Mill A Liquor As Received	Mill B Liquor As Received	ESP Ash Dissolved Brine	Lime Mud Solids	ESP Ash
Total solids content	50	47.20	25.7	67.400	
Na_2S	6.5	6.37		<0.01	
NaOH	5.9	5.08	<0.01		
$CO_3^=$	4.33	3.9	1.29	52.8	7.4
HCO_3^-			0.34		
$SO_4^=$	2.99	2.42	14.32	0.01	54.5
$S_2O_3^=$	4.52	3.02	<0.40	<0.01	
Cl^-	<0.2	0.337	4.27	<0.1	10.1
Na_2CO_3/Na_2SO_4	1.73	1.92	7.87		
Na	20.2	17.2	4.75	0.73	30.6
S	5.15	4.68	0.34	0.04	
K	0.54	1.34	0.34	0.004	1.77

6.3.1. Liquor Crystallization and Fouling Behavioral Study

Liquors from Mills A and B were used to study the crystallization behavior of sodium salts in black liquor when concentrated from below the solubility limit (usually less than 50% total solids content) up to between 70% and 75% total solids content. The experiments were conducted with the same rates of recirculation of black liquor, but the initial heat flux and the vapor pressure on the liquor side differed, Table 6.2 presents these differences.

Table 6.2: Operating conditions for all experiments using the two different mill liquors.

Mill	Initial Heat Flux (Wm^{-2})	Vessel Pressure (bara)
A	21000	1.496
B	13000	1.531

During the evaporation runs, steam pressure, liquor temperature, and condensate flow rates were measured every 0.1 min. for calculation of overall heat-transfer coefficients. Particle population data were collected by FBRM every 0.17 min. Filtered and unfiltered liquor samples were collected approximately every 30 min. during each run.

6.3.2. Black Liquor Inorganic Composition Study

Experiments were conducted using the liquor from Mill B, both as-received and with approximately 2.64 wt% of industrial grade anhydrous Na_2CO_3 added per initial mass of black liquor solids. These experiments were conducted to determine the influence of changes to the inorganic composition of black liquor on crystallization in the bulk liquor and on the heat-transfer surface. Two repeat experiments were conducted at the two different inorganic compositions.

6.3.3. Black Liquor Fouling Reduction Study

Five experiments were conducted to quantify repeatability in this work. Two experiments with the as-received black liquor from Mill A were conducted, followed by three experiments with the as-received black liquor with brine (an aqueous solution containing mainly Na_2SO_4) from the bleach plant added. These initial experiments were followed by a total of seven experiments designed to evaluate a number of potential methods to control fouling of heat-transfer surfaces in black liquor evaporators. Four materials were evaluated to determine if their effect on fouling and their potential to control it. They were (a) brine from the bleach plant, (b) dry precipitator ash (mainly Na_2SO_4) recovered from the recovery boiler (c) lime mud, and (d) anhydrous Na_2CO_3, which could be used as a makeup chemical to replace sodium losses.

The impact of adding dry precipitator ash on the fouling rate was evaluated. The dry ash was added to black liquor that had previously been concentrated to 58% total solids content. This was done to test whether the precipitator ash would reduce fouling by providing a greater surface area of crystalline material to relieve supersaturation via

crystal growth on that material. A total solids content of 58% was selected because it represented the typical concentration of black liquor from the C2 effect, and because it was above the solubility limit of Na_2CO_3 and Na_2SO_4 in the black liquor. This experiment was intended to determine whether or not the species crystallizing from the black liquor would crystallize on particles of dissimilar composition and crystal structure, potentially reducing the rate of deposition on the heat-transfer surface.

Anhydrous sodium carbonate was evaluated to determine if it would provide a surface for growth that would reduce dissolved sodium carbonate levels in the black liquor and postpone or eliminate fouling. One Na_2CO_3 experiment was conducted with the black liquor as received. A second experiment with Na_2CO_3 addition was conducted with as-received liquor to which brine had been added.

Calcium carbonate acts as an inhibitor for both nucleation and growth of crystals of Na_2CO_3 and Na_2SO_4 [1]. Lime mud was added to evaluate the hypothesis that it would produce calcium ions that would inhibit the nucleation of dicarbonate so that nucleation would not occur within the C1 effect.

The combined impacts of a longer residence time of black liquor in the evaporator sump and reduced heat flux on fouling of the heat-transfer surface were evaluated simultaneously in one experiment. The hypothesis was that both of these changes would reduce supersaturation, and therefore reduce the rate of fouling. The residence time of black liquor in the evaporator sump was increased by increasing the volume of black liquor in the sump while maintaining the same liquor circulation rate. In addition, the steam pressure was reduced by approximately 5-7 psig throughout the experiment, to lower the evaporation rate. This reduced the heat flux approximately 28%.

In all of the fouling reduction studies in which a solid material was added, the liquor was removed from the evaporator for the purpose of adding the material, as no *in situ* addition method was available. While the evaporator was empty, the heat-transfer surface was washed with water to remove any scale or dried liquor that might have remained on it when the liquor was removed. This was done so that the heat-transfer surface would be clean when evaporation began again.

Table 6.3 shows how the various liquor mixtures were prepared so as to conduct these experiments.

Table 6.3: Components in the black liquors used to test various options for reducing fouling. The liquors were all from Mill A.

Experiment	Starting Volume of Liquor, gallons	Initial Brine Added to BL	Added to BL at 55-59%
As Received	44 gal. Virgin BL		
As Received + Brine	44 gal. Virgin BL	4 gal. Brine	
Brine to C1	44 gal. Virgin BL		4 gal. Brine
Brine to C1	44 gal. Virgin BL		4 gal. Brine
Dry ash to 58% liquor	40 gal. Virgin BL		9.4 lb. dry ash
Na_2CO_3 – As Received	40 gal. Virgin BL		50 g Na_2CO_3
Na_2CO_3 – As Received + Brine	36 gal. Virgin BL	3.25 gal. Brine	50 g Na_2CO_3
Lime mud	40 gal. Virgin BL		83 g lime mud (wet)
Sump retention time	40 gal. Virgin BL	3.6 gal. Brine	

6.4. Results and Analysis

To analyze the experimental results for crystallization in the bulk liquor and on the heat-transfer surface, it is critical to have some understanding of the solubility of Na_2CO_3 and Na_2SO_4 in black liquor. Chapter 2 discusses the previous work on the solubility of sodium salts (particularly those composed of carbonate and sulfate), so for this chapter only the relevant information for how their solubility was estimated and the results are provided.

The solubility of Na_2CO_3 and Na_2SO_4 in the black liquors used in this study was estimated using the NAELS thermodynamic equilibrium software [2, 3]. Estimations

were made for the as-received black liquors and for those liquors after the addition of the applicable sodium salts. To simplify the presentation of results, the estimations were made at a single temperature of 130°C, rather than over the range of temperatures (normally 120°C to 135°C) encountered in each evaporation experiment This specific temperature was chosen because it was the average temperature at which fouling was observed.

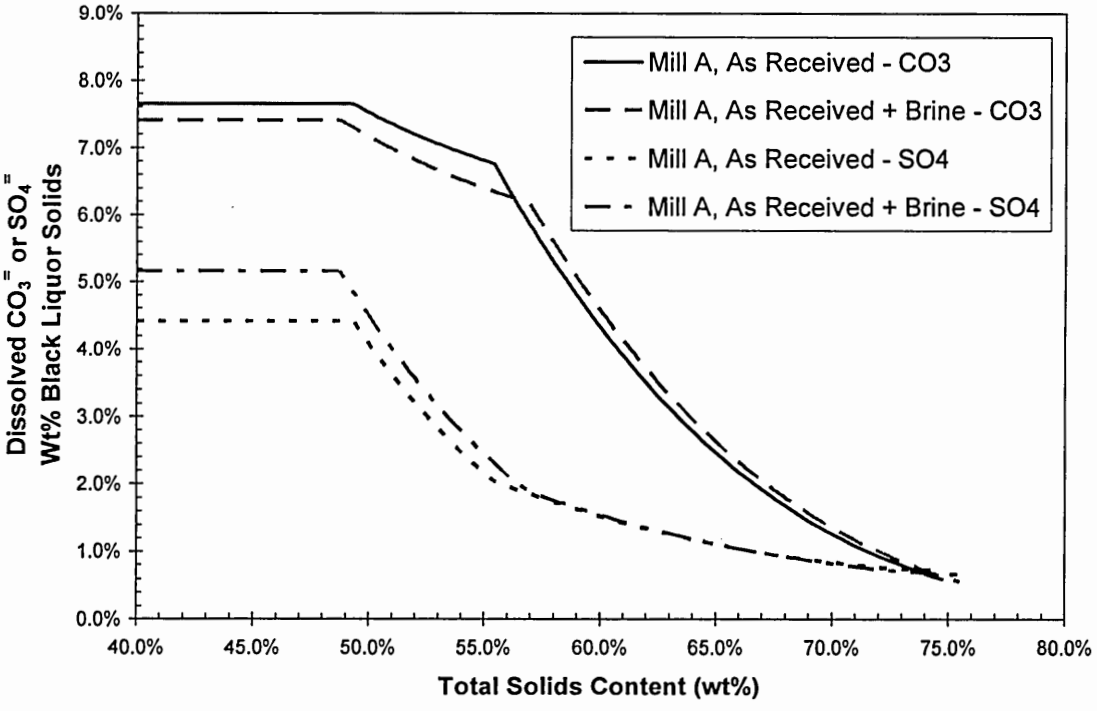

Figure 6.2: Carbonate and sulfate concentrations at equilibrium at 130°C versus total solids content for the as-received and modified Mill A black liquors

Figures 6.2 and 6.3 present the estimated solubility results. The curves in each figure represent the total amounts of CO_3^{2-} and SO_4^{2-} per unit of black liquor solids that would remain soluble at equilibrium as the black liquors were concentrated from 40% to 75% total solids content.

The results in Figures 6.2 and 6.3 indicate that addition of Na_2SO_4 or Na_2CO_3 to black liquor reduces the total solids content of the liquor at which it is saturated with

these two salts. Also, the location of the transition from burkeite to Na_2CO_3 as the crystalline species at equilibrium changes with the ratio of sodium carbonate to sodium sulfate in the liquor. An increase in this ratio lowers the total solids content at which the transition occurs, while a decrease has the opposite effect.

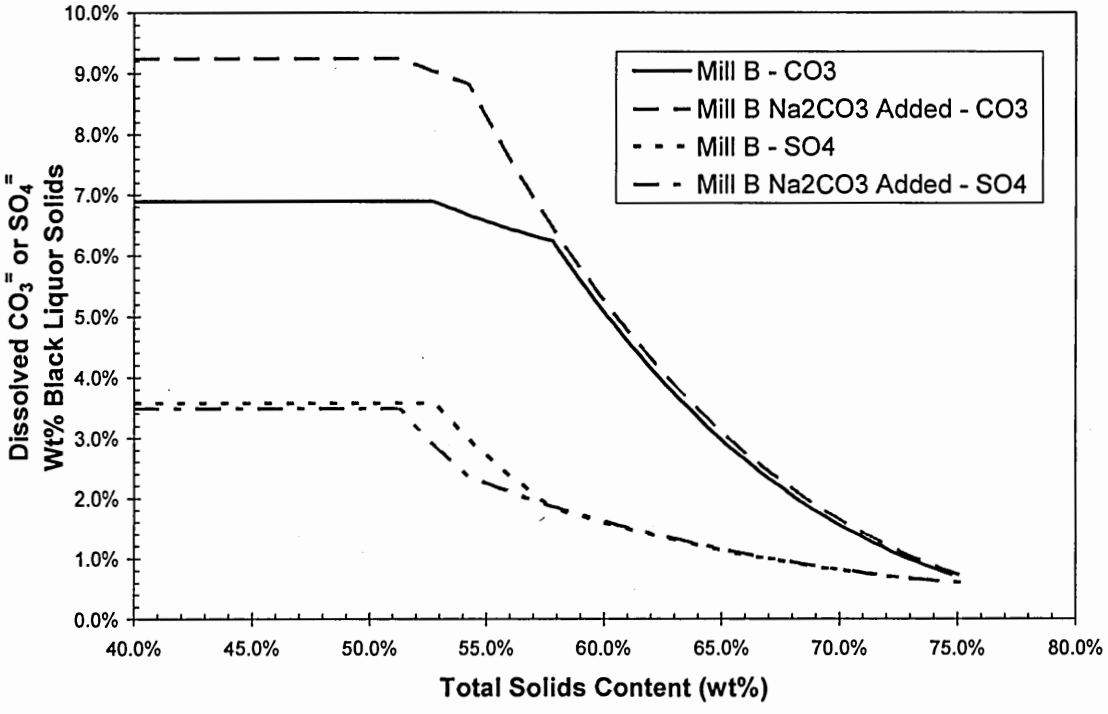

Figure 6.3: Carbonate and sulfate concentrations at equilibrium at 130°C versus total solids content for the as-received and modified Mill B black liquors.

6.4.1. Analysis of Heat Transfer and FBRM Results for Evaporation of Black Liquor Solutions

Heat transfer and crystallization data were acquired continuously for every run. Black liquor samples were collected periodically from the liquor recirculation line of the evaporator during each run. They were analyzed for total solids content to provide the relationship between time and total liquor solids content for that run.

The overall heat-transfer coefficients, *U(t)*, were used to evaluate the onset and rate of fouling. *U(t)* was calculated as:

$$U = \frac{q}{A\Delta T}. \tag{6.1}$$

In Equation 6.1, q is the rate of heat transfer from the condensing steam to the liquor. It is calculated from the measured steam condensate flow rate and the latent heat of vaporization evaluated at the measured steam pressure as discussed in Chapter 3 of this thesis. A is the heat-transfer surface area (12 ft^2 or 1.1 m^2) and ΔT is the difference between the saturation temperature of the condensing steam and the liquor temperature in the sump.

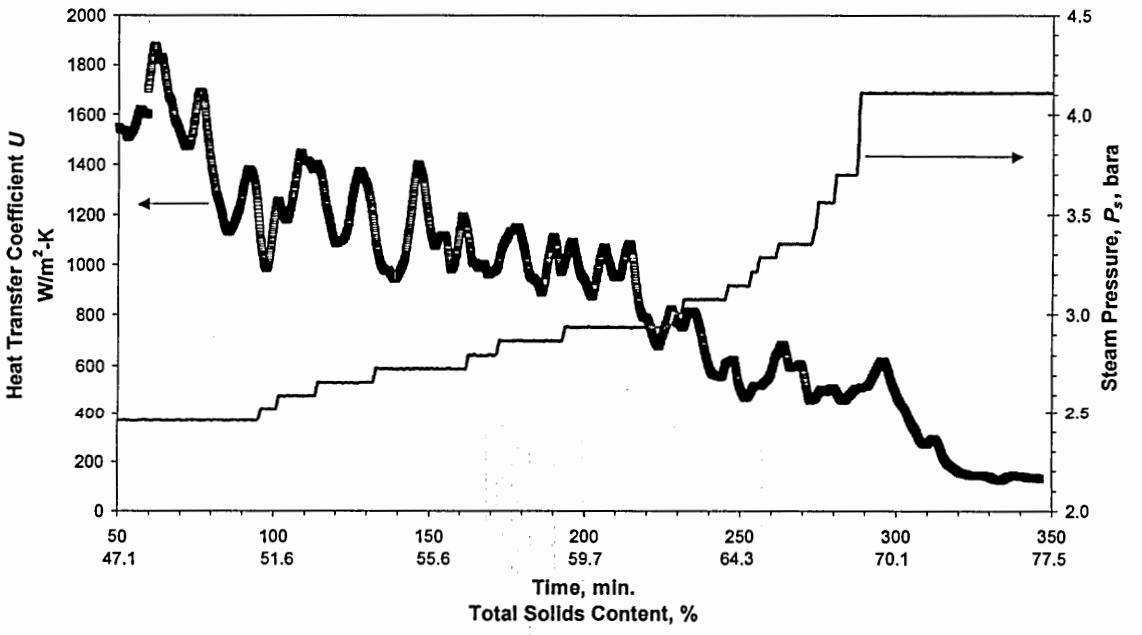

Figure 6.4: The apparent heat-transfer coefficient and steam pressure versus time and the corresponding total solids content of the black liquor during evaporation with black liquor from Mill B

Figure 6.4 shows the estimated heat-transfer coefficients during the experiment. As the liquor was concentrated, the temperature of the liquor increased for a given pressure in the vapor body due to the boiling point rise. In order to maintain a relatively

steady evaporation rate, the steam pressure had to be gradually increased as the run proceeded. Figure 6.4 also shows how the steam pressure was increased during the experiment.

Figure 6.4 also shows the effect of changes in viscosity on the heat-transfer coefficient that was discussed in Chapter 3 of this thesis. During the first part of the experiment a relatively constant reduction occurred in the heat-transfer coefficient. After approximately 300 minutes, this slow decrease transitioned to a rapid decline.

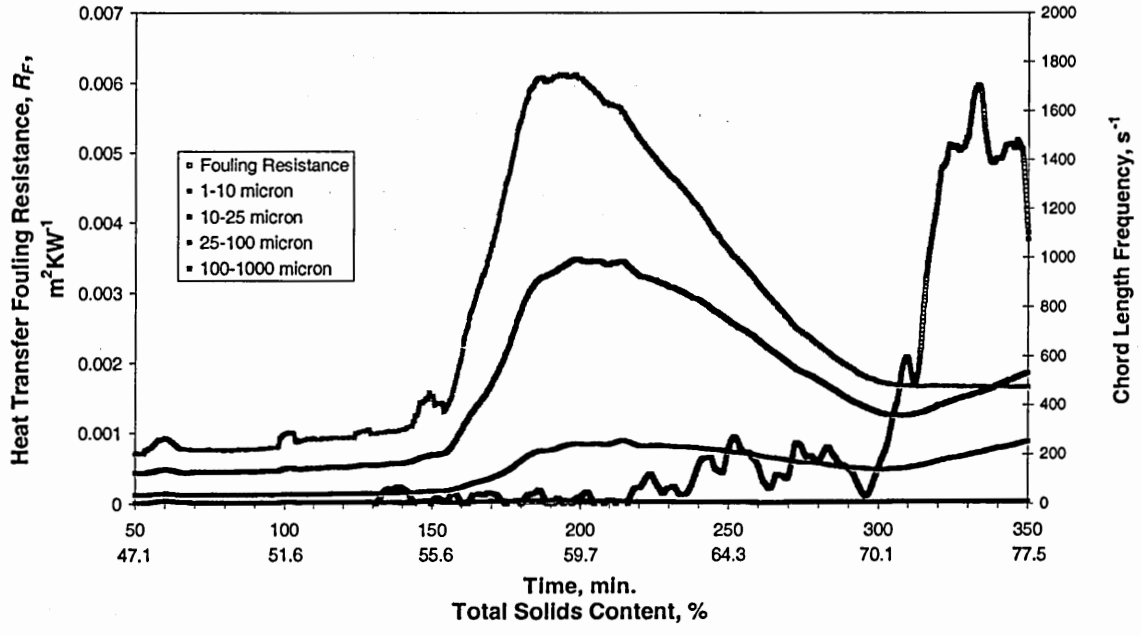

Figure 6.5: The heat-transfer resistance due to fouling and the number of crystals observed in four different chord length ranges versus time and the corresponding total solids content of the black liquor for the same experiment shown in Figure 6.4

Figure 6.5 shows the heat-transfer resistance due to fouling for this experiment after the heat-transfer resistance ($1/U$) has been corrected to account for the effects of viscosity. Figure 6.5 also shows FBRM particle population data for this experiment.

The particle population underwent three distinct transitions during the experiment shown in Figure 6.5. The first transition corresponds to bulk nucleation and is observed around 150 minutes (55% total solids content). The second transition is observed

between 200 and 300 minutes. No final conclusion for the cause of this transition has been reached. However, a number of potential explanations have been provided.

It should be noted that a declining particle population is not a cause for concern theoretically. In fact only the 3rd (mass) moment of a particle distribution should not decrease during a batch concentration of this type. And as previously mentioned, the 3rd moment should not be considered reliable when using FBRM data due to the concerns discussed in Chapter 4 of this thesis. There appears to be a two-fold answer to what is occurring in the second transition region. First, agglomeration combined with equipment scan depth limitations can explain the disappearance of smaller particles from the system without a simultaneous increase in larger particles. The least dramatic change in particle counts was observed in the smallest size range. Second, the presentation of particles to the FBRM probe may have changed in this region. At the same time the particle counts declined, the liquor viscosity was increasing to the point where the Reynolds number in the pipe where the FBRM probe is mounted became laminar. From an equipment standpoint, there were no changes that could be made to shift back into a turbulent regime, as the pipe diameter was already the minimum allowable for mounting the FBRM probe. Combining the agglomeration and viscosity issues provides a potential explanation for the population observations. Because of the ambiguity about the exact phenomena responsible for the second transition, this work has ignored this region of the particle population data and focused on the third characteristic transition instead.

The third transition was an apparent second nucleation point corresponding with nucleation of the dicarbonate double salt ($2Na_2CO_3 \cdot Na_2SO_4$). The salt species nucleating was confirmed using powder X-ray diffraction as shown in Figure 6.6. Due to

contamination with black liquor solids, the diffraction spectrum of the sample was particularly noisy. However, when compared to a clean diffraction spectrum for this crystal [1], four distinct peaks clearly identify this as a sample composed primarily of dicarbonate.

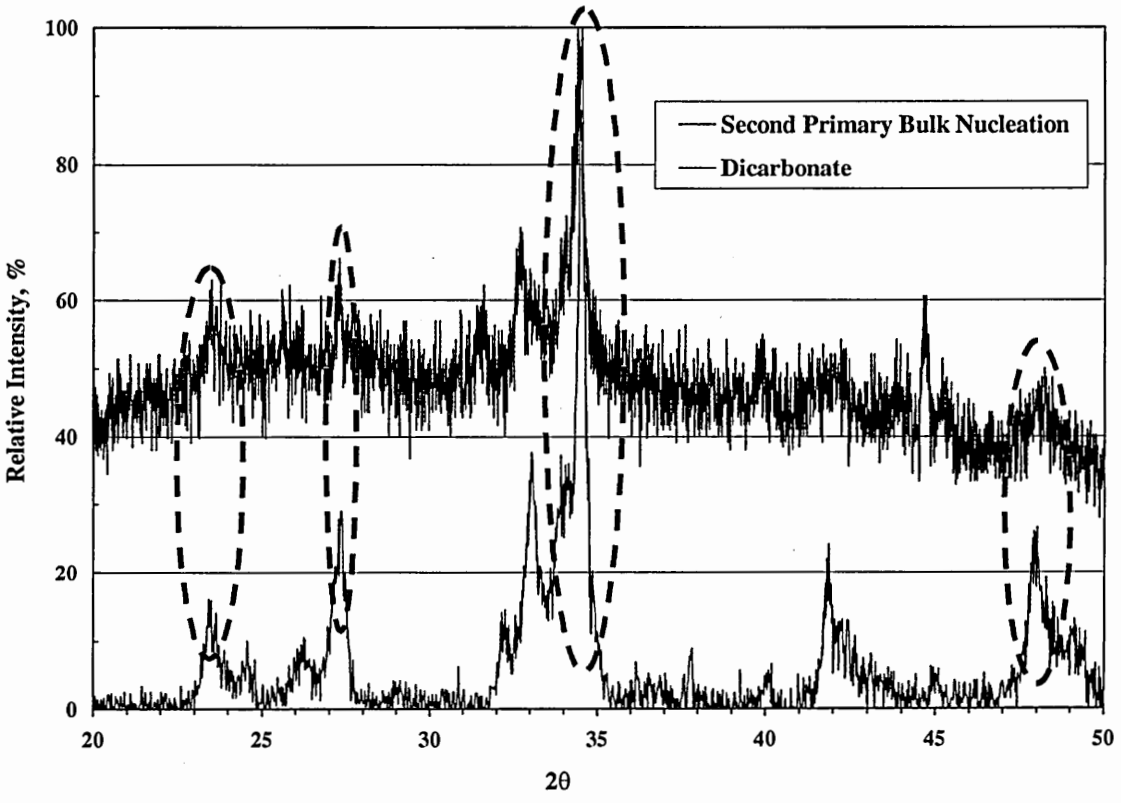

Figure 6.6: Powder x-ray diffraction spectra identifying the second salt nucleated as dicarbonate

In Figure 6.5, the second nucleation point was seen at 310 minutes as the particles counted in the two smallest size ranges begin to increase. This was confirmed by reviewing the 0^{th} moment of the particle population, that is, the total number of particles in the system. Figure 6.7 shows the trend for the 0^{th} moment in addition to the first derivative of this moment with time. The time derivative provided an estimation to be made of the two bulk nucleation rates, $J_{0,1}$ and $J_{0,2}$.

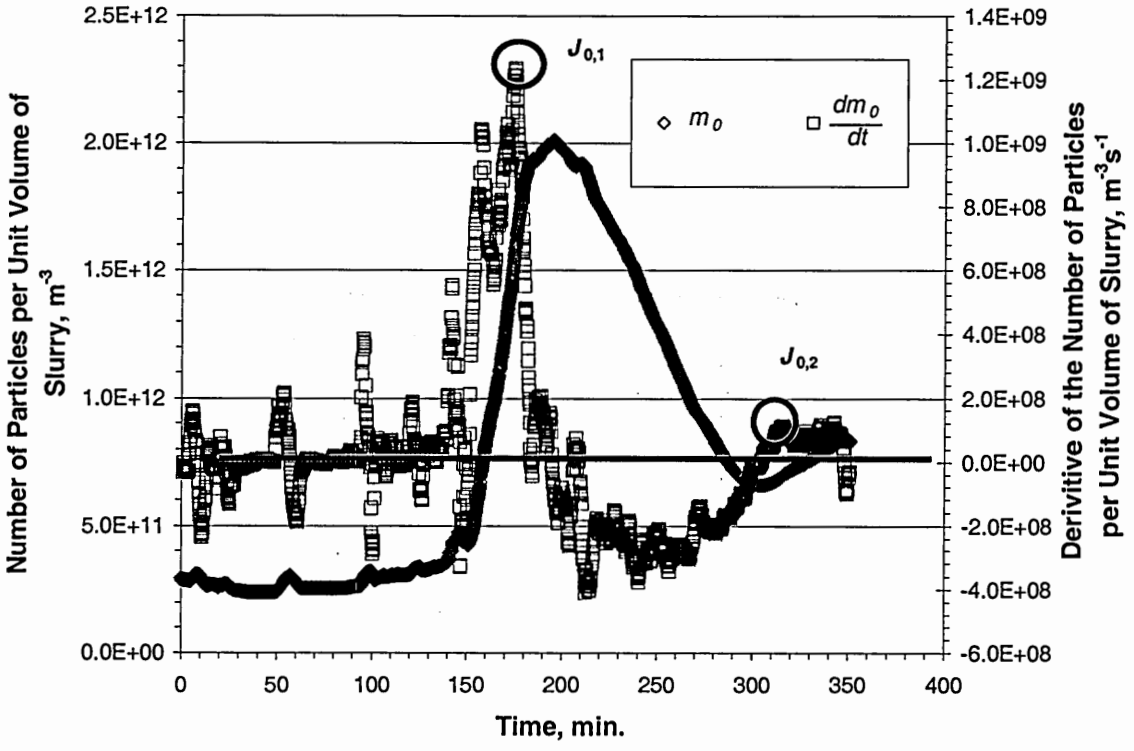

Figure 6.7: 0^{th} moment of the particle population and the time derivative of 0^{th} moment for the experimental data in Figure 6.5analyzed to determine the nucleation rates, $J_{0,1}$ and $J_{0,2}$

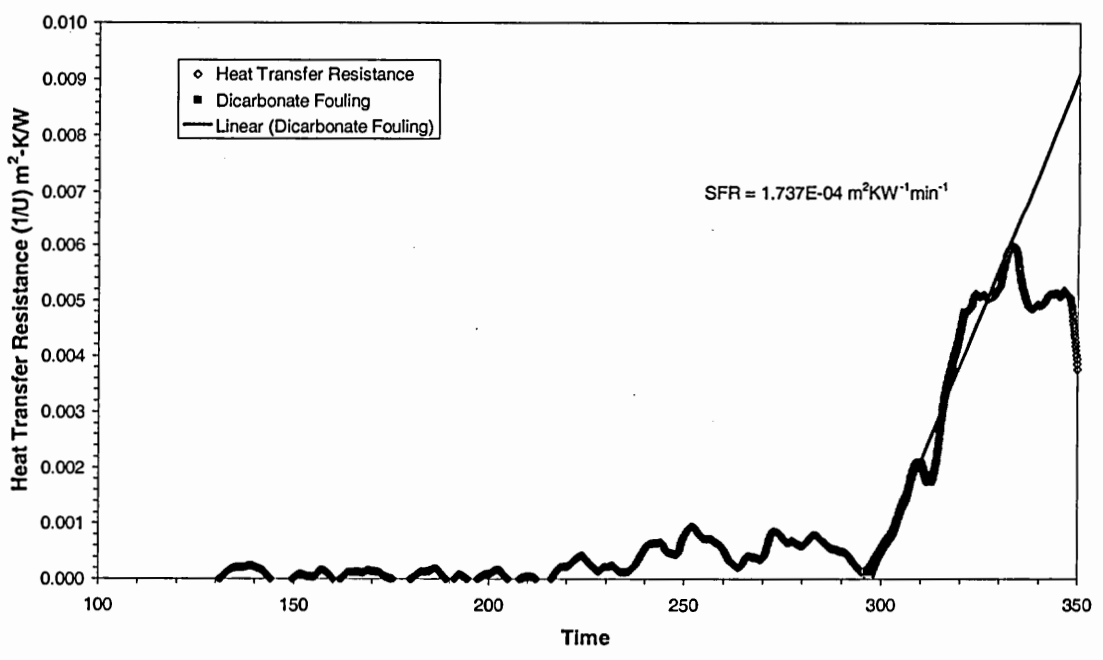

Figure 6.8: Determination of the surface-fouling rate from heat-transfer resistance data

Figure 6.8 presents the same heat transfer resistance data as Figure 6.5, but with a regression fit line added for the surface-fouling rate. The resistance behavior can be best described as constant through approximately 225 minutes. Between 225 minutes and 300 minutes fouling does appear to have occurred on the plate, but it was sporadic and appeared to slough off of the plate at times (at 255 minutes for example). After 300 minutes, rapid fouling occurred. The heat transfer resistance increased to a point where the maximum steam pressure was reached and the plate temperature could no longer be raised to drive evaporation. The estimated surface fouling rate in Figure 6.8 corresponds to $G_S = 5$ μm/s for a $k_F = 1.73$ $W \cdot m^{-1} K^{-1} m$. The thermal conductivity, k_F, was estimated by Smith [4].

This growth rate is high for an inorganic salt, but is certainly possible at high supersaturation [5, Table 6.1]. To determine the supersaturation required a number of assumptions be made.

Obtaining crystal-free samples of black liquor through a filter is extremely difficult. Several attempts to obtain filtered liquor samples for analysis in order to determine dissolved solids concentrations for the relevant species and use them to determine supersaturation were made during these studies. Sampling issues combined with analytical costs made this approach unworkable. Because of these difficulties, another method was developed to estimate supersaturation.

This estimation of the level of supersaturation was based on two key assumptions. The first assumption is that NAELS provides an accurate prediction of the inorganic ion composition of the liquor. This is important because the ratio of dissolved carbonate to sulfate determines what salt crystallizes from the solution [1]. The second assumption is

that the actual solution composition matches the solubility limit of any species when crystals of that species are present.

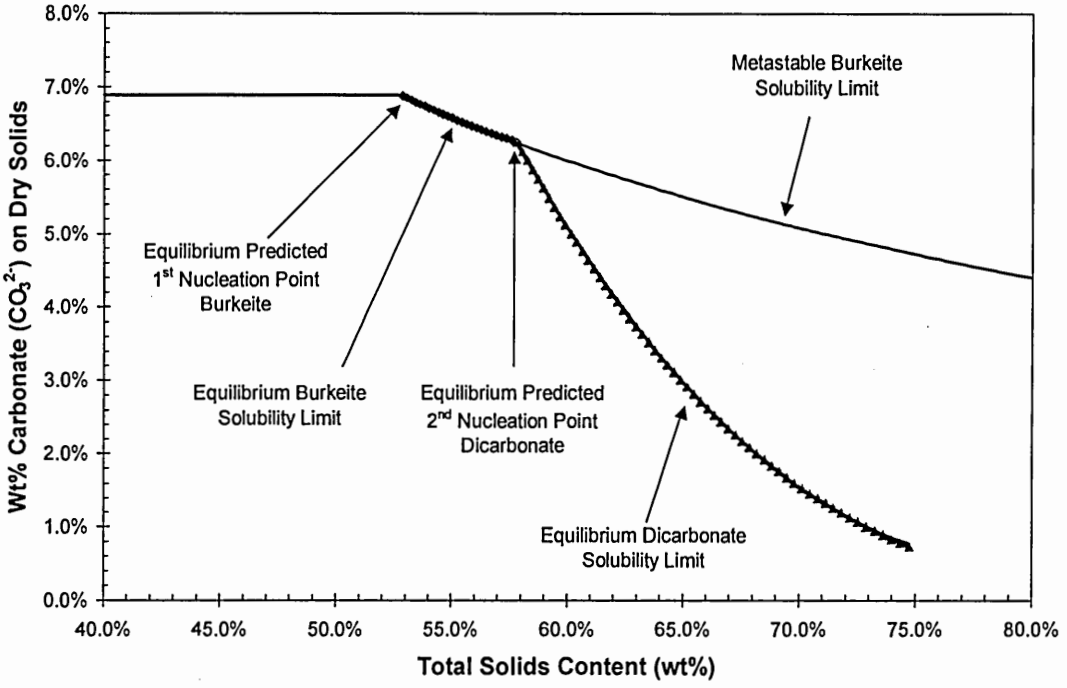

Figure 6.9: Representation of the solubility curves for burkeite and dicarbonate in black liquor.

Figure 6.9 shows the solubility and metastable behavior of burkeite as well as the presumed solubility of dicarbonate. The second assumption listed previously means that when burkeite crystals are present, the solution composition matches the burkeite solubility curve (either in the equilibrium or metastable region shown in Figure 6.9). As black liquor is concentrated and crystallization proceeds, the dissolved carbonate to sulfate ratio increases. However, the ratio of these anions in either burkeite or dicarbonate is nearly always less than in the solution from which they crystallize. This means that the dissolved carbonate to sulfate ratio is always increasing provided a double salt is being crystallized. This also means that relative supersaturation can be measured using the carbonate anion supersaturation. The relative supersaturation, σ, for $[CO_3]$ was used in this work to represent supersaturation,

$$\sigma = \frac{[CO_3] - [CO_3]^*}{[CO_3]^*}. \tag{6.1}$$

Equation 6.1 is the general definition of relative supersaturation. However, due to crystallization behavior, one small adjustment was made. During all of the black liquor experiments, the first primary nucleation in the bulk solution produced burkeite while the fouling on the heat-transfer surface and second primary nucleation in the bulk solution were dicarbonate. However, nucleation of burkeite did not always occur before the predicted transition to dicarbonate. In these cases, the relative supersaturation causing nucleation is not the supersaturation relative to the equilibrium condition, but rather the supersaturation relative to a metastable condition that is indicated in Figure 6.9. For these situations, the metastable solubility limit $[CO_3]^M$ was used in place of $[CO_3]^*$ in Equation 6.1.

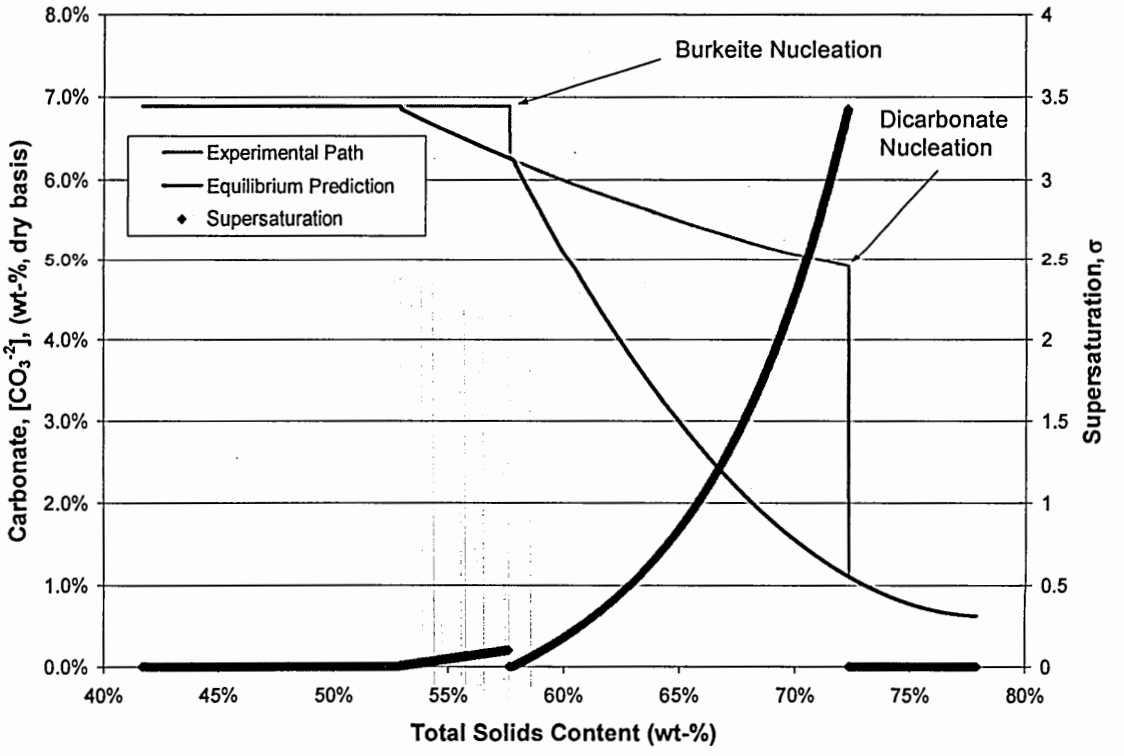

Figure 6.10: Estimate of the dissolved carbonate concentrations during an evaporation experiment and at equilibrium, and the relative supersaturation.

Applying this analysis method for to the experiment shown in Figure 6.5 produces the results shown in Figure 6.10. This figure indicates that the supersaturation at the actual burkeite nucleation point is only 0.1, similar to that seen in the aqueous salt solution work (where $0.1<\sigma<0.25$). This number compares well with the supersaturation seen in aqueous salt solutions where EDTA was added to bind the calcium ion.

The supersaturation at the point where fouling begins and the point where the second primary bulk nucleation event occurs are significantly greater if the assumptions used in this work are valid. For the experiment in Figure 6.10, fouling occurred at σ = 2.18 while secondary nucleation occurred at σ = 3.4. Both of these values are significantly greater than the supersaturation normally encountered in aqueous salt system (both sodium and other cations) [5, Table 6.1].

There are two possible reasons for this in black liquor. First, nucleation of dicarbonate is inhibited by calcium and at the higher liquor solids contents (and corresponding higher temperatures) where dicarbonate formed. At these temperatures, the concentration of calcium ions should increase because of the dissociation of calcium-organic complexes [6, 7]. Second, black liquor has a viscosity of several hundred centipoises in the solids content range where dicarbonate formed. This could cause nucleation to be inhibited by diffusion limitations.

For black liquor experimental work, two nucleation orders (values of *i*) can be obtained, one for each of the primary nucleation events in the bulk liquor. In the case of black liquor, no growth rate on the heat-transfer surface can be used to perform a fit like the one applied in Chapter 5 of this thesis for burkeite or dicarbonate due to differences in

the level of supersaturation when these events occurred. Instead, a least squares fit was applied using the data for the three repeat experiments conducted using as-received Mill A liquor with brine added. Using the empirical equation,

$$J_0 = k_N \sigma^i, \tag{6.2}$$

and knowing J_0 and σ, k_N was calculated, given an assumed i. Then, the square root of the sum of the errors squared for each individual k_N in the three experiments was calculated and minimized by adjusting i. This procedure yielded nucleation orders of 1.8 for burkeite and 1.6 for dicarbonate. These are both close to the 2.0 nucleation order for burkeite measured in aqueous salt solutions.

6.4.2. Influence of Na_2CO_3:Na_2SO_4 on Bulk Nucleation and Surface Fouling

This set of experiments was conduced to answer the fundamental question of how a change in the inorganic composition, specifically the ratio of Na_2CO_3:Na_2SO_4, would change the bulk and surface crystallization. As Figure 6.3 shows, the first predicted solubility limit for the liquor from Mill B as it was concentrated decreased by approximately 1.5 wt% total solids content when sodium carbonate was added to the black liquor. The transition from bukeite to dicabonate decreases by 3.6 wt% total solids content for the change in liquor composition.

Table 6.4: Nucleation and surface growth rate results from evaporation of black liquor from Mill B

Mill B Sample Description	1st Nucleation Solids Content	$J_{0,1}$ $m^{-3}s^{-1}$	2nd Nucleation Solids Content	$J_{0,2}$ $m^{-3}s^{-1}$	Surface Fouling Solids Content	G_S $m \cdot s^{-1}$
As Received	57.6%	1.23E+09	72.3%	1.13E+08	69.7%	5.01E-06
As Received	58.8%	2.35E+09	71.0%	7.68E+08	69.7%	2.17E-05
As Received+Na_2CO_3	55.2%	2.19E+08	69.0%	1.67E+08	61.7%	1.48E-06
As Received+Na_2CO_3	57.9%	9.16E+08	72.8%	8.42E+07	67.5%	3.22E-05

When the crystallization rates in Table 6.4 are analyzed, the average measured first nucleation point decreased by 1.6 wt-%, in the liquor spiked with Na_2CO_3, approximately equal to the solubility reduction predicted by NAELS. At the same time, the nucleation rate decreased by 68%. For the 2nd nucleation point, the decrease was only 0.75 wt-% total solids content. Given that the average nucleation rate decreased 71%, it appears that the nucleation process is dependant on both inorganic composition and supersaturation as the nucleation rate decreased substantially while the totals solids content at which nucleation occurred (an indicator of developed supersaturation) remained nearly constant. Despite a 5 wt-% total solids content decrease in the solids concentration at which fouling begins in the higher carbonate to sulfate ratio black liquor solution, the most significant finding of this analysis is that the growth rate on the heat-transfer surface actually increased 26%.

Table 6.5 contains the rate parameters determined from the nucleation orders and the estimated levels of supersaturation for the as-received black liquor and the as-received liquor with Na_2CO_3 added. The rate parameter for growth on the heat-transfer surface was estimated from,

$$G_S = k_{G,S}\sigma\,. \tag{6.3}$$

Table 6.5: Rate parameters calculated from the experimental measurements of nucleation and fouling of the heat transfer surface during evaporation of black liquor from Mill B, with and without addition of Na_2CO_3, and on estimated solubility and supersaturation of sodium carbonate

Mill B Sample Description	1st Nucleation σ_1	1st Nucleation $k_{N,1}$ $m^{-3}s^{-1}$	2nd Nucleation σ_2	2nd Nucleation $k_{N,2}$ $m^{-3}s^{-1}$	Surface Fouling σ_F	Surface Fouling $k_{G,S}$ $m \cdot s^{-1}$
As Received	0.10	6.99E+10	3.43	1.57E+07	2.18	1.46E-06
As Received	0.13	9.23E+10	2.72	1.55E+08	2.14	8.01E-06
As Received+Na_2CO_3	0.06	2.88E+10	2.85	3.13E+07	0.77	5.22E-07
As Received+Na_2CO_3	0.58	2.41E+09	2.85	1.57E+07	2.21	1.13E-05

In Table 6.5, the rate parameter for the first primary nucleation decreased by 80% when sodium carbonate was added. The rate parameter for the second primary nucleation decreased by 72% and the rate parameter for growth on the heat-transfer surface increased 25%.

This study indicated that increasing the ratio of dissolved carbonate to sulfate by addition of sodium carbonate changed the crystallization behavior. Both the crystallization rates and the estimated rate parameters show that nucleation was reduced for both burkeite and dicarbonate while the growth rate for dicarbonate on the heat-transfer surface increased. From this work, it is impossible to decouple the two phenomena and determine if the increased fouling behavior reduced the nucleation of dicarbonate. Theoretically these phenomena are coupled because the rate of fouling reduces the relative supersaturation prior to nucleation.

It is also impossible to conclude from this work whether or not the trace calcium added with the sodium carbonate may have influenced the results. The dissolved, non-organically bound, calcium ion concentration was not measured as no procedures exist for measuring it independently of the total soluble calcium in black liquor. Without a better determination of the non-organically bound calcium in black liquor, it is impossible to determine if the trace contaminant levels in the anhydrous sodium carbonate are significant enough to have caused additional inhibition of crystal nucleation and growth. This is one area that should be explored further.

Another plausible explanation for the observed reduction in the nucleation rate is that enriching the carbonate relative to the sulfate in black liquor may hinder the nucleation of burkeite. The reasoning for this is based on the structure of burkeite, which

Shi outlined in greater detail as a part of his calcium substitution arguments [1]. The burkeite crystal unit cell contains places for eight sodium cations and 4 anions. The most stable structure contains 3 sulfate anions and 1 carbonate anion. To obtain lower ratios, such as the nominal 2:1 ratio of sulfate to carbonate, a significant degree of substitution must occur. However, each of the substitutions exacts a cost in thermodynamic stability. Adding additional dissolved carbonate relative to the dissolved sulfate should make substitution of carbonate for sulfate into the lattice structure more likely if we assume that the instabilities for this substitution are only observed across the extended crystal lattice. The added carbonate may tend to inhibit development of the crystal past a critical nucleus size, effectively decreasing the nucleation rate as the carbonate to sulfate ratio increases.

What is clear from this study is that relatively small changes in the carbonate to sulfate ratio (2.6 to 3.6 moles Na_2CO_3 per mole Na_2SO_4) in the range where Shi's model [1] predicts burkeite as the first species to nucleate can lead to a significant change in the bulk nucleation and growth of fouling deposits on a heat-transfer surface for a black liquor as it is concentrated..

6.4.3. Analysis of Hypothetical Fouling Reduction Opportunities

The final set of black liquor experiments conducted as a part of this research examined the benefit of a number of potential schemes to control evaporator fouling at Mill A. Table 6.6 contains the results of the three reproducibility runs that were made with the black liquor from Mill A, with brine added to it. The repeatability of the black liquor solids content at nucleation and at the onset of fouling, and fouling rates presented in Table 4 is surprisingly quite good. The 1st, and 2nd nucleation events and the onset of

fouling occurred at 54.8 ± 3.0%, 65.8 ± 1.3%, and 65.1 ± 1.0% total solids content, respectively. For the estimated rate constants for dicarbonate nucleation and for fouling, the relative standard deviations were 72.2% and 1.9%, respectively. The rate constant for fouling is remarkably reproducible, especially considering that the growth rate itself had a relative standard deviation of 21.3%.

Table 6.6: Reproducibility of nucleation events, fouling rate, and rate parameters for the black liquor from Mill A with brine added.

Mill A Sample Description	1st Nucleation Solids Content	σ_1	$J_{0,1}$ $m^{-3}s^{-1}$	$k_{N,1}$ $m^{-3}s^{-1}$	2nd Nucleation Solids Content	σ_2	$J_{0,2}$ $m^{-3}s^{-1}$	$k_{N,2}$ $m^{-3}s^{-1}$
As Received+Brine	56.5%	0.19	1.12E+09	2.02E+10	64.4%	0.88	1.24E+08	1.53E+08
As Received+Brine	51.4%	0.07	1.90E+08	2.11E+10	66.5%	1.38	6.52E+07	3.90E+07
As Received+Brine	56.5%	0.20	1.43E+09	2.54E+10	66.7%	1.42	1.06E+08	6.02E+07
Average	*54.8%*	*0.15*	*9.12E+08*	*2.23E+10*	*65.8%*	*1.23*	*9.85E+07*	*8.41E+07*
St. Dev.	*3.0%*	*0.07*	*6.44E+08*	*2.77E+09*	*1.3%*	*0.30*	*3.03E+07*	*6.08E+07*
St Dev/Average	*5.4%*	*47.4%*	*70.6%*	*12.5%*	*1.9%*	*24.6%*	*30.8%*	*72.2%*

Mill A Sample Description	Surface Fouling Solids Content	σ_F	G_S $m \cdot s^{-1}$	$k_{G,S}$ $m \cdot s^{-1}$
As Received+Brine	65.7%	0.88	9.89E-07	1.13E-06
As Received+Brine	65.6%	1.16	1.34E-06	1.16E-06
As Received+Brine	63.9%	0.78	9.07E-07	1.17E-06
Average	*65.1%*	*0.94*	*1.08E-06*	*1.15E-06*
St. Dev.	*1.0%*	*0.20*	*2.30E-07*	*2.13E-08*
St Dev/Average	*1.6%*	*20.8%*	*21.3%*	*1.9%*

Some general comments and observations can be made from an inspection of the data in Table 6.6. The onset of rapid fouling occurred consistently at a slightly lower total solids content (0.9 to 5.5% less) than the total solids content at which the 2nd bulk nucleation event occurred. This is probably due to the inverse solubility of Na_2CO_3 and Na_2SO_4 with temperature, and the fact that the heat-transfer surface is hotter than the bulk liquor. Dicarbonate was apparently deposited on the hot surface, as detected by decreases in the heat-transfer rate, before nucleation occurred in the bulk solution as detected by increases in the particle counts from the FBRM measurements.

With the repeatability of the experimental procedure detailed in Table 6.6, it was possible to compare each of the proposed fouling control scenarios. To compare the various fouling control options tested to the base case, a simple statistical analysis was

used to analyze the potential effectiveness of each of the schemes. Assuming a normal distribution of the data, a fouling control scheme has a significant effect, with 90% confidence, when z, the measured effect, falls outside ±1.65 standard deviations from the base case average. This test was used to determine whether the measured rate parameters were significantly different when scale control schemes were implemented in the pilot evaporator experiments compared to the base case of the as-received liquor with brine added.

Looking only at the data in Table 6.6, it is clear that the two most repeatable parameters are the first nucleation rate parameter and the surface growth rate parameter. From a fouling perspective the first (burkeite) nucleation rate parameter was of less interest since there is no fouling associated with the first nucleation event. Instead, the second nucleation rate and more importantly, the rate parameter for growth on the heat-transfer surface were considered. The excellent repeatability for the growth rate on the heat-transfer surface is very useful with regard to understanding dicarbonate fouling.

Table 6.7: Rates of nucleation and fouling of the heat transfer surface, and the total solids contents of the black liquors at their onset, for evaporation experiments performed with black liquor from Mill A, both as received and with various additives.

Mill A Sample Description	1st Nucleation Solids Content	$J_{0,1}$ $m^{-3}s^{-1}$	2nd Nucleation Solids Content	$J_{0,2}$ $m^{-3}s^{-1}$	Surface Fouling Solids Content	G_S $m \cdot s^{-1}$
As Received	56.7%	2.19E+09	68.0%	4.03E+08	64.8%	9.94E-07
Brine to C1	56.1%	1.26E+09	73.7%	1.30E+08	64.5%	8.26E-07
Dry Ash	58.6%	7.01E+08	66.5%	1.93E+08	61.2%	3.64E-07
As Received+Na_2CO_3 (s)	55.6%	1.16E+09	-	-	67.7%	7.05E-07
As Received+Brine+Na_2CO_3 (s)	56.4%	1.25E+09	69.1%	1.94E+08	64.8%	1.99E-07
Lime Mud	57.2%	8.64E+08	72.2%	1.82E+08	61.7%	1.27E-07
Sump Retention (Low Heat Flux)	57.2%	8.71E+08	70.2%	1.63E+08	66.6%	8.96E-07

Table 6.7 presents each of the measured values for the various scale reduction strategies. For all of the strategies, the measured growth rate was reduced. As most strategies involved making a change in the composition of black liquor *after* the nucleation of burkeite, it would be expected that the nucleation rates for burkeite in these

experiments would be similar, and they were. Because the data associated with the first nucleation event provided no information about fouling reduction strategies, they were not analyzed further than what is presented in Table 6.7. The nucleation rate data for the second nucleation event for each of the strategies were also within an order of magnitude of the base case. This implies that the rate was not affected by the changes.

Table 6.8: Supersaturation at the onset of the second nucleation event and of fouling of the heat transfer surface, their rate parameters, and the level of certainty of the significance of each.

Mill A Sample Description	2nd Nucleation σ_2	$k_{N,2}$ $m^{-3}s^{-1}$	Significance	Surface Fouling σ_F	$k_{G,S}$ $m \cdot s^{-1}$	Significance	Reduction in $k_{G,S}$
Virgin	2.33	1.04E+08	0.32	1.25	7.95E-07	-16.67	30.9%
Brine to C1	5.72	7.93E+06	-1.25	1.17	7.04E-07	-20.94	38.8%
Dry Ash	1.76	7.80E+07	-0.10	0.58	6.28E-07	-24.48	45.4%
Virgin+Na_2CO_3 (s)	-	-	-	2.20	3.21E-07	**-38.90**	**72.1%**
Virgin+Brine+Na_2CO_3 (s)	2.29	5.15E+07	-0.54	0.97	2.06E-07	**-44.32**	**82.1%**
Lime Mud	4.67	1.54E+07	-1.13	0.65	1.97E-07	**-44.74**	**82.9%**
Sump Retention (Low Heat Flux)	2.79	3.15E+07	-0.87	1.39	6.47E-07	-23.63	43.8%

Table 6.8 presents the statistical analysis for the fouling control strategies. The first major observation is that all of the hypothetical solutions produce significant reductions in the fouling behavior of Mill A's black liquor at a confidence level of 90% (or 1.65 standard deviations). The significance value represent the number of standard deviations the rate constant is from the base case mean, with a positive value indicating an increase and a negative value indicating a decrease. The implication of this statement is that Mill A might reduce its evaporator fouling by implementing any of these strategies. The fouling reduction value represents the percent reduction in the surface growth rate constant from the base case mean.

One issue to consider for a production facility with a given set of equipment is that even if fouling rates are significantly lower, if the total solids content at which fouling occurs also shifts, the change may not prove beneficial. For example each of the optional solutions outlined in Table 6.8 shows significant reductions in the surface growth rate constant. However, only for the virgin liquor with solid Na_2CO_3 and the

sump retention trial did the fouling begin at greater total solids content than in the basis case as indicated in Table 6.7. A potential trade-off is being made for any of the other strategies. Fouling may potentially occur at lower total solids content (perhaps even in a different effect), but should be slower.

Because most of the tested scale control strategies showed lower total solids concentrations at the start of surface fouling, they should not be considered. The best choice is either processing only virgin liquor and adding solid anhydrous sodium carbonate crystals as a seed material prior to the first concentrator where fouling is occurring or increasing the sump retention time for supersaturation reduction.

From a purely crystallization perspective, aside from benefits to Mill A in particular, one interesting observation stands out in Table 6.8 as well. Each of the experiments where solids material was added showed a rate parameter for growth on the heat-transfer surface reduction two times greater than the other changes. In the case of anhydrous sodium carbonate it can be assumed that this was due to the added surface area for growth of sodium carbonate and the consequent reduction in the relative supersaturation. In the case of lime mud ($CaCO_3$) it is more difficult determine the reason for the change. Shi showed that $CaCO_3$ is not a favorable nucleation seed for burkeite [1], actually inhibiting burkeite nucleation and growth instead. If this holds true for the double crystal dicarbonate as well, then it can be concluded that it is the calcium inhibition effects that are influencing the changes. This would explain the nearly four-fold increase in the supersaturation required for the nucleation of dicarbonate. However, the slight decrease in supersaturation and significantly lower solids at which fouling

occurs in the lime mud experiment is not explained well using calcium inhibition reasoning.

6.5. Pilot-Scale Black Liquor Experimental Conclusions

The pilot evaporation experiments with black liquor presented in this chapter are the first investigation of the simultaneous bulk and surface crystallization behavior Na_2CO_3 and Na_2SO_4 from black liquor. Three main conclusions can be made based on this work.

First, this work has shown the value of *in situ* particle population analysis in combination with heat-transfer measurements for fouling rate estimation. Prior to this work, *in situ* particle population of black liquor had never been undertaken. The quantifiable nucleation behavior observed using FBRM technology in black liquor provides a better understanding about the phenomena occurring during the concentration-driven crystallization from such a complex fluid. Relating the measured particle population data with the estimated ion concentrations has provided a means to calculate nucleation rate parameters. These rate parameters can be compared quantitatively between different experiments.

Second, this work has shown that increasing the carbonate to sulfate ratio in black liquors whose compositions were such that burkeite crystallized from them, had a negative influence on the nucleation of both burkeite and dicarbonate. In addition, increasing the carbonate to sulfate ratio increased growth rates of dicarbonate on the heat transfer surface. Because each of these phenomena was driven by supersaturation but also affect supersaturation, they are not independent.

Third, the addition of solid particles to black liquors whose total concentration was above the solubility limit for burkeite substantially reduced the surface growth rate parameter. However, in two of the three experiments with addition of solid materials, the addition also reduced the total solids content at which fouling occurred. Thus, even though the fouling rate parameters were reduced, fouling would begin at an earlier point in the evaporation process. Also, it is possible that crystallization on the anhydrous sodium carbonate reduced the dissolved Na_2CO_3 content of the liquor and delayed the onset of fouling.

6.6. Acknowledgements

Portions of the experimental work reported in the chapter in conjunction with the Weyerhaeuser sponsored black liquor work were conducted by Steve Lien and Gary Heedick from the Institute of Paper Science and Technology. Data analysis and interpretation is the author's. Special thanks to Wolfgang Schmidl and Steve Lien from IPST, and Pete Thorn and Phil Smith from Weyerhaeuser Company for their help and insight in developing the fouling reduction opportunity work.

6.7. Variables

G Growth rate, ms^{-1}

J_O Nucleation rate, $m^{-3}s^{-1}$ (Volume) or $m^{-2}s^{-1}$ (Surface)

k_G Growth rate constant, ms^{-1}

k_N Nucleation rate constant, $m^{-3}s^{-1}$

m_0 0^{th} chord length distribution moment, m^{-3}

R Thermal resistance – subscript indicates what the resistance is measured through, m^2KW^{-1}

P_S Steam pressure, bara

SFR Surface fouling rate, $m^2KW^{-1}s^{-1}$

T Temperature, K

t Time, s

U Overall heat transfer coefficient, $Wm^{-2}K^{-1}$

z Measured effect

σ Relative supersaturation

Super and Subscripts

$_1$ First event

$_2$ Second event

$_F$ Fouling

^{i} Nucleation order

^{M} Metastable condition

$_S$ Surface

* Chemical equilibrium

6.8. Bibliography

1. Shi, B., Crystallization of Solutes that Lead to Scale Formation in Black Liquor Evaporation, *Ph.D. Thesis*, Georgia Institute of Technology, 2002.

2. Sinquefield, S.A, A Microcomputer Software Package for Simulation of Non-Ideal Aqueous Electrolyte Systems at Equilibrium, *M.S. Thesis*, Oregon State University, 1991
3. Golike, G.P., Q. Pu, K.L. Holman, K.R. Carlson, P.C. Wollwage, H.G. Folster and S. Rankin, NAELS: A New Method for Calculating Equilibrium Solubility of Burkeite and Sodium Carbonate in Black Liquor, *1998 International Chemical Recovery Conf.* pp. 403-418
4. Smith, J.B., Sodium Salt Scaling in Falling Film Black Liquor Evaporators, *Ph.D. Thesis*, Georgia Institute of Technology, 2000
5. Mullin, J.W., *Crystallization*, 3rd Edition, Butterworth Heinemann, Boston, 1997
6. Westervelt, H.H., W.J. Frederick, E.W. Malcolm, and D.B. Easty, "The Determination and Temperature Dependence of the Stability Constant of the Calcium - Catechol-4-Sulfonate Complex in Alkaline, Aqueous Media", *Analytica Chimica Acta*, 138, pp. 237-243. (1982)
7. Westervelt, H.H., W.J. Frederick, E.W. Malcolm, and D.B. Easty, "New Evidence Concerning the Role of Black Liquor Organics in Calcium Carbonate Scale Formation," *TAPPI*, 65(5):179-80 (1982).

Chapter VII: Bench-Scale Surface Crystallization

7.1 Objective

There will be two major objectives for the experiments conducted using the bench-scale surface crystallizer. The first objective will be to observe and identify the mechanism(s) by which fouling by salts composed of Na_2CO_3 and Na_2SO_4 is initiated on a heat-transfer surface from aqueous solutions of Na_2CO_3 and Na_2SO_4. The second objective will be to: (a) measure the sizes of crystals on the heat-transfer surface as a function of time to determine the rate of growth, (b) measure the heat-transfer resistance due to fouling with time to estimate a fouling rate and (c) determine the relationship between the fouling rate and the growth rate of crystals observed on the heat-transfer surface.

7.2. Introduction

Pilot-scale experiments provided results for bulk crystallization and for surface fouling phenomena in aqueous solutions of sodium salt and in black liquor. However, they could not provide a microscopic observation of the heat-transfer surface, nor did they allow determination of the specific mechanism for scale initiation on the surface or a direct measurement of the growth rate of crystals on the surface.

Two primary mechanisms have been proposed and discussed for initiation of crystallization fouling [1, 2]. For the first mechanism, supersaturation develops to the point at which direct nucleation on the heat-transfer surface occurs. The crystal nucleus develops directly on the heat transfer surface, although subsequent growth may not be in

contact with the surface [2-4]. The second mechanism for scale initiation involves the adhesion of particles to the surface. If a particle comes into contact with the heat-transfer surface, where the flow velocity is negligible due to the no-slip flow condition, then the particle could adhere to the surface by growing into the void space in the microstructure of the surface.

Supersaturation can be generated in the system of interest by increasing the temperature and/or solvent evaporation. In this work, supersaturation can be developed at the heat-transfer surface due to its higher temperature, even if the bulk solution is at equilibrium. Supersaturation in the solution due to prior evaporation of the solvent that has not been reduced through crystallization is also possible. Hedrick and Kent referred to supersaturation present for this reason as residual supersaturation [5].

7.3. Procedure

The bench-scale surface crystallizer apparatus was discussed extensively in Chapter 3. Thus, only the operational details and any experimentally relevant apparatus changes are discussed in this section.

The bench-scale surface crystallizer experimental work was broken down into two series of experiments. The first series was conducted with no supersaturation due to evaporation of the solvent. Only the supersaturation due to the inverse relationship between solubility and temperature at the heat-transfer surface acted as the driving force for crystallization. Evaporation from the bulk solution was used in the second series to increase the supersaturation to a level above that which could be developed only by the inverse relationship between solubility and temperature at the heat-transfer surface. This

study was conducted to determine the supersaturation required for rapid crystallization on the heat-transfer surface.

7.3.1. Generation of Supersaturation at the Heat-Transfer Surface

An experimental method was developed to measure crystallization on a heat-transfer surface from aqueous slurries of Na_2CO_3 at equilibrium. The aqueous slurries were prepared with deionized water and industrial grade Na_2CO_3. Anhydrous sodium carbonate was added to the water to create a slurry at approximately 50°C. The slurry temperature was raised to 110°C and left for a minimum of 8 hours to equilibrate. This preparation method guaranteed that at the operating temperature of 110°C the slurry would not be supersaturated. A number of possible equipment configurations were considered for forming scale from the equilibrated slurry. Figure 7.1 presents the four options considered.

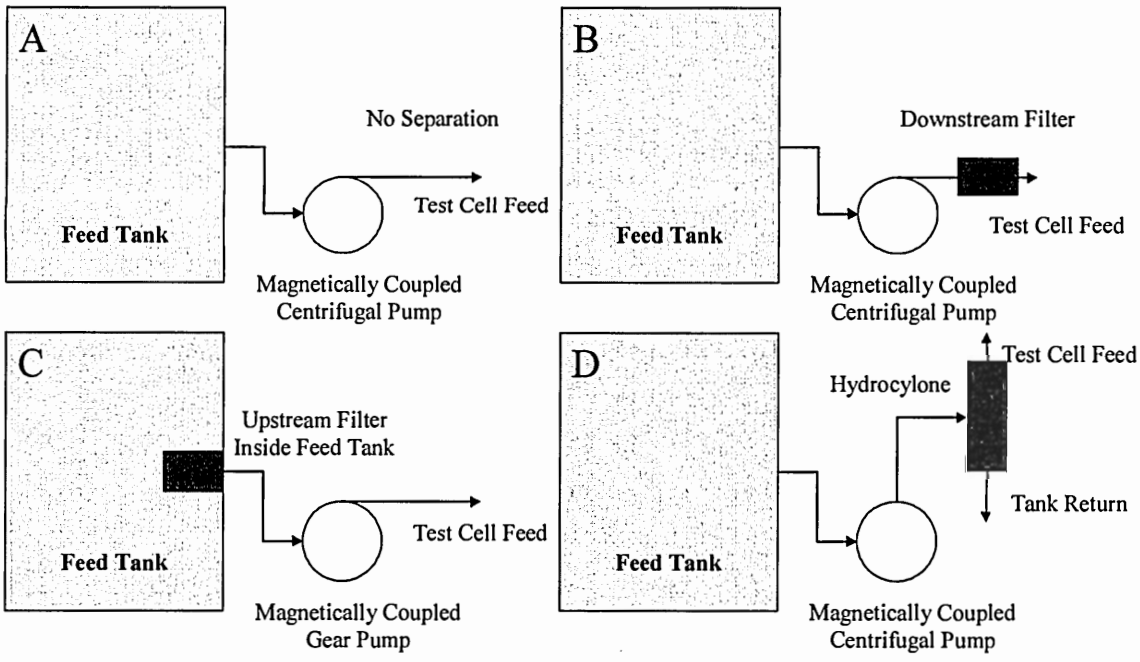

Figure 7.1: Experimental apparatus configurations considered for experimental studies with the bulk solution at equilibrium

The option in Figure 7.1A was the easiest to try. Unfortunately, crystals in the bulk slurry clouded the digital imagery of the surface, preventing observation of crystals on the surface. The remaining three possibilities were also tested experimentally.

The options in Figures 7.1B and 7.1C proved unacceptable due to standard design concerns. In the case of a downstream filter (Figure 7.1B), the pressure drop across the filter increased rapidly. Because of this, the flow rate decreased and, without additional control equipment, was determined to be unreliable. An upstream filter inside of the tank was considered a possible solution to filter plugging (Figure 7.1C). In this case, the feed tank mixing would have a tendency to remove crystals from the filter surface. Indeed this hypothesis proved true during room temperature tests. However, when the feed solution was raised to operating temperatures, with the corresponding saturated vapor/solution and solution/solid conditions, a 10°C decrease in temperature between the feed tank and the test cell inlet was observed. This temperature decrease was attributed to flashing that occurred due to the pressure drop across the filter. The pressure drop across the filter was caused by the pump, which pulled a slight suction to maintain the set point for flow rate. The flashing also led to crystallization on the inside surface of the filter, which increased the pressure drop.

Finally, as shown in Figure 7.1D, a small hydrocyclone was added to the apparatus to act as a downstream particle separator. Placing the hydrocyclone downstream of the pump alleviated both the plugging and the flashing problems previously experienced. While this arrangement was not perfect, it did allow important conclusions to be reached.

7.3.2. Generation of Supersaturation from Evaporation and Increased Temperature

These experiments were conducted using the experimental apparatus configuration as detailed in Chapter 3. Initial runs were performed on solutions of aqueous Na_2CO_3. The total solids content of the solution was raised from below the solubility limit to above it by evaporating water from the solution. Bulk nucleation of Na_2CO_3 occurred when the relative supersaturation in the bulk solution reached approximately 0.1. No fouling was observed either before or after bulk nucleation.

Table 7.1: Bench-scale surface crystallizer batch evaporator experimental outline.

C:S mole ratio	T_B, °C	EDTA* Added (g)
2.67	110	-
2.67	110	-
2.67	110	-
2.67	110	30
6.0	110	-
6.0	115	-
6.0	115	9.5
6.0	115	28.5

*** Ethylene-Diamine-Tetraacetic Sodium Salt**

Solutions described in Table 7.1 were prepared from ACS grade sodium carbonate and sodium sulfate dissolved in 0.030 m^3 deionized water. The initial concentrations ranged between 28.1% total solids content and 29.6% total solids content, but all experiments were conducted at a target evaporation rate of 8.4×10^{-4} g H_2O/min/g initial salt mass. This value was approximately the maximum evaporation rate from the feed tank that could be maintained while still maintaining a constant temperature in the feed tank; it is lower than the value obtained during experiments with the pilot apparatus. This specific evaporation rate implied that the residual supersaturation increased at the same rate in all experiments. The 2.67:1 and 6.0:1 carbonate-to-sulfate mole ratios were

chosen in order to obtain burkeite and dicarbonate, respectively, as the crystallizing species [6].

Experiments were conducted at 110°C and 115°C for reasons that will be outlined in the results and analysis section. The flow rate through the test cell for all experiments except one was 600 ml/min. The applied voltage for heating in all experiments was 93 V, which corresponded to an applied power of 290 W.

EDTA was added in three of the experiments to sequester calcium. Calcium levels in the sampled solutions were between 150 and 200 ppm on a dry mass basis.

In each experiment, the solution was concentrated by evaporation from below the solubility limit until crystals were observed on the heat-transfer surface. At this point, evaporation was halted to maintain a constant supersaturation while measuring growth rates. In cases where primary bulk nucleation preceeded surface growth, evaporation was continued until either crystals were observed on the surface, or until crystals in the bulk slurry caused the circulation line to plug.

7.4. Results and Analysis

The bench-scale surface crystallizer was able to provide results on the initiation mechanisms for crystallization fouling from double salts composed of Na_2CO_3 and Na_2SO_4 and the subsequent growth rates for the crystals in the deposit.

7.4.1. Fouling from Aqueous Na_2CO_3 at Equilibrium

As previously described, an aqueous solution of Na_2CO_3 was circulated through the test cell after the crystals were separated using the hydrocyclone. The experiment

was conducted a number of times varying both the circulation rate through the test cell and the thermal driving force, ΔT, between the heated stainless-steel plate and the aqueous sodium carbonate solution. Crystallization on the heated plate was not observed in any of the experiments.

An explanation for the lack of crystal formation is based on the solubility behavior of aqueous sodium carbonate. From work in Chapter 5 and 6, it was found that a value of σ greater than 0.1 was necessary for crystallization in either the bulk solution or on the heat-transfer surface. This is also the order of magnitude often observed for the heterogeneous primary bulk nucleation of a number of salts [7, Table 6.1].

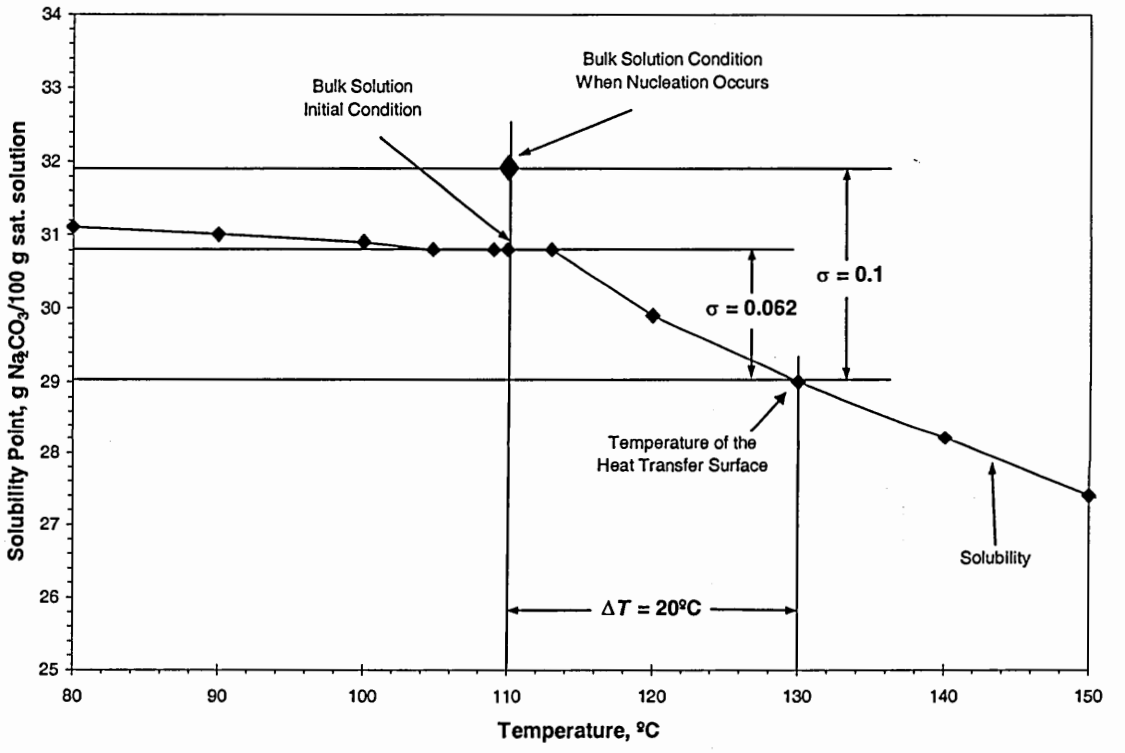

Figure 7.2: Solubility diagram for aqueous Na_2CO_3 indicating experimental conditions and estimated supersaturation required for nucleation.

The solubility of aqueous Na_2CO_3 is shown as a function of temperature in Figure 7.2. The bulk temperature in the experiments was 110°C, with a corresponding Na_2CO_3

solubility of approximately 30.8 wt%. With a maximum temperature difference of 20°C allowed before nucleate boiling occurred, the plate could be heated to a surface temperature of 130°C. This corresponded to a solubility of 29 wt%. Since,

$$\sigma = \frac{C_{\text{Feed}}^{*} - C_{\text{Plate}}^{*}}{C_{\text{Plate}}^{*}}, \tag{7.1}$$

where the concentrations are measured as the weight percent Na_2CO_3 in the solution, a relative supersaturation of only 0.062 could be achieved through developed supersaturation at the heat transfer surface without moving into the nucleate boiling regime.

If a linear relationship between solubility and temperature is assumed then C_{Plate}^{*} - $C_{\text{Feed}}^{*} = \Delta C = m\Delta T$, where ΔT is T_{Plate} - T_{Feed}. Since $\sigma = (C_{\text{Feed}}^{*} - C_{\text{Plate}}^{*})/C_{\text{Plate}}^{*}$, a general relationship can be derived to determine when surface nucleation might be expected. Namely,

$$m = -\frac{C^{*}\sigma}{\Delta T}, \tag{7.2}$$

where m is the slope of the linear relationship between solubility and temperature (i.e. m will be a negative number for any solute that is inversely soluble with temperature).

Given the restriction that $\sigma > 0.1$ and not allowing nucleate boiling to occur at the heat-transfer surface (i.e. $\Delta T < 20°C$), Equation 7.2 becomes

$$m \leq -0.005C^{*} \text{ (concentration/K)} \tag{7.3}$$

Equation 7.3 allows a prediction of the minimum inverse solubility behavior required for rapid initiation of surface scale. Using this model and the solubility behavior for aqueous sodium carbonate, rapid initiation of surface fouling was not predicted. Based on several

concentration-temperature solubility profiles for solutions of different Na_2CO_3:Na_2SO_4 predicted with the NAELS chemical equilibrium software, rapid initiation of surface fouling would not be expected from aqueous solutions of sodium carbonate and sodium sulfate either.

This implies that the initiation of fouling of Na_2CO_3-Na_2SO_4 salts is not due to supersaturation generated solely from increased temperatures at the heat-transfer surface.

7.4.2. Initiation Mechanisms for Fouling when Evaporation was used to Generate Supersaturation

Evaporation was used to generate supersaturation in aqueous solutions of Na_2CO_3 and then Na_2CO_3 and Na_2SO_4. Work started with aqueous Na_2CO_3 and progressed to solutions with compositions more representative of black liquor.

Only primary nucleation in the bulk solution was observed during four evaporation experiments with aqueous sodium carbonate. After σ increased to values greater than 0.1 in the solution, primary nucleation in the bulk solution occurred, and no subsequent fouling was observed on the heat-transfer surface. This observation indicated that the metastable limit for bulk nucleation was lower than that for surface nucleation.

After evaporation experiments with aqueous sodium carbonate did not produce crystallization on the heat-transfer surface, solutions with burkeite as the expected solute were tested, followed by experiments with dicarbonate as the expected solute.

Because the relative supersaturation when bulk nucleation occurred in the aqueous Na_2CO_3 had a standard deviation relative to the average value observed of less than 10%, it was assumed that the experimental procedures were repeatable and only two

experiments were conducted with aqueous solutions having Na_2CO_3:Na_2SO_4 molar ratios of 2.67:1. These experiments were conducted to determine the mechanism for scale initiation. Analysis of microscopic digital imagery of a section of the heat-transfer surface taken during the experiments showed crystals on the surface before crystals were observed in the bulk solution. From this, the mechanism for the initiation of burkeite deposits on the heat-transfer surface was identified as nucleation directly on the heat-transfer surface rather than adhesion. It is possible that adhesion of crystals smaller than the observable limit ($d_p < 30$ μm) due to early bulk nucleation acted as the mechanism. However, crystals from early nucleation were not observed at any time either in the digital imagery of the surface or by visual observation of the flow across the surface. In one experiment, bulk crystallization was observed approximately 20 minutes after surface fouling was first observed and evaporation stopped. In the second experiment, sloughing of scale pieces restricted flow and required the experiment to be stopped before bulk nucleation was observed.

An aqueous solution with a Na_2CO_3:Na_2SO_4 molar ratio of 6.0:1 was tested to determine the mechanism for the initiation of dicarbonate scale. The initial experiment was conducted at 110°C to allow for comparison to the burkeite experiments. During this experiment, bulk nucleation occurred prior to surface nucleation. Analysis of microscopic digital imagery of a section of the heat-transfer surface taken during the experiments indicated that the initiation mechanism was adhesion of crystals to the heat-transfer surface after their nucleation in the bulk solution. The habit of the crystals on the heat-transfer surface appeared to be quite different from that observed previously with burkeite. Crystals from the 6.0:1 solution displayed a more facetted nature than those

from burkeite. Differences in appearance coupled with the fact that sodium carbonate monohydrate can form below 109°C (the feed temperature to the cell was slightly below this value) led to the conclusion that the crystals nucleating could be sodium carbonate monohydrate.

Shi conducted all of his dicarbonate experiments at bulk conditions of 115°C [6], so the next 6.0:1 solution experiment was conducted at 115°C. This experiment also showed bulk nucleation followed by surface adhesion to be the initiation mechanism for scaling. The crystal habit observed was closer to that seen for burkeite than to the 6.0:1 experiment conducted with a bulk solution temperature of 110°C. The difference observed in crystal habit for the deposits coupled with differences in the effective thermal conductivity, which will be discussed later, indicated that dicarbonate was crystallizing at the higher temperature. Thus, it was concluded that the initiation mechanism for surface fouling of dicarbonate was adhesion followed by growth. The rapid nucleation that caused an opaque white solution observed for burkeite did not occur with dicarbonate. Rather, the nucleation rate for dicarbonate in the bulk solution appeared to be much lower. Bulk nuclei were observed in the microscopic imagery, but were barely discernable visually.

The image capture and analysis software provided numerous images of crystals on the heat-transfer surface for review. Several of these will be presented and discussed.

Figure 7.3 shows the habit of burkeite crystals on the heat-transfer surface. The tooling marks on the stainless steel are observed as the straight white lines on the surface. Crystal masses that were growing toward the center of the image from three directions are seen in this figure. Later, these three masses grew together to form one large mass.

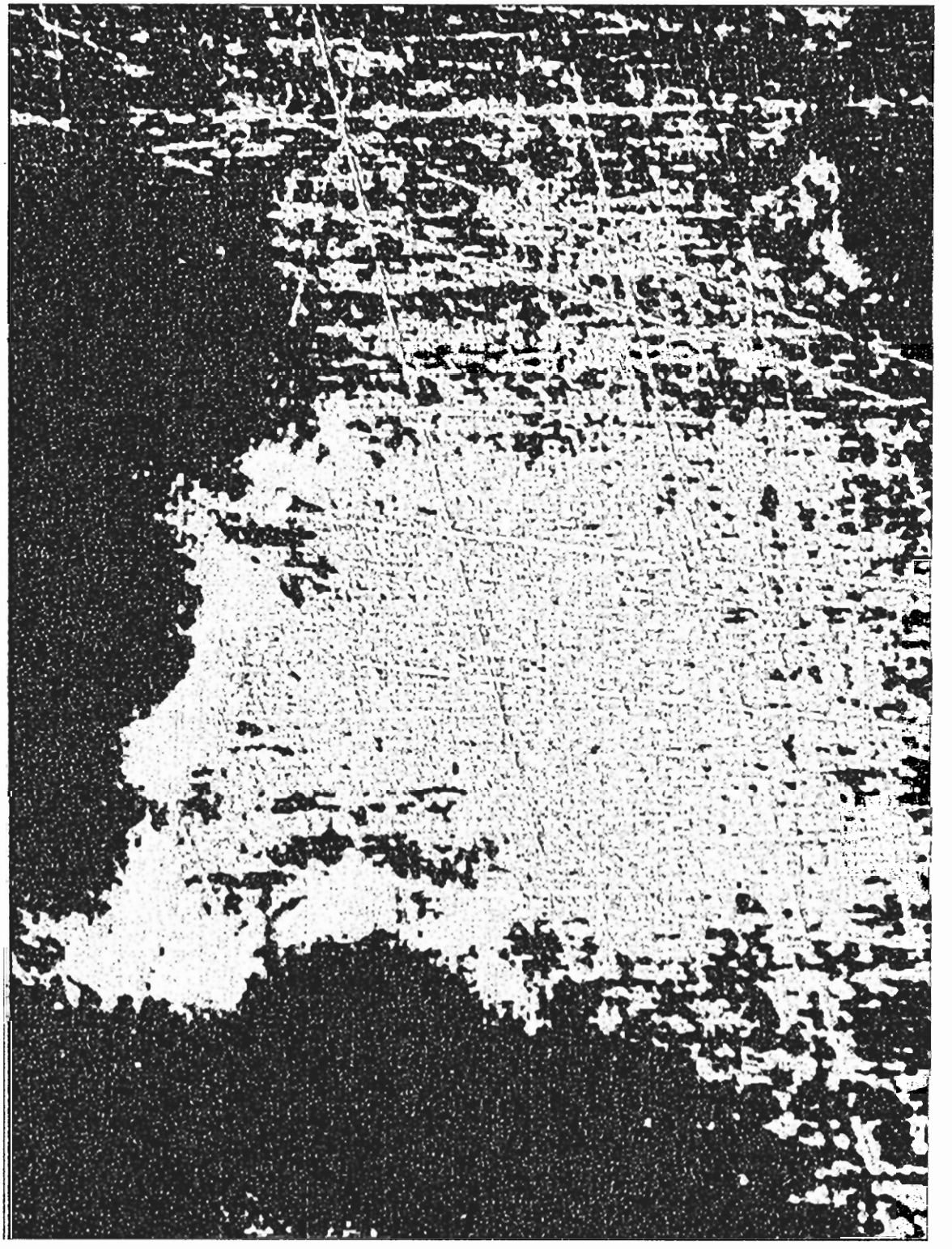

Figure 7.3: Microscopically observed habit of burkeite crystals on the heat-transfer surface (imaged area shown is 2700 μm in height)

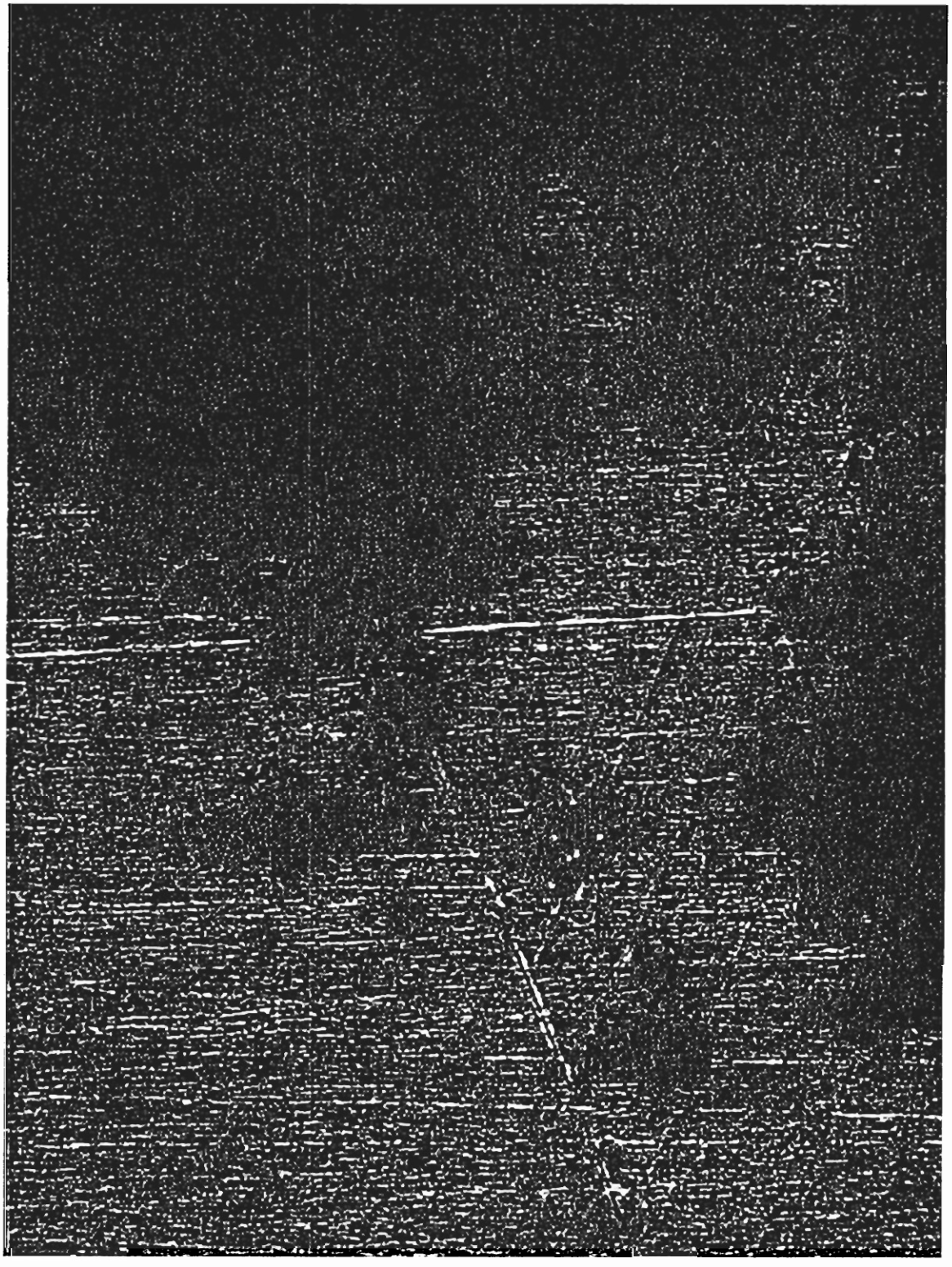

Figure 7.4: Microscopically observed habit of sodium carbonate monohydrate crystals on the heat-transfer surface (imaged area shown is 2700 μm in height)

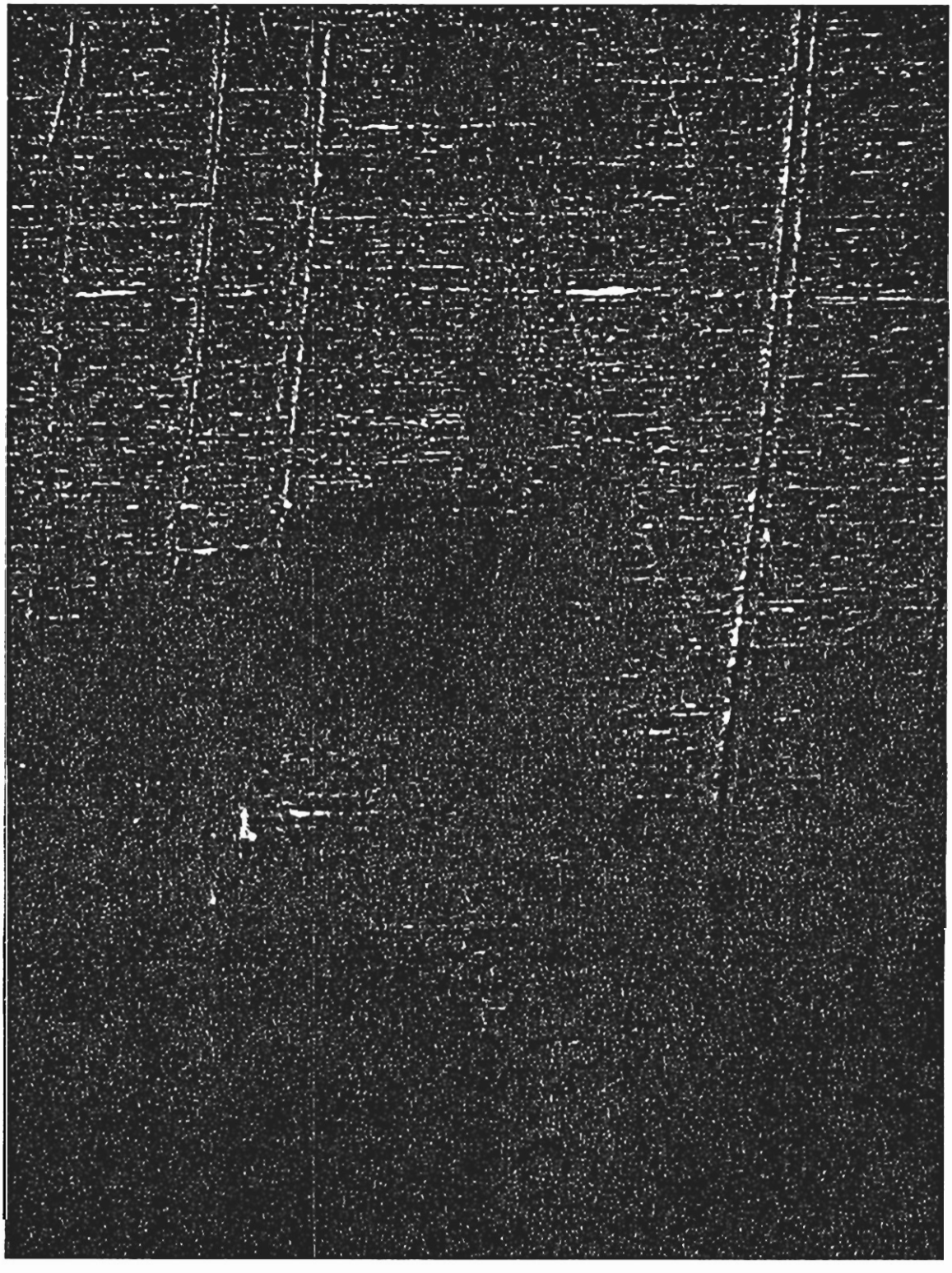

Figure 7.5: Microscopically observed habit of dicarbonate crystals on the heat-transfer surface (imaged area shown is 2700 μm in height)

For burkeite, no clearly defined faces are observed. Rather, the crystalline masses had the appearance of large agglomerates composed of individual crystals that were small enough to not be discernable in the microscopic imaging. One possible cause of this appearance might have been a combination of concurrent nucleation and growth on the existing crystal surfaces. This is what Linnikov referred to as crystal splitting [2]. It is more accurately described as dendritic growth [7].

Figure 7.4 shows a different crystal habit from that seen in Figure 7.3. While the crystalline mass was not a perfect crystal, it did display a facetted nature not observed in Figure 7.4. This was probably due to a reduction in the dendritic behavior because the relative supersaturation was lower (0.33 for burkeite, 0.19 for sodium carbonate monohydrate). The difference may also be partially explained by the initiation mechanism. Bulk nucleation followed by adhesion of the crystals to the heat-transfer surface could lead to individual crystals on the heat-transfer surface. Also, sodium carbonate monohydrate has been shown to form good individual crystals with defined edges [6].

Figure 7.5 shows the surface crystal habit observed for the 6.0:1 solution after the temperature was increased to 115°C. The appearance was different from both Figure 7.3 and in Figure 7.4. In Figure 7.5, the deposit appears to be an agglomerate, but the individual crystal structures do not appear to be as small as those in Figure 7.3. The habit in Figure 7.5 might be explained by noting that dicarbonate bulk nuclei are typically small agglomerates [6], but the initiation mechanism was adhesion. Thus, the size of individual crystal structures on the heat-transfer surface was not as small as it was for burkeite due to less crystal splitting because the supersaturation was lower. Yet, the

deposits on the heat-transfer surface did not have the facetted nature of sodium carbonate monohydrate because the dicarbonate crystals adhering to the surface are themselves agglomerates.

7.4.3. Measurement of Heat-Transfer, Nucleation and Grow Rates for Crystals on the Heat-Transfer Surface

Measurement of the heat-transfer coefficient, nucleation rate on the heat-transfer surface and the subsequent growth rate would provide important data for modeling the process of fouling on heat-transfer surfaces. For this reason, an attempt was made to develop this data.

While digital images of crystals on the heat-transfer surface were being collected, temperatures and voltage applied to heat the surface were also collected using a data acquisition system. These data allowed the heat-transfer coefficient to be determined. Only the overall heat transfer coefficient, U, was determined since only inlet and outlet temperatures were measured. For the bench-scale surface crystallizer then,

$$U = \frac{q}{A\left(T_P - \frac{T_I + T_O}{2}\right)}, \tag{7.4}$$

where q is the heat generated by the resistance heater calculated from, $q = V^2/R_E$. Figure 7.6 presents the heat-transfer coefficient and thermal resistance due to fouling for a sample experiment.

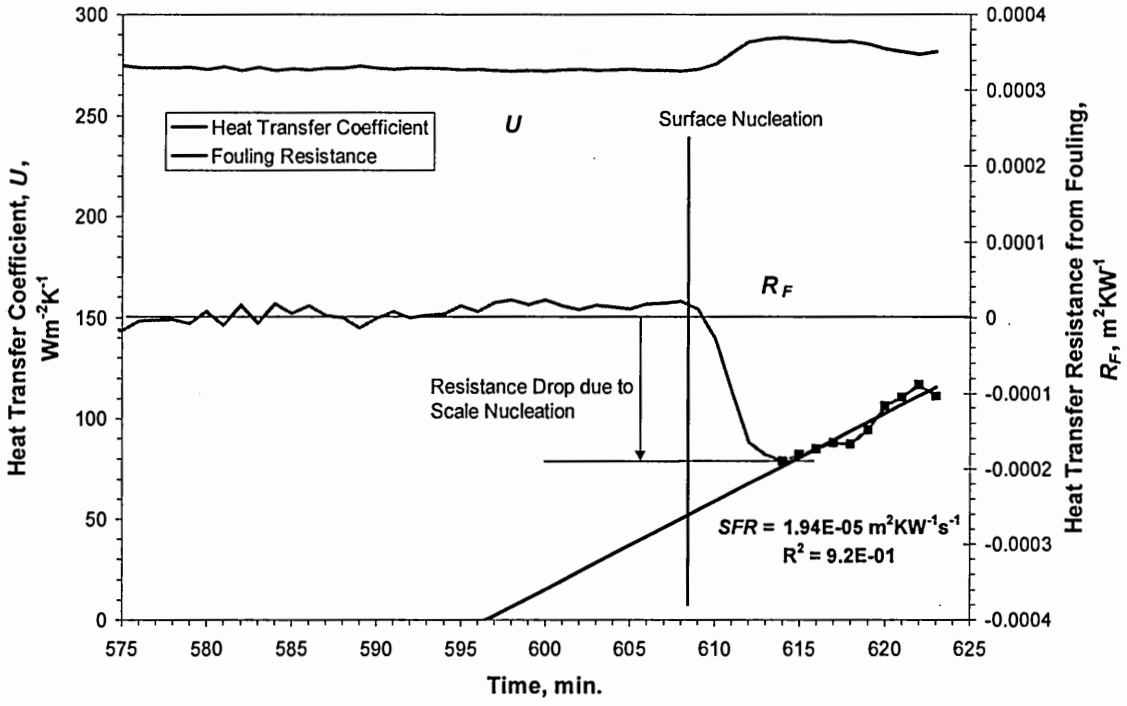

Figure 7.6: Overall heat-transfer coefficient and estimations of thermal resistance due to fouling for the crystallization of burkeite on a heat-transfer surface

The data in Figure 7.6 show negligible resistance due to fouling prior to initiation of scale on the heat-transfer surface. At approximately 608 minutes, the heat-transfer coefficient increased approximately 5% for a short period of time before beginning a steady decline. The drop in heat-transfer resistance at this time was explained as a transient effect due to the nucleation of scale. As scale nucleates on a heat-transfer surface, it temporarily provides additional surface area for heat transfer without changing the thermal driving force. Possibly more importantly, the scale also perturbs the flow which can also increase the heat-transfer coefficient. The net result was an apparent increase in the heat-transfer coefficient. At the end of this transient period, the resistance increased due to growth of the crystals on the heat-transfer surface. The surface fouling rate, *SFR*, was determined during this region.

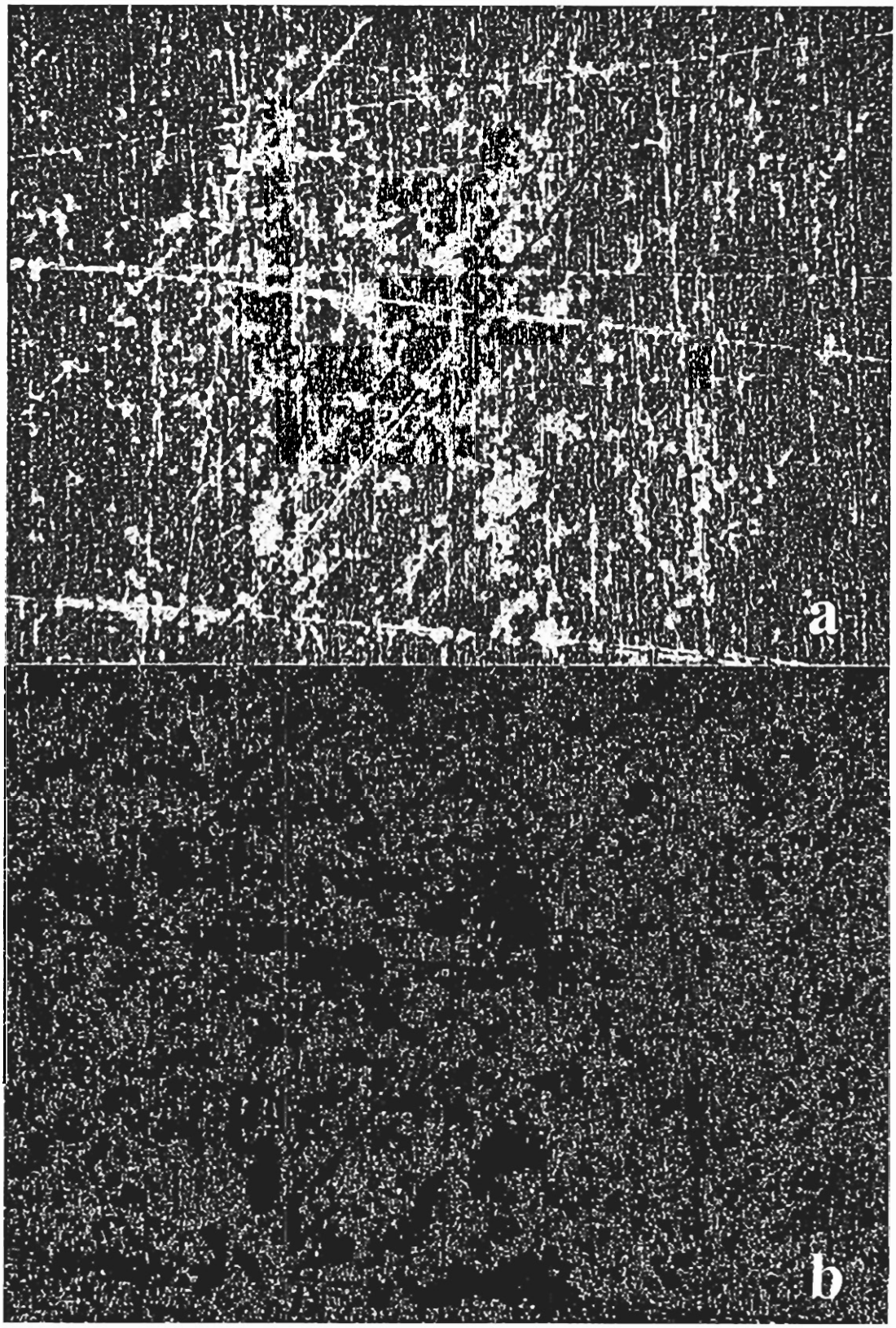

Figure 7.7: Imagery of nucleation on the heat-transfer surface (a) first image after surface nucleation (b) computer filtered analysis of nuclei

Due to the somewhat random locations at which surface nucleation occurred, and the limitation of digitally imaging one fixed location, it was impossible to determine reproducible nucleation rates. However, nucleation of burkeite on the heat-transfer surface occurred at the imaging location in one experiment. This observation provided an opportunity to discuss how nucleation on the surface could be studied given three-dimensional computer control of the location being imaged.

Even when a clear image of the surface nuclei was obtained, as displayed in Figure 7.7a, it was challenging to analyze the image in order to determine the number of nuclei. Image analysis is highly subjective because of the filtering options before the software counts the nuclei. The white lines in Figure 7.7a represent tool marks on the heat-transfer surface. The light gray regions are nuclei on the surface.

After one set of color and light filters were used, as shown in Figure 7.7b, the Image Pro-Plus software counted 3918 nuclei (the white dots in Figure 7.7b). This corresponded to a nucleation rate on the heat-transfer surface, $J_{0,S}$, of 4.73×10^9 $m^{-2}s^{-1}$.

Together, known values of $J_{0,S}$ and the drop in thermal resistance, ΔR_F, allowed an estimation of the initial radius of a deposit on the heat-transfer surface, $r_{C,S}$, to be made. If the apparent drop in resistance is due only to the increase in the surface area for heat-transfer because of nucleation, and if the nuclei are hemispherical in geometry, then a straightforward estimation can be made.

Derived from the thermal resistance due to fouling,

$$\Delta R_F = \frac{\Delta T}{q} \Delta A, \tag{7.5}$$

Equation 7.5 shows how an apparent change in the resistance could be due to a change in the area for heat-transfer. Because each hemisphere of radius $r_{C,S}$ had a surface area of

$2\pi r_{C,S}^2$ and was covering a circle on the heat-transfer surface of area $\pi r_{C,S}^2$, the net gain in area was $\pi r_{C,S}^2 J_{0,S}$. Thus, the size of the critical radius can be estimated from

$$\Delta R_F = -\frac{\Delta T}{q} \pi r_{C,S}^2 J_{0,S} . \tag{7.6}$$

For the nucleation event pictured in Figure 7.7, the estimated size of a critical nucleus was 0.37 μm. Estimating $r_{C,S}$ in this manner could prove to be a useful tool for future work with equipment that can image larger portions of the surface area and capture reproducable images of nucleation events on the heat-transfer surface.

Time-lapse digital imagery of the heat-transfer surface was used to identify and track stable crystal structures on the surface. After calibration using a slide etched with 1-mm marks, the Image Pro Plus software package allowed measurement of crystal lengths in individual digital images. This process is illustrated in Figure 7.8. By plotting the different lengths measured as a function of time as shown in Figure 7.9, an average surface growth rate was determined for each of the bench-scale experiments where crystallization on the heat-transfer surface was observed.

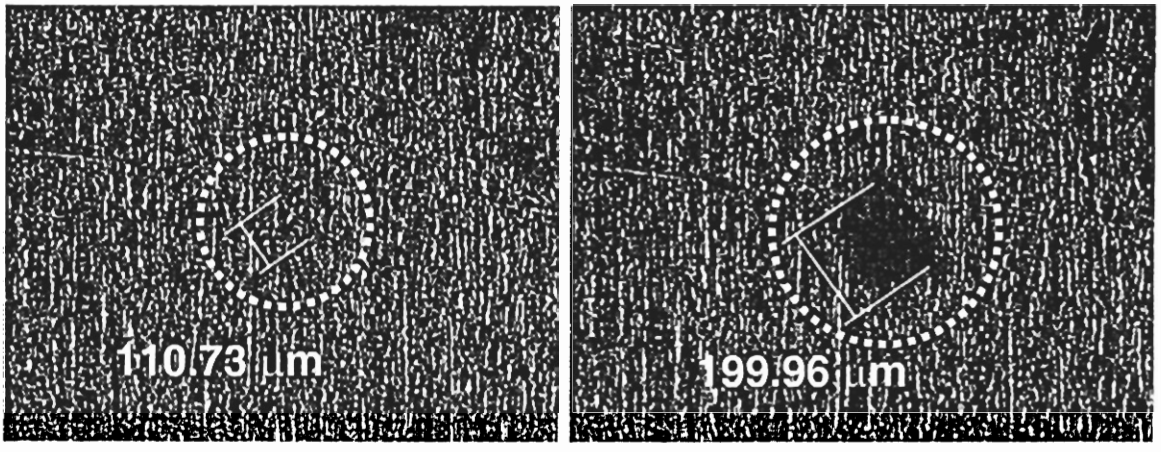

Figure 7.8: Analysis of time-lapse images showing a growing crystal on the heat-transfer surface at two different times

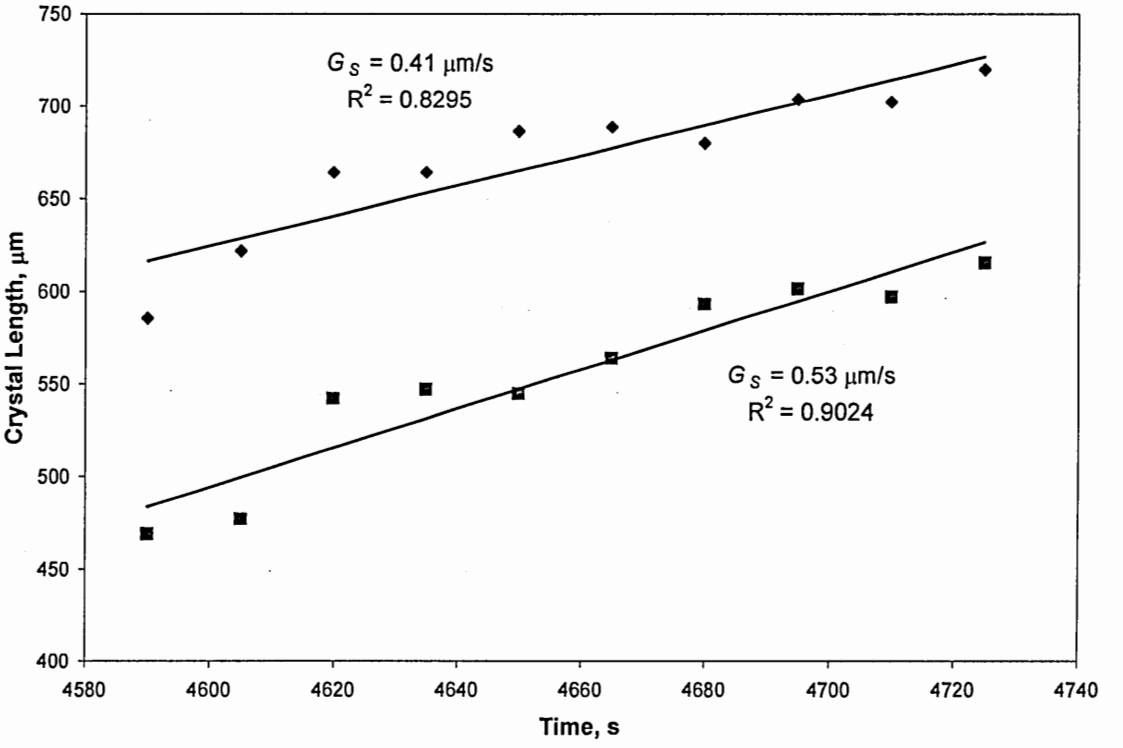

Figure 7.9: Example of the estimation of growth rates for crystals on the heat-transfer surface derived using measurements of crystal length from analysis of time-lapse imagery

Table 7.2: Bench-scale surface crystallizer growth rate kinetic estimations

C:S mole ratio	T_B, °C	Mass EDTA, g	G_S, m·s^{-1}	σ_S	k_S, m·s^{-1}	St. Dev. k_S, m·s^{-1}
2.67	110	-	3.14E-07	0.32	9.83E-07	1.58E-07
2.67	110	-	3.18E-07	0.34	9.49E-07	
2.67	110	-				
2.67	110	30		0.19		
6.0	110	-	1.71E-07	0.23	7.61E-07	
6.0	115	-	4.63E-07	0.14	3.35E-06	6.01E-07
6.0	115	9.5	1.11E-06	0.12	9.21E-06	
6.0	115	28.5	*	0.09		

***Moments after surface crystals were observed in this experiment, bulk crystals plugged the circulation line and no growth rate data was determined.**

Growth rate parameters were estimated for all of the bench-scale surface crystallization experiments where crystal growth could be measured using the methods outlined in Chapter 5. The growth rates and growth rate parameters from the bench-scale surface crystallizer are presented in Table 7.2. For the experiments where multiple

crystals were observed, the standard deviation of the growth rate parameter is also presented in Table 7.2.

The standard deviation of the growth rate for burkeite during a single experiment where growth rates were measured for several different crystals on the heat-transfer surface was only 16% of the average measured value. The standard deviation of the average growth rate parameters estimated for the two burkeite experiments conducted under the same conditions was 2.5% of the average of the estimated values. The standard deviation of growth for different dicarbonate crystals during the same experiment was approximately 18% of the average measured value. A direct comparison between burkeite and dicarbonate is not possible due to different bulk temperatures and supersaturation gradients (as defined by differing *m*-values for their respective concentration-temperature solubility curves). An indirect comparison of the rate parameters indicates that dicarbonate growth may be one order of magnitude greater than burkeite.

7.4.4. Estimation of Effective Thermal Conductivity from Observed Growth Rates and Heat-Transfer Resistance.

The model for dependence of fouling crystallization on the heat-transfer surface used in Chapters 5 and 6 is

$$SFR = \frac{1}{k_F} G_S , \tag{7.7}$$

where the effective thermal conductivity of the fouling deposit was assumed to be 1.73 $Wm^{-1}K^{-1}$, the value previously reported by Smith [8]. The method for estimating surface-fouling rates was presented previously in this chapter. With the surface-fouling rate and

measured growth rate of crystals on the heat-transfer surface, it was possible to estimate the thermal conductivity of the fouling deposit on the heat transfer surface. The results are presented in Table 7.3.

Table 7.3: Surface fouling rates and estimations of the thermal conductivity for crystal deposits on the heat-transfer surface from experiments with the bench-scale surface crystallizer.

C:S mole ratio	T_B, °C	Mass of EDTA, g	G_S, $m \cdot s^{-1}$	SFR, $m^2KW^{-1}s^{-1}$	k_F, $Wm^{-1}K^{-1}$
2.67	110	N	3.14E-07	1.94E-07	1.61
2.67	110	N	3.18E-07	2.09E-07	1.52
2.67	110	N			
2.67	110	Y - 30 g			
6.0	110	N	1.71E-07	9.33E-08	1.84
6.0	115	N	4.63E-07	1.22E-07	3.80
6.0	115	Y - 9.5 g	1.11E-06	2.80E-07	3.95
6.0	115	Y - 28.5 g	*		

***Moments after surface crystals were observed in this experiment, bulk crystals plugged the circulation line and no growth rate data was determined.**

The effective thermal conductivities measured using the bench-scale surface crystallizer for burkeite compared well to the value of 1.73 $Wm^{-1}K^{-1}$ previously reported [8]. The experimental values varied between 6 and 12% from the previously reported value. The first experiment with an aqueous solution of Na_2CO_3:Na_2SO_4 molar ratio 6.0:1 that was conducted at 110°C also had a value similar to that previously reported for burkeite (6% variation) and used for sodium carbonate monohydrate in the pilot-scale experiments. However, when the temperature was raised to 115°C at the same molar ratio, the effective thermal conductivity more than doubled. This further justifies the previous conclusion that different salts were crystallizing at these two different bulk solution temperatures with sodium carbonate monohydrate the likely crystal formed at 110°C and dicarbonate at the higher temperature.

7.4.5. Influence of Calcium on Crystallization of Double Salts of Na_2CO_3 and Na_2SO_4 on a Heat-Transfer Surface

The final remaining question for this chapter is how calcium affected the results reported in this chapter when calcium was not sequestered. To determine the effect, EDTA was added in a series of experiments using different solutions. The exact amounts added to each experiment are listed in Table 7.1.

EDTA was added to the solutions expected to produce burkeite to obtain a 4:1 mole ratio of EDTA molecules to calcium ions. Shi identified that a ratio between 2 and 4:1 totally sequestered the calcium and eliminated its inhibiting effects [5]. However, this left the question of what influence EDTA might have on the surface crystallization process. For this reason, the experiments with solutions expected to produce dicarbonate had EDTA added to produce a 0.5:1 molar ratio in the first experiment and a 1.5:1 mole ratio in the second experiment.

Differences in the supersaturation where initiation occurred and differences in growth rate for crystals on the heat-transfer surface were expected when EDTA was added. The values were tabulated in Table 7.2. For dicarbonate the rate parameter increased by 275% when a small amount of EDTA was added. The kinetic parameters in Table 7.2 indicate that calcium played a significant role in the crystallization phenomenon. These results were not unexpected given the results in Chapter 5.

Differences in the initiation mechanism, or lack thereof, provided an additional indication of the influence of calcium on crystallization on the heat-transfer surface. Any change in habit might have indicated an influence of EDTA on the surface crystallization process.

In the case of solutions expected to produce burkeite, when EDTA was added no crystallization on the heat-transfer surface was observed. Instead, at a relative supersaturation of 0.15 in the bulk solution, primary nucleation occurred. No subsequent adhesion of crystals to the heat-transfer surface was visible. This implies that nucleation directly on the surface observed from solutions expected to produce burkeite without EDTA added was caused in part by calcium inhibition. From crystallization theory, the interfacial free energy for a surface crystal should be lower than for a bulk crystal since one crystal face is in contact with the heated surface, not the solution. Calcium ions increase the interfacial free energy by introducing lattice defects. Without the calcium inhibition, the supersaturation required to cause nucleation directly on the surface is not reached and primary bulk nucleation occurs instead.

In solutions expected to produce dicarbonate, when EDTA was added adhesion of crystals to the heat-transfer surface still occurred. However, the number of stable initiation sites for fouling decreased with the increasing level of EDTA in the solution. The apparent reason for this is the reduction in supersaturation and the consequent reduction in growth rates. In adhesion fouling of this type, growth of the crystal into the microstructure of the surface is required to create a stable site.

Table 7.4 presents each of the experiments and the mechanism of initiation for fouling of the heat-transfer surface in each case. The one experiment not discussed previously is the reduced circulation rate experiment. The parameters for this experiment are located in the third row from the top in Table 7.4. Here the circulation rate was reduced by 33% to determine what impact this variable might have on fouling. Instead of influencing fouling, the pre-bulk nucleation crystals formed in solutions expected to

produce burkeite when calcium is present caused the circulation piping to plug numerous times.

Table 7.4: Mechanism for initiation of fouling on the heat-transfer surface observed during experiments with the bench-scale surface crystallizer

C:S mole ratio	T_B, °C	Mass of EDTA, g	Results
2.67	110	-	Direct Surface Nucleation before Bulk Nucleation
2.67	110	-	Direct Surface Nucleation
2.67	110	-	Lower Circulation Led to Particle Settling & Line Plugged
2.67	110	30	Bulk Nucleation - No Surface Adhesion
6.0	110	-	Bulk Nucleation - Surface Adhesion & Growth
6.0	115	-	Bulk Nucleation - Surface Adhesion & Growth
6.0	115	9.5	Bulk Nucleation - Surface Adhesion & Growth
6.0	115	28.5	Bulk Nucleation - Surface Adhesion & Growth

Table 7.5: Relative supersaturation at primary bulk nucleation (or where surface fouling was observed)

C:S mole ratio	T_B, °C	Mass of EDTA, g	σ_B
2.67	110	-	0.29
2.67	110	-	0.30
2.67	110	-	
2.67	110	30	0.15
6.0	110	-	0.20
6.0	115	-	0.11
6.0	115	9.5	0.10
6.0	115	28.5	0.06

Table 7.5 shows that EDTA did in fact act to sequester calcium as the relative supersaturation levels required for nucleation were significantly reduced. For burkeite the relative supersaturation required was reduced by 50%. For dicarbonate, the relative supersaturation was reduced by just under 50%. What is interesting is that only a slight decrease in the relative supersaturation required for bulk nucleation of dicarbonate was observed for the first level of EDTA. It was only at the higher EDTA level that the relative supersaturation was significantly reduced. This result agrees with the observation of Shi that a small amount of calcium can have a large influence on crystallization of double salts containing Na_2CO_3 and Na_2SO_4 [6].

7.5. Conclusions

Results of experiments conducted using the bench-scale surface crystallizer were used to identify the mechanism by which fouling was initiated on the heat-transfer surface for both burkeite and dicarbonate. For burkeite, initiation of the fouling deposit occurred by direct nucleation of crystals on the heat-transfer surface. For dicarbonate, initiation of the fouling deposit occurred after bulk nucleation through adhesion of the crystals in solution to the heat-transfer surface. Growth rates for crystals on the heat-transfer surface were measured and heat-transfer resistances due to fouling were estimated using the bench-scale surface crystallizer apparatus. In addition, a method for determining nucleation rates was presented, but requires additional refinement.

Burkeite fouling was due in part to calcium inhibition. The inhibiting effects of calcium on burkeite crystallization allowed the supersaturation to reach a level at the heat-transfer surface where nucleation occurred before the metastable limit in the bulk solution was reached. When EDTA was added to sequester the calcium ions, primary bulk nucleation occurred before the initiation of fouling and no subsequent fouling was observed.

For dicarbonate, the growth rate parameter increased with the sequestering of calcium by EDTA. Sequestering calcium with EDTA also reduced the relative supersaturation at which crystallization occurred for both dicarbonate and burkeite. The relative supersaturation at which burkeite nucleation occurred was generally higher than that for dicarbonate.

7.6. Variables

C Concentration, wt-%

d_p Bulk particle diameter, m

G_S Surface growth rate, ms^{-1}

$J_{0,S}$ Surface nucleation rate, $m^{-2}\ s^{-1}$

k_F Effective thermal conductivity of fouling material, $Wm^{-1}K^{-1}$

k_S Surface growth rate parameter, ms^{-1}

m Inverse solubility profile slope, K^{-1}

q Heat transfer rate, W

SFR Surface fouling rate, $m^2KW^{-1}s^{-1}$

R_E Electrical Resistance, Ω

R_F Fouling Thermal Resistance, m^2KW^{-1}

T Temperature, K

U Overall heat transfer coefficient, $Wm^{-2}K^{-1}$

V Voltage, V

σ Relative supersaturation

τ Scale initiation time, s

Superscripts and Subscripts

* Solubility limit

$_B$ Bulk Condition

$_I$ Inlet Condition

$_O$ Outlet Condition

s Surface Condition

7.7. Bibliography

1. Hasson, D., "Precipitation Fouling," *Fouling of Heat Transfer Equipment*, 527-568, Hemisphere Publishing Corporation, New York, 1981
2. Linnikov, Oleg D., "Investigation of the initial period of sulphate scale formation Part 1. Kinetics and mechanism of calcium sulphate surface nucleation at its crystallization on a heat-exchange surface," *Desalination*, 122:1-14 (1999)
3. Linnikov, Oleg D., "Investigation of the initial period of sulphate scale formation Part 2. Kinetics of calcium sulphate crystal growth at its crystallization on a heat-exchange surface," *Desalination*, 128:35-46 (2000)
4. Linnikov, Oleg D., "Investigation of the initial period of sulphate scale formation Part 3. Variations of calcium sulphate crystal growth rates at its crystallization on a heat-exchange surface," *Desalination*, 128:47-55 (2000)
5. Hedrick, R.H., Kent, J.S., "Crystallizing sodium salts from black liquor," *TAPPI Journal*, 75:12, 107-111 (1992)
6. Shi, B., "Crystallization of Solutes that Lead to Scale Formation in Black Liquor Evaporation," *Ph.D. Thesis*, Georgia Institute of Technology, 2002
7. Mullin, J.W., *Crystallization 3rd Edition*, Butterworth-Heinemann, 1997
8. Smith, J.B., Sodium Salt Scaling in Falling Film Black Liquor Evaporators, *Ph.D. Thesis*, Georgia Institute of Technology, 2000

Chapter VIII: Summary of the Research

8.1. Introduction

The research undertaken and reported in this thesis had four objectives: (1) to determine the initiation mechanisms for heat-transfer fouling by double salts composed of Na_2CO_3 and Na_2SO_4; (2) to develop a methodology for the estimation of rate parameters for primary nucleation and growth of crystals in bulk solutions and growth of crystals on heat-transfer surfaces; (3) to determine the effect of calcium on the crystallization behavior of double salts of Na_2CO_3 and Na_2SO_4, particularly as it relates to fouling of heat-transfer surfaces; and (4) to determine the dependence of fouling on the composition of black liquor, and particularly the influence of the transition in crystallizing species from burkeite to dicarbonate, and on nucleation phenomena.

8.2. Initiation Mechanisms for Heat-Transfer Fouling by Na_2CO_3-Na_2SO_4 Based Salts

Fouling of heat-transfer surfaces by double salts composed of Na_2CO_3 and Na_2SO_4 was found to be a caused by two different crystallization phenomena. In the case of burkeite, direct nucleation was determined to be the mechanism by which the initiation of fouling occurred. For dicarbonate, primary bulk nucleation at relatively high supersaturation followed by surface adhesion was identified as the mechanism for the initiation of fouling.

Results from this work indicate that primary nucleation of two separate crystal species of Na_2CO_3 and Na_2SO_4 can occur when black liquor is being concentrated.

Primary nucleation first occurs shortly after the solubility limit is exceeded, when burkeite begins to crystallize out of solution. At greater total solids content, as the dissolved sulfate content in the liquor is reduced, dicarbonate begins to crystallize out of solution. In black liquor, no fouling by burkeite was observed, while fouling due to dicarbonate was substantial.

Finally, the level of supersaturation that resulted from inverse solubility behavior and temperature of the heat-transfer surface alone was not sufficient to cause rapid fouling. Rather, this supersaturation combined with additional supersaturation developed by evaporation led to rapid initiation of scale on the heat-transfer surface, and subsequent fouling.

8.3. Estimation and Application of Rate Parameters for Primary Nucleation and Growth in Bulk Solutions and Growth of Crystals on a Heat-Transfer Surface

Nucleation rates were estimated for the first time from Focused-Beam Reflectance Measurements (FBRM). Rate parameters for primary bulk nucleation and for growth on a heat-transfer surface of crystals that contained Na_2CO_3 and Na_2SO_4 were estimated using conventional crystallization models. The rate parameters estimated were used to determine the influence of changes in experimental variables on the fouling process and to evaluate potential strategies to reduce fouling on heat-transfer surfaces.

Correlative models for the dependence of the rate parameters for primary bulk nucleation and for crystal growth on the heat-transfer surface from aqueous solutions of sodium carbonate and sodium sulfate were developed through this research. The rate parameter for primary bulk nucleation in an aqueous solution of Na_2CO_3 and Na_2SO_4

depended directly on the thermal driving force and inversely on the rate of recirculation of the aqueous solution over the heat transfer surface and on the Na_2CO_3:Na_2SO_4 in solution. The rate parameter for growth of crystals on the heat-transfer surface depended inversely on the rate of recirculation of the aqueous solution over the heat transfer surface rate and on the Na_2CO_3:Na_2SO_4 in solution. The ratio of the salts in solution was raised to the ¼ power.

The dependence of the rate parameters for primary bulk nucleation and for crystal growth on the heat-transfer surface on the composition of black liquor solutions was also determined through this research. The rate parameters for both the first and the second nucleation events decreased in black liquor when the Na_2CO_3:Na_2SO_4 ratio was increased. The rate parameter for crystal growth on the heat-transfer surface decreased when the Na_2CO_3:Na_2SO_4 ratio was increased. In addition, the viability of a number of potential strategies that could be employed to reduce fouling at an industrial facility was determined by comparison of their estimated rate parameters. Of the alternatives studied, adding crystal of anhydrous sodium carbonate to black liquor above its solubility limit provided to be the best method to reduce fouling of the heat-transfer surface in the pilot evaporator.

The growth rate of a layer of crystals on a heat-transfer surface was estimated from the heat-transfer resistance and thermal conductivity of the fouling deposit from

$$\frac{d\left(1/U\right)}{dt} = \frac{d\Delta x_F}{k_F\, dt}. \tag{8.1}$$

Recognizing that $d\Delta x_F/dt$ is actually a growth rate, a conventional model for growth rates of crystals of the form,

$$G_S = k_S \sigma , \tag{8.2}$$

was substituted into Equation 8.1 for $d\Delta x_F/dt$. This created a model for crystallization fouling,

$$\frac{d\left(1/U\right)}{dt} = \frac{k_S \sigma}{k_F} . \tag{8.3}$$

The sizes of crystals on the heat-transfer surface were measured as a function of time from digital imagery. The rate of growth of these crystals was determined using the measurements obtained.

The estimated thermal conductivity, k_F, for burkeite was estimated from the growth rates of crystals observed on the heat-transfer surface and surface fouling rates determined from estimated heat-transfer coefficients. The thermal conductivity estimated was within 10% of the value reported by Smith [1]. An advancement of this model taking into account fouling initiation rate would be useful but was not undertaken as a part of this research because nucleation rates on the heat-transfer surface could not be measured sufficiently accurately, given the limitations of the experimental apparatus.

8.4. Influences of Calcium on the Crystallization of Na_2CO_3-Na_2SO_4 Based Salts.

Sequestering calcium ions with EDTA allowed bulk nucleation to occur in burkeite-producing solutions before any crystals were observed on the heat-transfer surface. No subsequent adhesion of crystals to the surface, as seen with dicarbonate, occurred. For dicarbonate, when calcium was sequestered, surface adhesion and growth occurred with molar ratios of EDTA to calcium ion as low as 1.5:1. However, the number of nucleation sites observed decreased when the concentration of EDTA was

increased. Also, the rate parameter for crystal growth on the heat-transfer surface increased when the concentration of EDTA was increased.

8.5. Future Research Opportunities

While this research provided a better understanding of the relationship between crystallization phenomena and fouling of heat transfer surfaces during evaporation of black liquor, it also raised several new questions. Those questions are included here as guidance for future research on this topic.

One key question is the exact nature of EDTA-calcium interactions and their influence on the crystallization of burkeite and dicarbonate. This work clearly shows that the crystallization behavior for both crystals is altered by the addition of EDTA to sequester calcium. However, no consideration has been given to whether or not EDTA itself might inhibit crystallization in Na_2CO_3-Na_2SO_4 salts. The only way to evaluate this is to completely remove calcium from the system, and no practical method of separation has been determined to accomplish this task.

One experimental difficulty that was not overcome was the quantitative measurement of the composition of the dissolved species in black liquor during evaporation. It was difficult to collect samples that were completely free of crystals. Also, the small changes in composition with time during evaporation were difficult to detect because of the difficulty in sampling and analytical errors. An *in situ* measurement of the dissolved sodium carbonate and dissolved sodium sulfate concentrations is needed. It would be valuable for experimental measurements and for on-line monitoring and control of supersaturation in industrial black liquor evaporators.

There is currently no way of estimating the solubility of Na_2CO_3 and Na_2SO_4 in black liquor that accounts for the differing composition of burkeite and dicarbonate crystals with solution composition. In addition, dicarbonate may not be a thermodynamically stable chemical species. Methods of accounting for the variable composition of burkeite in equilibrium calculations, and for predicting crystallization of dicarbonate as a non-equilibrium species need to be developed.

One final area for additional research would be to determine the influence of viscosity on the processes of crystallization. The experimental work conducted for this thesis used the plate Reynolds number as an indication of the flow behavior. However, this value is primarily influenced by the flow velocity for these experiments. If the crystallization process has any bulk transport limitations, then the viscosity of the solution may play a significant role in the fouling process.

8.6. Bibliography

1. Smith, J.B., Sodium Salt Scaling in Falling Film Black Liquor Evaporators, *Ph.D. Thesis*, Georgia Institute of Technology, 2000

References

Adams, T.N., Frederick, W.J., Grace, T.M., Hupa, M., Iisa, K., Jones, A.K., Tran, H., *Kraft Recovery Boilers*, TAPPI Press, Atlanta, 1997

Arhippainen, B. and Jungerstam, B., "Operating Experience of Black Liquor Evaporation to High Dry Solids Content," TAPPI Journal, 52(6): 1095-1099 (1969)

Barrett, P., Glennon, B., "In-line FBRM Monitoring of Particle Size in Dilute Agitated Suspensions," Part. Part. Syst. Charact. 16 (1999) 207-211.

Berry, L.R., "Black Liquor Scaling in Multiple Effect Evaporators," *TAPPI Journal*, 49(4): 68A-71A (1966)

Branch, C.A., "Heat Transfer and Heat Transfer Fouling in Evaporators with Kraft Pulp Black Liquor," *Ph.D. Thesis*, University of Auckland, 1991

Branch, Craig A. and Hans M. Müller-Steinhagen, "Fouling during heat transfer to kraft liquor. Part 1: Experimental results," *Appita* 48:1 pp. 45-50 (1995)

Braatz, R.D., Fujiwara, M., Ma, D.L., Togkalidou, T., Tafti, D.K., "Simulation and New Sensor Technologies for Industrial Crystallization: A Review," International Journal of Modern Physics B, Vol 16, Nos 1 & 2 pp. 346-353 (2002)

Custers, J.P.A., Hersmis, M.C., Meuldijk, J., Vekemans, J.A.J.M., Hulshof, L.A., "3,4,5-Tri-Dodecyloxybenzoic Acid: Combining Reaction Engineering and Chemistry in the Development of an Attractive Tool to Assist in Scaling Up Solid-Liquid Reactions," Organic Process Research & Development, 2002, 6, 645-651.

Dowding, P.J., Goodwin, J.W., Vincent, B., "Factors governing emulsion droplet and solid particle size measurement performed using the focused beam reflectance technique," Colloids and Surfaces A: Physicochemical and Engineering Aspects 192 (2001) 5-13.

Euhus, D.D., Rousseau, R.W., Frederick Jr., W.J., Lien, S.J., "Black Liquor Evaporation: Links between Nucleation in the Bulk and Fouling of Heat Transfer Surfaces," Separations Technology Topical Conference, AIChE, New York, 2001, pp. 236-241.

Euhus, D.D., Rousseau, R.W., Frederick Jr., W.J., Lien, S.J., "Sodium Salt Fouling of Falling-Film Evaporators: A Pilot Study," International Chemical Recovery Conference, Oral Presentations, PAPTAC, Montreal, 2001, pp. 183-193.

Euhus, D.D., Shi, B., Rousseau, R.W., Frederick Jr., W.J., "Control of Soluble Scale in Black Liquor Evaporators and Concentrators: Part 1. Pilot Plant Studies," Proceedings of the 2002 TAPPI Fall Technical Conference, TAPPI Press, Atlanta, 2002

Felder, R.M., Rousseau, R.W., *Elementary Principles of Chemical Processes, 3rd Edition*, John Wiley & Sons, New York, 2000

Frederick, W.J., B. Kelly, H.C. Kim, M.J. McIntyre, and J.P. Danko, "Modeling Electrolyte Behavior in Pulp and Paper Processes," in *Chemical Engineering Technology in Forest Products Processing*, B. Crowell, editor, AIChE Forest Products Division, Tacoma, WA (1988), pp. 87-96.

Frederick Jr., W.J., Euhus, D.D., Shi, B., Rousseau, R.W., "Control of Soluble Scale in Black Liquor Evaporators and Concentrators: Part 2. Interpretation of Crystallization Results," Proceedings of the 2002 TAPPI Fall Technical Conference, TAPPI Press, Atlanta, 2002

Frederick Jr., W.J., Schmidl, G.W., Verrill, C.L., Rousseau, R.W., Shi, B., Euhus, D.D., Chen, F.C., Gao, Z., *Control of Soluble Scale Fouling in High-Solids Black Liquor Concentrators: Final Technical Report*, DOE Contract DE-FC36-99-GO10387,A003, April 28, 2003

Gao, S.-X., C.-B. Gu, Z.-L. Jiao, Y.-C. Li, D. Luo, L. Niu, D.-B. Shi and J.-S. Wang, "Falling-Film Flow on Vertical Plate and Evaporating Test Reseearch as well as Primary Test on the Concentration of Black Liquor from Wheat-Straw Pulp," *Int. Nonwood Fiber Pulping & Pmkg. Conf. (Beijing) Proc. Vol. 2*: 865-876 (July 11-14, 1988)

Golike, G.P., Nakamura, N., "Global Evaporator: New Technology for Black Liquor Heating and High-Solids Evaporation," *1989 CPPA/TAPPI Int. Chem. Recovery Conf. Preprints*: 183-189, (Ottawa, April 3-6, 1989)

Golike, G.P., Q. Pu, K.L. Holman, K.R. Carlson, P.C. Wollwage, H.G. Folster and S. Rankin, "NAELS: A New Method for Calculating Equilibrium Solubility of Burkeite and Sodium Carbonate in Black Liquor," *Proceedings of the 1998 International Chemical Recovery Conference. Part 1 (of 3)*: 403-418, TAPPI Press (Tampa, FL. Jun 1-4, 1998)

Grace, T.M., *Solubility Limits in Black Liquor Project 3136*, Institute of Paper Chemistry (February 22, 1974)

Grace, T.M., *A Survey of Evaporator Scaling in the Alkaline Pulp Industry Project 3234 Report 2*, Institute of Paper Chemistry (September 22, 1975)

Grace, T.M., "Solubility Limits in Black Liquors," *AIChE Symposium Series*, 72(157): 73-82 (1976)

Grace, T.M. and B.D. Andrews, *Study of Evaporator Scaling: Soluble Carbonate-Sulfate Scales Project 3234 Report 2*, Institute of Paper Chemistry (January 25, 1977)

Grace, T.M., "Evaporator Scaling," *Southern Pulp and Paper Manufacturer*, 42(8): 16-23 (1977)

Grace, T.M., *Pulp and Paper Manufacture Series Volume 5: Alkaline Pulping: Chapter 18, Overview of Kraft Recovery*, Edited by Kocurek, M.J., Grace, T.M., and Malcolm, E., Joint Textbook Committee of the Paper Industry, 1989

Grace, T.M., *Pulp and Paper Manufacture Series Volume 5: Alkaline Pulping: Chapter 19, Black Liquor Evaporation*, Edited by Kocurek, M.J., Grace, T.M., and Malcolm, E., Joint Textbook Committee of the Paper Industry, 1989

Green, R.P., Hough, G, *Chemical Recovery in the Alkaline Pulping Processes Revised Edition*, TAPPI Press, Atlanta, 1992

Green, S. and Frattali, F., "The System Sodium Carbonate-Sodium Sulfate-Sodium Hydroxide-Water at 100°C," *Journal of American Chemistry Society*, 68: 1789-1794 (1946)

Harrison, R., "New operating strategies for kraft evaporators can reduce scale," *Pulp and Paper*, March: 156-159, 1980

Harvie, Charles E.; Weare, John H. The prediction of mineral solubilities in natural waters: the sodium-potassium-magnesium-calcium-chlorine-sulfate-water system from zero to high concentration at 25° *Geochimica et Cosmochimica Acta* (1980), 44(7), 981-97.

Harvie, Charles E.; Eugster, Hans P.; Weare, John H. Mineral equilibriums in the six-component seawater system, sodium-potassium-magnesium-calcium-sulfate-chloride-water at 25°C. II: Compositions of the saturated solutions. *Geochimica et Cosmochimica Acta* (1982), 46(9), 1603-18.

Harvin, Richard L. Thermal and physical properties and heat-transfer coefficients of sulfate paper mill black liquor. Ph.D. dissertation, Univ. of Florida (1955), 154 pp.

Hasson, D., "Precipitation Fouling," *Fouling of Heat Transfer Equipment*, 527-568, Hemisphere Publishing Corporation, New York, 1981

Hedrick, R.H., Kent, J.S., "Crystallizing sodium salts from black liquor," *TAPPI Journal*, 75:12, 107-111 (1992)

Hukkanen, E.J., Braatz, R.D., "Measurement of Particle Size Distribution in Suspension Polymerization Using In Situ Laser Backscattering," Submitted Article provided by the Authors.

Kern, D.Q., Seaton, R.E., "A theoretical analysis of thermal surface fouling," British Chemical Engineering, 4:5, pp. 258-262 (1959)

Kim, W.T., Bai, C., Cho, Y.I., "A study of $CaCO_3$ fouling with a microscopic imaging technique," *International Journal of Heat and Mass Transfer*, 45:597-607 (2002)

Kim, W.T., Cho, Y.I., "Experimental Study of the Crystal Growth Behavior of $CaCO_3$ Fouling Using a Microscope," *Experimental Heat Transfer*, 13:153-161 (2002)
Incropera, F.P., DeWitt, D.P., *Introduction to Heat Transfer, Third Edition*, John Wiley & Sons, 1996

Lamy, E.J., "Process changes reduce mill's concentrator fouling problems," *Pulp and Paper*, December: 92-95, 1979

Lavery, H.P., Grace, T.M., and Frederick, W.J., "Slug and Churn Flow Heat Transfer in the Long Tube Vertical Evaporator," *Svensk Papperstidning*, Research Section, pp.R72-80 (1983).

Linnikov, Oleg D., "Investigation of the initial period of sulphate scale formation Part 1. Kinetics and mechanism of calcium sulphate surface nucleation at its crystallization on a heat-exchange surface," *Desalination*, 122:1-14 (1999)

Linnikov, Oleg D., "Investigation of the initial period of sulphate scale formation Part 2. Kinetics of calcium sulphate crystal growth at its crystallization on a heat-exchange surface," *Desalination*, 128:35-46 (2000)

Linnikov, Oleg D., "Investigation of the initial period of sulphate scale formation Part 2. Variations of calcium sulphate crystal growth rates at its crystallization on a heat-exchange surface," *Desalination*, 128:35-46 (2000)

Makela, A., "TUBEL – a new black liquor concentrator technology for modern mill demands," *Proceedings of the 1998 International Chemical Recovery Conference. Part 1 (of 3)*: 393-401, TAPPI Press (Tampa, FL. Jun 1-4, 1998)

MINITAB User's Guide 1: Data, Graphics, and Macros, Release 13, 1999

MINITAB User's Guide 2: Data Analysis and Quality Tools, Release 13, 1999

Mullin, J.W., *Crystallization 3rd Edition*, Butterworth-Heinemann, 1997

Novak, L., "Sodium Salt Scaling in Connection with Evaporation of Black Liquors and Pure Model Solutions," *Ph.D. Thesis*, Chalmers University of Technology, 1979

Novak, L., "Sodium Salt Scaling in Connection with Evaporation of Black Liquors and Pure Model Solutions," *Swedish Paper Journal*, 8: 240-245 (1979)

Osborne, D.M., "Evaporation to High Solids," *1993 Kraft Recovery Operations Short Course Notes*: 119-128, TAPPI (Orlando, Jan. 3-8, 1993)

Pitzer, K.S., *Theory: Ion interaction Approach. Activity Coefficients in Electrolyte Solutions*, vol. 1 R.M. Pytkowicz, ed., CRC Press, 1979

Randolph, A.D., M.A. Larson, Theory of Particulate Processes, 2nd ed., Academic Press, 1988

Rieke, J., Drone, K., Cox, D., Clark, C., "Willamette uses enhanced forced circulation to reach 80% solids," *Pulp and Paper*, 74(7): 37-41, (2000)

Rousseau, R.W., "Crystallization Processes," *Encyclopedia of Physical Science and Technology, Third Edition, Volume 4*, Academic Press, 2002

Ruf, A., Worlitschek, J., Mazzotti, M., "Modeling and Experimental Analysis of PSD Measurements through FBRM," Part. Part. Syst. Charact. 17 (2000) 167-179.

Schmidl, Wolfgang and Frederick, Wm. James, "Current Trends in Evaporator Fouling," *Proceedings of the 1998 International Chemical Recovery Conference. Part 1 (of 3)*: 367-377, TAPPI Press (Tampa, FL. Jun 1-4, 1998)

Seidell, A. and W. Linke, *Solubility of Inorganic and Metal Organic Compounds*, Vol. II, 4th ed.: 1121, Van Nostrand, Princeton (1965)

Shi, B., "Crystallization of Solutes that Lead to Scale Formation in Black Liquor Evaporation," *Ph.D. Thesis*, Georgia Institute of Technology, 2002

Shi, B., Euhus, D.D., Rousseau, R.W., Frederick, Jr., W.J., "Crystallization and Control of Sodium Salt Scales in Black Liquor Concentrators," Submitted to *TAPPI Journal*

Sinquefield, S.A, A Microcomputer Software Package for Simulation of Non-Ideal Aqueous Electrolyte Systems at Equilibrium, *M.S. Thesis*, Oregon State University, 1991

Smith, J.B., Sodium Salt Scaling in Falling Film Black Liquor Evaporators, *Ph.D. Thesis*, Georgia Institute of Technology, 2000

Somerscales, E.F.C., Knudsen, J.G., *Fouling of Heat Transfer Equipment*, Hemisphere Publishing Corporation, New York, 1981

Stenuf, T.J., Liu, H.-S., "Heat Transfer to Black Liquor in a Falling-Film Evaporator," *ESPRI Research Reports*, 79:IX SUNY College of Environmental Science and Forestry (Syracuse) (NY) 80 October 15, 1983

Tadayyon, A., Rohani, S., "Determination of Particle Size Distribution by Par-Tec ® 100: Modelling and Experimental Results," Part. Part. Syst. Charact. 15 (1998) 127-135.

Verrill, C.L., Schmidl, W., Ball, A.R., Frederick Jr., W.J., DeMartini, N., Experimental Determination and Modeling of Sodium Salt Solubilities in High Solids Kraft Black Liquor – Accepted for Presentation at the *2003 TAPPI Fall Technical Conference*

Westervelt, H.H., W.J. Frederick, E.W. Malcolm, and D.B. Easty, "The Determination and Temperature Dependence of the Stability Constant of the Calcium - Catechol-4-Sulfonate Complex in Alkaline, Aqueous Media", *Analytica Chimica Acta*, 138, pp. 237-243. (1982)

Westervelt, H.H., W.J. Frederick, E.W. Malcolm, and D.B. Easty, "New Evidence Concerning the Role of Black Liquor Organics in Calcium Carbonate Scale Formation," *TAPPI*, 65(5):179-80 (1982).